CENTRO UNIVERSITÁRIO SENAI CIMATEC

PROGRAMA DE POS-GRADUAÇÃO STRICTO SENSU

MODELAGEM COMPUTACIONAL E TECNOLOGIA INDUSTRIAL

PAULO ROBERTO FREITAS NEVES

Modelagem computacional para aperfeiçoamento de tecnologia de descontaminação instantânea de superfícies por meio de aspersão de agente biocida

Salvador, 2021

PAULO ROBERTO FREITAS NEVES

Modelagem computacional para aperfeiçoamento de tecnologia de descontaminação instantânea de superfícies por meio de aspersão de agente biocida

Dissertação de Mestrado apresentada ao Programa de Pós-Graduação de Modelagem Computacional e Tecnologia Industrial, Curso de Mestrado em Modelagem Computacional e Tecnologia Industrial do Centro Universitário SENAI CIMATEC, como requisito para a obtenção do título de Mestre em Modelagem Computacional e Tecnologia Industrial.

Orientador: Prof. Dr. Alex Álisson Bandeira Santos

Orientadora: Prof[a]. Dr[a]. Bruna Aparecida Souza Machado

Salvador, 2021

Ficha catalográfica elaborada pela Biblioteca do Centro Universitário SENAI CIMATEC

N511m Neves, Paulo Roberto Freitas

Modelagem computacional para aperfeiçoamento de tecnologia de descontaminação instantânea de superfícies por meio de aspersão de agente biocida / Paulo Roberto Freitas Neves. – Salvador, 2021.

123 f. : il. color.

Orientador: Prof. Dr. Alex Álisson Bandeira Santos.
Orientadora: Profª. Drª. Bruna Aparecida Souza Machado.

Dissertação (Mestrado em Modelagem Computacional e Tecnologia Industrial) – Programa de Pós-Graduação, Centro Universitário SENAI CIMATEC, Salvador, 2021.
Inclui referências.

1. SARS-CoV-2. 2. Câmara de desinfecção. 3. Agente biocida. 4. Descontaminação – Superfícies contaminadas - SARS-CoV-2. 5. Water-Sensitive Paper - WSP. 6. *C*omputational Fluid Dynamics - CFD. I. Centro Universitário SENAI CIMATEC. II. Santos, Alex Álisson Bandeira. III. Machado, Bruna Aparecida Souza. IV. Título.

CDD 620.00113

NDI - 03

Sistema FIEB | SENAI CIMATEC
PELO FUTURO DA INOVAÇÃO

CENTRO UNIVERSITÁRIO SENAI CIMATEC

Mestrado Acadêmico em Modelagem Computacional e Tecnologia Industrial

A Banca Examinadora, constituída pelos professores abaixo listados, aprova a Defesa de Mestrado, intitulada **"Modelagem computacional para aperfeiçoamento de tecnologia de descontaminação instantânea de superfícies por meio de aspersão de agente biocida**" apresentada no dia 18 de junho de 2021, como parte dos requisitos necessários para a obtenção do Título de Mestre em Modelagem Computacional e Tecnologia Industrial.

Orientador: **Prof. Dr. Alex Álisson Bandeira Santos**
SENAI CIMATEC

Bruna Aparecida Souza Machado
Assinado de forma digital por Bruna Aparecida Souza Machado
Dados: 2021.06.21 11:58:10 -03'00'

Orientadora: **Prof. Dr. Bruna Aparecida Souza Machado**
SENAI CIMATEC

Membro Interno: **Prof. Dr. Davidson Martins Moreira**
SENAI CIMATEC

Membro Externo: **Prof. Dr. Antônio Gabriel Souza Almeida**
IFBA

DEDICATÓRIA

Dedico este trabalho à toda minha família e amigos

AGRADECIMENTOS

Agradeço primeiramente a Deus por me conceder saúde e permitir mais esta conquista.

À minha família, em especial à minha esposa e filha, Priscila e Celina por todo amor, incentivo e dedicação, aos meus pais, Amarildo (in memorian) e Eliane, por todo amor, dedicação e pelos ensinamentos de vida, aos meus irmãos, Carlos e Ramon, pela parceria de sempre e a minha querida tia Sônia Marlene (in memorian) que me proporcionou muitos momentos felizes.

Aos meus parentes mais próximos, sogro, sogra, cunhados, cunhadas e sobrinhas por estarem sempre ao meu lado proporcionando momentos felizes.

Aos meus orientadores, Prof. Dr. Alex Santos e Profª. Dra. Bruna Machado, por acreditarem no meu potencial, pelas sugestões, esclarecimentos, paciência e dedicação.

Aos membros da banca pela disponibilidade em avaliar e realizar comentários construtivos, contribuindo com a evolução do trabalho.

Ao Prof. Dr. Luis Alberto Brêda Mascarenhas, por todo apoio nas discussões técnicas e confiança depositada.

Aos professores e colegas dos Programas de Pós-Graduação do SENAI CIMATEC, pela contribuição a cada apresentação e durante as aulas.

Aos membros do Laboratório Energia, Luzia Tofaneli, Turan Oliveira, Paulo Reis e Tarcísio Magalhães, por todo apoio no desenvolvimento do trabalho e pela parceria de sempre.

Ao ITS, em especial à Profª Dra. Leticia Rodrigues, Fabrícia Oliveira, Katharine Hodel, Laerte Santos e Eduardo Silva por todo apoio e esclarecimentos no desenvolvimento do trabalho.

À Marinilda Souza, pela amizade e incentivo de sempre.

Ao SENAI CIMATEC por todo o apoio, pela infraestrutura computacional e disponibilidade de equipe, fundamentais para o desenvolvimento deste trabalho.

A todos aqueles que contribuíram de forma direta ou indireta. Foram muitos que apoiaram esse desenvolvimento. Meus sinceros agradecimentos.

RESUMO

A transmissão do SARS-CoV-2 através do contato com superfícies contaminadas no ambiente ou por objetos vem sendo cada vez mais descrita como uma importante forma de transmissibilidade. Desta forma, o objetivo deste trabalho foi de projetar e avaliar o desempenho de uma câmara de desinfecção por spray para aspersão instantânea de solução de agente biocida, por meio de ensaios experimentais e modelagem computacional, bem como, propor os ajustes necessários na configuração para melhorar a aspersão sobre superfícies e, consequentemente, a eficácia do equipamento desenvolvido. Sete microrganismos teste foram preparados e inoculados na superfície de sete tipos de EPI (máscara respiratória, protetor facial, sapato, luva, touca, óculos de segurança e jaleco). Os testes foram realizados em EPIs previamente contaminados utilizando um manequim com dispositivo de movimento para exposição à câmara com agente biocida (hipoclorito de sódio). Simulações CFD da presente tecnologia (câmara com 6 bicos nebulizadores) também foram realizadas aplicando o método dos volumes finitos e o modelo de turbulência SST k – ω e validadas por meio de comparações, de forma qualitativa e quantitativa, com ensaios experimentais realizados utilizando o método Water-Sensitive Paper (WSP). Após avaliação, foi identificado que o sistema de aspersão com o agente biocida foi eficaz na redução da carga microbiana, sendo a redução percentual igual a> 99% e, consequentemente, trazendo o número de células viáveis para <10 UFC / mL e <0,33 UFC / cm² após tempos de exposição de 10 e 30 s em 96,93% nas condições experimentais analisadas. Além disso, foi proposto um novo procedimento de passagem para a câmara com seis bicos e uma nova configuração da câmara de desinfecção. Na câmara com 6 bicos foi identificada deficiência em sua região central, onde a concentração de gotas suspensas era próxima a zero. No entanto, com o procedimento de nova passagem, houve um aumento significativo na molhabilidade da superfície. Com a proposição da câmara com 12 bicos, a concentração de gotas em suspensão nas diferentes regiões foi maior, com um aumento médio de 266%. Os resultados experimentais da nova configuração comprovaram que houve um aumento

da molhabilidade em todos os momentos de exposição, sendo mais significativo para uma exposição de 30 s.

Palavras-chave: SARS-CoV-2; câmara de desinfecção; spray; agente biocida; descontaminação; Water-sensitive paper; CFD.

ABSTRACT

The transmission of SARS-CoV-2 through contact with contaminated surfaces in the environment or by objects has been increasingly described as an important form of transmissibility. Thus, the objective of this work was to design and evaluate the performance of a spray disinfection chamber for instant sprinkling of biocidal agent solution, by means of experimental tests and computational modeling, as well as to propose the necessary adjustments in the configuration to improve sprinkling on surfaces and, consequently, the effectiveness of the developed equipment. Seven test microorganisms were prepared and inoculated on the surface of seven types of PPE (respiratory mask, face shield, shoe, glove, cap, safety glasses and lab coat). The tests were performed on previously contaminated PPE using a mannequin with a movement device for exposure to the chamber with a biocidal agent (sodium hypochlorite). CFD simulations of the present technology (chamber with 6 nebulizer nozzles) were also performed using the finite volume method and the SST k - ω turbulence model and validated through comparisons, qualitatively and quantitatively, with experimental tests performed using the method Water-Sensitive Paper (WSP). After evaluation, it was identified that the spray system with the biocidal agent was effective in reducing the microbial load, with the percentage reduction equal to> 99% and, consequently, bringing the number of viable cells to <10 CFU / mL and <0 , 33 CFU / cm² after exposure times of 10 and 30 s in 96.93% in the experimental conditions analyzed. In addition, it was proposed a new passage procedure for the chamber with six nozzles and a new configuration of the disinfection chamber. In the chamber with 6 nozzles, a deficiency was identified in its central region, where the concentration of suspended droplets was close to zero. However, with the new pass procedure, there was a significant increase in surface wettability. With the proposition of the chamber with 12 nozzles, the concentration of drops in suspension in the different regions was higher, with an average increase of 266%. The experimental results of the new configuration proved that there was an increase in wettability at all times of exposure, being more significant for an exposure of 30 s.

Keywords: SARS-CoV-2; disinfection chamber; spray; biocidal agent; decontamination; Water-Sensitive Paper; CFD.

LISTA DE TABELAS

LISTA DE FIGURAS

LISTAS DE SIGLAS E ABREVIATURAS

A	Área [m^2]
ANVISA	Agência Nacional de Vigilância Sanitária
arg_1	Parâmetro do modelo de turbulência SST k – ω
arg_2	Parâmetro do modelo de turbulência SST k – ω
C_D	Coeficiente de arrasto
$CD_{k\omega}$	Parâmetro do modelo de turbulência SST k – ω
CFD	Fluidodinâmica Computacional
CFU	Colony-Forming Unit
COVID-19	*Coronavirus Disease* 2019
C_μ	Constante do modelo de turbulência k – ε
$C_{\varepsilon 1}$	Constante do modelo de turbulência k – ε
$C_{\varepsilon 2}$	Constante do modelo de turbulência k – ε
d	Diâmetro [m]
DIVISA	Diretoria de Vigilância Sanitária e Ambiental
EPA	US Environmental Protection Agency
EPI	Equipamento de Proteção Individual
f	subscrito indicador de fluido
F_1	Função de mistura do modelo SST k – ω
F_2	Função de mistura do modelo SST k – ω
g	Aceleração da gravidade [m/s^2]
HCWs	Healthcare workers
k	Energia cinética turbulenta [$m^2.s^{-2}$]
K	Condutividade térmica [W/m.K]
lm	Comprimento de mistura [m]
m	Massa [kg]
MERS	Síndrome Respiratória do Oriente Médio
MVF	Método dos Volumes Finitos
OMS	Organização Mundial da Saúde

$_p$	Subscrito indicador de partícula
$\boldsymbol{p}$	Pressão
PC	Principal Component
PCA	Principal Component Analysis
$\mathbf{P_K}$	Produção de turbulência devido a forças viscosas [kg/m.s^3]
PPE	Personal Protective Equipment
PVC	Policloreto de Vinila
RANS	Reynolds Averege Navier-Stokes
$\mathbf{R_e}$	Número de Reynolds
RT-PCR	Reverse Transcription - Polymerase Chain Reaction
S	Taxa de Deformação [1/s]
$\bar{S}$	Valor médio do termo fonte
SARS-CoV-2	Coronavírus da Síndrome Respirtória Aguda Grave
SESAB	Secretaria de Saúde do Estado da Bahia
$\mathbf{S_{Mx}}$, $\mathbf{S_{My}}$, $\mathbf{S_{Mz}}$	Termos fonte de momento nas direções x, y e z, respectivamente [kg/m^2.s^2]
SST	Shear Stress Transport
$\boldsymbol{S_k}$	Termo fonte da energia cinética turbulenta
$\boldsymbol{S_\omega}$	Termo fonte da frequência turbulenta
$\boldsymbol{S_\phi}$	Termo fonte de propriedade escalar genérica
t	Tempo [s]
U	Valor médio constante da velocidade no tempo [m/s]
$\boldsymbol{UV}$	Ultravioleta
UV-C	Ultravioleta-C (radiação de ondas curtas de 100 nm até 280 nm)
$\boldsymbol{u_*}$	Velocidade de atrito [m/s]
$\vec{\boldsymbol{u}}$	Vetor velocidade tridimensional [m/s]
$\boldsymbol{u(t)}$	Velocidade no tempo [m/s]
$\boldsymbol{u'(t)}$	Componente flutuante da velocidade no tempo [m/s]
u,v,w	Velocidades nas direções cartesianas (x, y, z), respectivamente [m/s]

u',v',w'	Componentes flutuantes das velocidades nas direções cartesianas (x, y, z), respectivamente [m/s]
USA	United States of America
UFBA	Universidade Federal da Bahia
V	Velocidade de escoamento do fluido [m/s]
VOF	Volume de Fluido
ν	Velocidade cinemática [m/s]
$\boldsymbol{\upsilon_t}$	Viscosidade cinemática turbulenta [m^2/s]
(W, P, E)	Pontos nodais
We	Número de Weber
$\mathbf{We_{crit}}$	Número de Weber crítico
$\mathbf{We_{max}}$	Número de Weber máximo
WHO	World Health Organization
WSP	Water-Sensitive Paper
x,y,z	Direções cartesianas [m]
y	Distância perpendicular à parede [m]
$\boldsymbol{y_p}$	Distância à parede mais próxima
$\mathbf{y^+}$	Distância adimensional da parede
$\boldsymbol{\alpha}$	Constante do modelo de turbulência k – ω
$\boldsymbol{\alpha_1}$	Constante do modelo de turbulência k – ω para modelagem SST k – ω
$\boldsymbol{\alpha_2}$	Constante do modelo de turbulência k – ε para modelagem SST k – ω
$\boldsymbol{\beta}$	Constante dos modelos de turbulência k – ω
$\boldsymbol{\beta_1}$	Constante do modelo de turbulência k – ω para modelagem SST k – ω
$\boldsymbol{\beta_2}$	Constante do modelo de turbulência k – ε para modelagem SST k – ω
$\boldsymbol{\beta'}$	Constante dos modelos de turbulência k – ω
$\boldsymbol{\Gamma}$	Coeficiente de difusão
ΔX	Comprimento do volume de controle [m]
ΔV	Volume
$\mathbf{\delta X_{WP}}$	Distância entre os nós oeste e central [m]
$\mathbf{\delta X_{PE}}$	Distância entre os nós central e leste [m]

δX_{we}	Distância entre as faces oeste e leste do volume de controle [m]
δX_{xP}	Distância entre a face oeste do volume de controle e o nó central [m]
δX_{Pe}	Distância entre o nó central e a face oeste do volume de controle [m]
ε	Taxa de dissipação de energia cinética turbulenta [$m^2.s^{-2}$]
κ	Constante de Von Kármán
μ	Viscosidade dinâmica [Pa.s]
μ_t	Viscosidade turbulenta [Pa.s]
ρ	Massa específica de um fluido [kg/m^3]
σ_κ	Constante dos modelos de turbulência k – ε e k – ω
σ_ε	Constante do modelo de turbulência K – ε
σ_ω	Constante dos modelos de turbulência k – ω
$\sigma_{\kappa 1}$	Constante do modelo de turbulência k – ω para modelagem SST k – ω
$\sigma_{\kappa 2}$	Constante do modelo de turbulência k – ε para modelagem SST k – ω
$\sigma_{\omega 1}$	Constante do modelo de turbulência k – ω para modelagem SST k – ω
$\sigma_{\omega 2}$	Constante do modelo de turbulência k – ε para modelagem SST k – ω
τ_0	Tensão de cisalhamento na superfície [N/m^2]
ϕ	Propriedade escalar genérica
φ	Variável escalar
ω	Frequência de dissipação de energia cinética turbulenta [1/s]

SUMÁRIO

1. INTRODUÇÃO

A COVID-19 (do inglês: *Coronavirus Disease* 2019), doença que tem como característica uma síndrome respiratória aguda grave, é causada pelo coronavírus-2 (SARS-CoV-2), que surgiu na cidade de Wuhan, localizada na província de Hubei na China e que se disseminou pelo mundo em semanas [1–4]. Em 11 de março de 2020 a Organização Mundial de Saúde (OMS) declarou a COVID-19 como uma pandemia [5], e mais de 160 milhões de casos já foram notificados em todo o mundo até maio de 2021, onde, Estados Unidos, Índia e Brasil são os três países com o maior número de casos notificados e juntos representam 43,8% do total de infectados pelo SARS-CoV-2 no mundo [6]. A Figura 1 apresenta o cenário mundial de casos de infecção por COVID-19 confirmados.

Figura 1: Casos de infecção por COVID-19 confirmados no mundo [6].

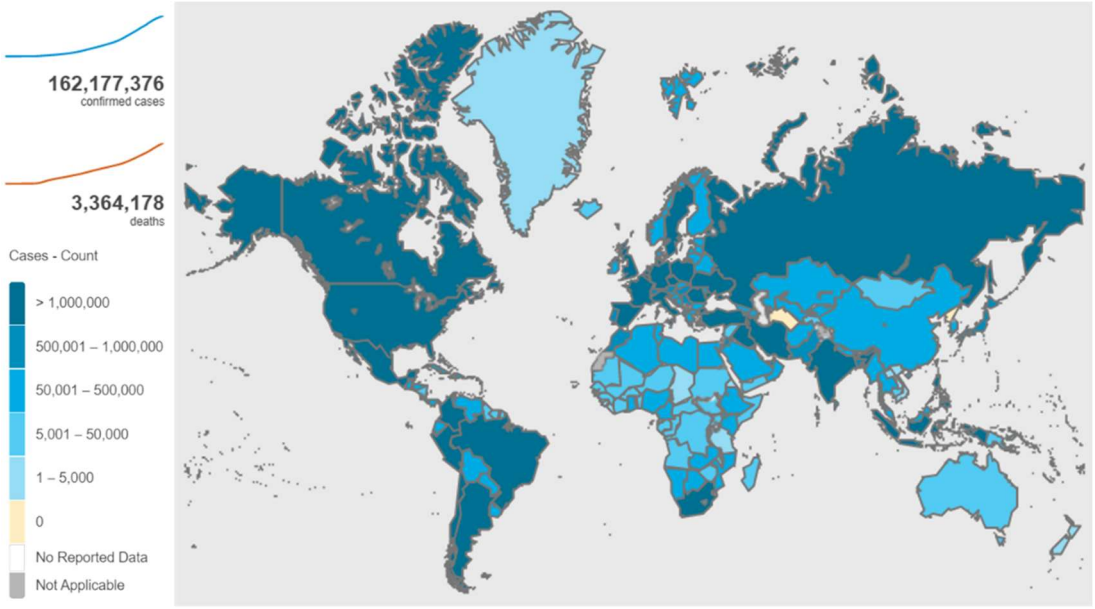

Embora tenha havido alerta sobre a ameaça do vírus que causam doenças respiratórios [7], o SARS-CoV-2 se espalhou a uma taxa sem precedentes, sendo urgente a necessidade de várias abordagens para enfrentamento dessa crise [8–10]. A transmissão do SARS-CoV-2 pode ocorrer por meio de contato direto com superfícies contaminadas ou pelo ar e, principalmente, através de contato direto com pessoas

contaminadas e secreções biológicas [11–16]. Desde o início da pandemia, diversos países têm adotado diferentes medidas desafiadoras para reduzir as taxas de infecção e, consequentemente, evitar o colapso dos sistemas de saúde [17]. Dessa forma, uma variedade de intervenções não farmacêuticas foi adotada, como os bloqueios regionais completos, fechamentos de atividades/comércio não essenciais, testagem em massa da população, medidas de quarentena, rastreamento de infectados, construção de hospitais destinados para o tratamento da COVID-19 e desenvolvimento de novas tecnologias de desinfecção [18,19].

É importante destacar que a pandemia causada pelo vírus SARS-CoV-2 afetou inúmeras pessoas em todo o mundo. O controle desta pandemia em tempo real é agora uma grande prioridade da comunidade científica e governos de diferentes partes do mundo [20]. As medidas de precaução durante e após a pandemia despertou o papel da sanitização na contenção da propagação de doenças. O objetivo do processo de sanitização é a remoção de microrganismos e inativação através de uma ou ambas etapas: (i) tratamento mecânico ou térmico e/ou (ii) uso de agentes antimicrobianos para descontaminar as partes do corpo, objeto ou superfícies, conforme apresentado na Figura 2 [21].

Até este momento, o distanciamento social surgiu como uma ferramenta útil para desacelerar a propagação do vírus SARS- CoV-2. Em locais públicos, entretanto, é difícil manter o distanciamento social por um longo período. Para diminuir a propagação da doença, um sistema de sanitização foi desenvolvido para interromper a cadeia de propagação do vírus em locais públicos, independentemente das condições de higiene das pessoas [22].

Figura 2: Métodos usados para a higienização e desinfecção de pessoas, objetos e espaços infectados [21].

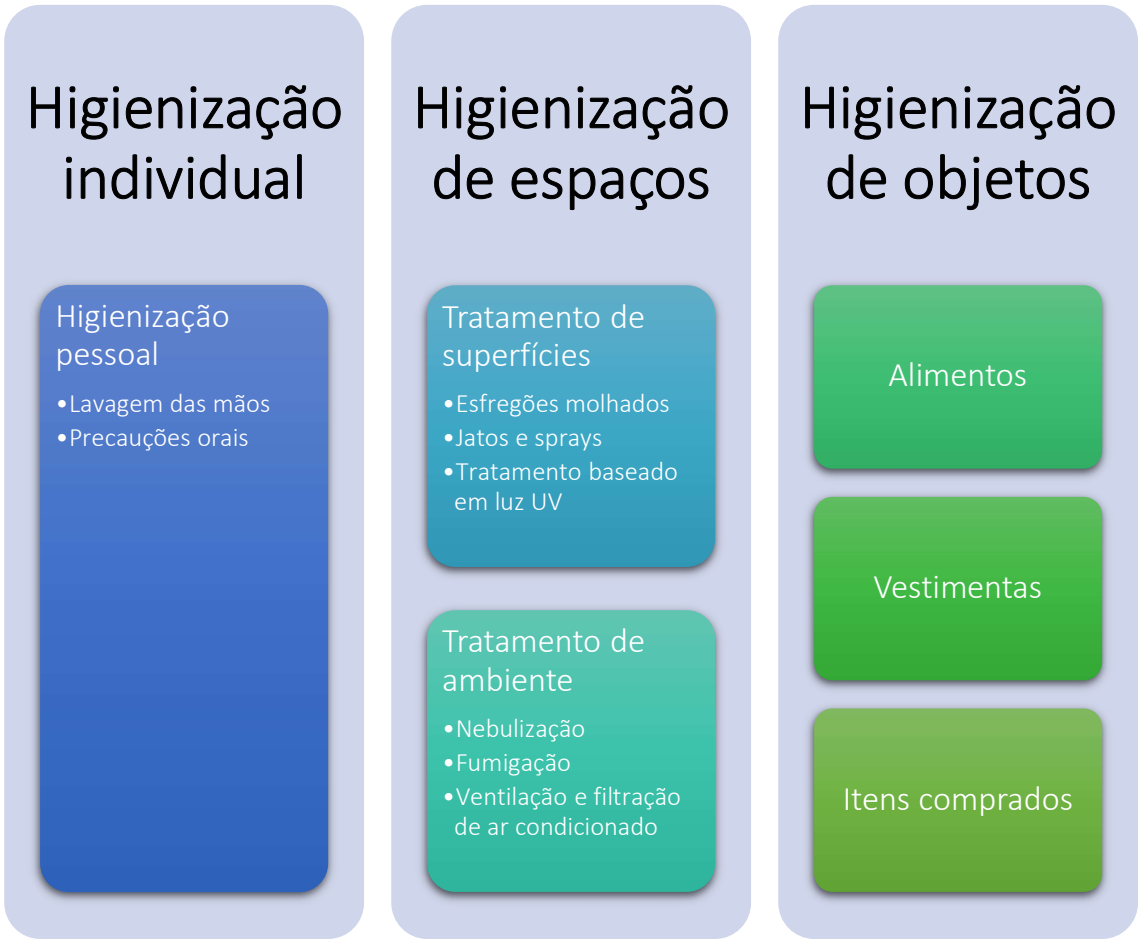

1.1. Justificativa

A transmissão através do contato com superfícies contaminadas no ambiente ou por objetos vem sendo cada vez mais descrita como uma importante forma de transmissibilidade [23,24] que, inclusive, já foi demonstrada para o SARS-CoV-2 [25,26]. A busca e avaliação da eficácia de alguns agentes biocidas e tecnologias que fazem uso desses agentes para a desinfecção de ambientes e superfícies contaminadas tem como base estudos anteriores, principalmente com vírus relacionados, como o SARS-CoV (coronavírus da Síndrome Respiratória Aguda Grave) e o MERS (coronavírus da Síndrome Respiratória do Oriente Médio) [27–29]. Mesmo com a descoberta de vacinas capazes de combater o vírus e com aproximadamente 1,4 bilhões de pessoas imunizadas em todo o mundo [30], as medidas de desinfecção podem potencialmente, desde que

comprovadas sua segurança de utilização, ajudar na inibição da transmissibilidade do vírus [1].

Desde o início da pandemia, novas tecnologias e protocolos passaram a ser desenvolvidos com o propósito de exercer o controle microbiano de forma eficiente, possibilitando uma redução da taxa de infecção [31,32]. Tecnologias essas que passaram a ser adotadas para auxiliar no combate a contaminação por SARS-CoV-2. Por exemplo, estudos anteriores demonstraram os benefícios do uso de dispositivos de luz ultravioleta para desinfecção de ambientes hospitalares [33], dispositivos portáteis com sistemas de pulverização para descontaminação de superfície [34] e câmaras de desinfecção com diferentes agentes biocidas [35]. Esses novos desenvolvimentos têm demonstrado auxiliar no controle da carga microbiana com base em evidências de testes em diferentes microrganismos, principalmente em ambientes nosocomiais, um dos principais problemas de saúde pública em todo o mundo [36] e, portanto, representam grande potencial de aplicação durante e após a pandemia causada pelo SARS-CoV-2.

Nesse contexto, os túneis/câmaras de desinfecção surgiram como uma medida de sanitização. Eles podem ser instalados em diversos locais, principalmente os quais podem ter grande circulação de pessoas (Figura 3). O primeiro túnel foi instalado na China e foi desenvolvido por outros países. Essas estruturas portáteis são feitas de aço e policloreto de vinila (PVC) com distâncias variando de 4 a 8 metros e podem ser do tipo estático e dinâmico. No tipo estático, a pessoa gira dentro da estação por 10-15 segundos, e o desinfetante é pulverizado a partir de bicos dispostos em toda a circunferência. O tipo dinâmico é uma passagem em que a pessoa se move por 4–8 metros e o dispositivo pulveriza o desinfetante por todo o caminho. Esses túneis são equipados com detectores infravermelhos (baseados em sensores) que ativam o spray desinfetante sempre que uma pessoa entra [37].

Basicamente, esses túneis borrifam uma névoa de uma solução desinfetante. Entretanto, a pulverização ou nebulização de certos produtos químicos, como formaldeído ou compostos de amônio quaternário, não é recomendado pela Organização Mundial da Saúde (OMS) e ANVISA (Nota Técnica n° 30/2020), pois não há nenhuma evidência científica sobre a eficácia, bem como, pelos efeitos adversos à saúde [38].

Figura 3: Túnel de passagem de desinfetante instalado em Islamabad, Paquistão [38].

Neste sentido, recentemente foi desenvolvido um equipamento que promove a aspersão de solução do agente biocida para a desinfecção instantânea dos equipamentos de proteção individual (EPIs) e que está sendo utilizado em alguns dos hospitais de referência para o tratamento da COVID-19 no Brasil. A avaliação de sua eficácia, segurança e aceitação entre os profissionais foram realizadas por meio de ensaios experimentais utilizando superfícies previamente contaminadas e analisando de forma qualitativa a deposição de partículas nas regiões de estudo [39], bem como, pela coleta de informações utilizando questionários estruturados envolvendo mais de 400 profissionais usuários [40].

O uso de desinfetantes no controle de infecções e os custos associados às infecções associadas à saúde são extremamente importantes, visto que podem ser usados em superfícies e/ou objetos inanimados para eliminar a maioria dos microrganismos patogênicos [41].

Diferentes tipos de microrganismos variam em sua resposta a ação de desinfetantes devido as suas características estruturais, composição e fisiologia celular, conforme apresentados na Tabela 1. De um modo geral, bactérias e fungos possuem uma resistência intrínseca para reduzir a permeabilidade de antissépticos e desinfetantes através da parede celular e uma resistência adquirida por mutações ou

aquisição de plasmídeos [42,43]. Os vírus possuem características únicas e específicas que influenciam a inativação por desinfetantes, como o tamanho (vírus maiores são mais sensíveis) e a presença do envelope celular, que é necessário para a infecção e, portanto, uma interferência no envelope pode reduzir a infectividade viral. Vírus Herpes Simplex, Vírus da imunodeficiência humana (HIV), Influenza e coronavírus são exemplos de vírus envelopado com baixa resistência aos desinfetantes [44].

Tabela 1: Aplicação de hipoclorito de sódio em diferentes concentrações na inativação de vírus, bactérias e fungos [45–54].

Desinfetante	Morte microbiana	Tempo de contato	Aplicação
NaClO (2,5% e 5,25%)	Biofilmes de *Enterococcus faecalis*, *Staphylococcus aureus*, *Candida albicans*, *Porphyromonas gingivalis, P. endodontalis, Prevotella intermedia* e *Fusobacterium nucleatum*	30 segundos, exceto para *C. albicans* e *S. aureus* (300 segundos)	Odontologia
NaClO (1 e 5%)	*E. faecalis, S. aureus, Escherichia coli, P. gingivalis* e *F. nucleatum*	Imediato	Odontologia
NaClO (0,21%)	Vírus da hepatite murina*	30 segundos	Descontaminação ambiental
NaClO (0,08 - 6%)	*E. faecalis, S. epidermidis, C. albicans e E. coli*	30 segundos	Odontologia
NaClO (0,5%, 2,5% e 5,25%)	*E. faecalis*, *C. albicans* e associação destes.	24 horas (antibiograma)	Odontologia
NaClO (1%) aerossolizado	*S. aureus* sensível *à meticilina*, *S. aureus* resistente *à meticilina*, *Pseudomonas aeruginosa* e *Bacillus subtilis* subsp. *spizizenii*	30 minutos	Descontaminação ambiental
Solução irrigante de NaClO (2,5%)	Biofilme de *E. faecalis*	10 minutos	Odontologia
NaClO (2,5% e 5,25%)	*Biofilme de E. faecalis*	30 minutos	Odontologia
NaClO (0,228g/L) disperso em umidificador ultrassônico	Vírus da diarreia epidêmica suína*	10 minutos	Descontaminação de EPI
NaClO (0,1 e 0,525%)	Coronavírus humano (HCoV 229e)	15 segundos	Descontaminação ambiental

* modelo com propriedades biofísicas e estrutura genômica semelhantes aos coronavírus humanos.

Além das propriedades de desinfecção da solução utilizada, a eficácia dessa tecnologia é também dependente da configuração e forma de uso do equipamento. A

disposição de bicos e procedimento de passagem podem influenciar na molhabilidade das superfícies de estudo e, consequentemente, no desempenho da desinfecção. [55].

Simulações numéricas tem se mostrado úteis para avaliação de fluxo de ar e trajetória de material particulado onde é importante a compreensão do fenômeno físico para fins médicos e de pesquisa [56–58]. Alguns estudos apresentaram desenvolvimento de câmaras de desinfecção por meio de fluidodinâmica computacional (CFD) e ilustraram técnicas de validação por meio deste tipo de simulação [55, 59]. Dessa forma, CFD pode ser uma alternativa interessante para avaliar tecnologias já desenvolvidas ou novas proposições.

1.2. Objetivos

1.2.1. Objetivo Geral

O objetivo geral deste trabalho foi de projetar e avaliar o desempenho de uma câmara de desinfecção por spray para aspersão instantânea de solução de agente biocida, por meio de ensaios experimentais e modelagem computacional, bem como, propor os ajustes necessários na configuração para melhorar a aspersão sobre superfícies e, consequentemente, a eficácia do equipamento desenvolvido.

1.2.2. Objetivos Específicos

- Projetar câmara de desinfecção por aspersão de agente biocida
- Realizar ensaios experimentais para avaliar a eficácia do agente biocida na inativação de bactérias e fungos em tempos de exposição de 10 e 30 segundos;
- Realizar simulações CFD de bico nebulizador e câmara de desinfecção aplicando o método dos volumes finitos e o modelo de turbulência SST k – ω;
- Avaliar a molhabilidade da câmara de desinfecção por meio de ensaios experimentais expondo WSP aplicados ao corpo em tempos de 10 e 30 segundos;

- Propor nova configuração da câmara de desinfecção aumentando o número e posições dos bicos nebulizadores.

1.3. Estrutura do Trabalho

Este trabalho foi organizado no formato de capítulos para uma melhor apresentação e entendimento do mesmo, possuindo no total cinco capítulos, conforme descrito a seguir:

O **capítulo 1** constitui a introdução, os objetivos e a estrutura desta dissertação. Neste capítulo o contexto geral que sustenta a importância do desenvolvimento da dissertação é discutido, evidenciando suas principais contribuições científicas.

O **capítulo 2** apresenta a revisão bibliográfica que é dividida em três tópicos. O primeiro traz tecnologias de desinfecção desenvolvidas para descontaminação de superfícies. O segundo aprofunda sobre os modelos matemático e numérico aplicados para simulação CFD de bicos nebulizadores. O terceiro apresenta trabalhos correlatos.

O **capítulo 3** apresenta um artigo publicado na PloS One (junho de 2021), como parte do desenvolvimento dos objetivos específicos desse trabalho. Refere-se à avaliação da eficácia do agente biocida utilizado na pesquisa para inativação de diferentes microrganismos, incluindo bactérias e fungos. Os resultados deste trabalho evidenciam a viabilidade da técnica baseada na descontaminação de superfícies de EPI's por meio de aspersão de agente biocida e sustentam o aprofundamento do estudo a partir de modelagem computacional.

O **capítulo 4** apresenta um artigo publicado na PloS One (maio de 2021), constituindo o desenvolvimento do modelo computacional para avaliação da eficácia e proposição de nova configuração da tecnologia, atendendo aos objetivos específicos desse trabalho. Neste capítulo são apresentadas as etapas do processo de caracterização do bico nebulizador, desenvolvimento do modelo computacional, ensaios experimentais e resultados.

O **capítulo 5** consiste na conclusão do trabalho e apresenta sugestão para trabalhos futuros.

REFERÊNCIAS

1. Weber DJ, Kanamori H, Rutala WA. “No touch” technologies for environmental decontamination: Focus on ultraviolet devices and hydrogen peroxide systems. Curr Opin Infect Dis 2016 Aug; 29(4):424–31. https://doi.org/10.1097/QCO.0000000000000284.

2. Donskey CJ. Decontamination devices in health care facilities: Practical issues and emerging applications. Am J Infect Control. 2019 Jun;47S:A23–A28. https://doi.org/10.1016/j.ajic.2019.03.005.

3. Shereen MA, Khan S, Kazmi A, Bashir N, Siddique R. COVID-19 infection: origin, transmission, and characteristics of human coronaviruses. Journal Of Advanced Research. 2020 Jul;24:91-98.http://dx.doi.org/10.1016/j.jare.2020.03.005.

4. Wang L, Didelot X, Yang J, et al. Inference of person-to-person transmission of COVID-19 reveals hidden super-spreading events during the early outbreak phase. Nat Commun 11.2020 Oct;5006:1-65006.https://doi.org/10.1038/s41467-020-18836-4.

5. World Health Organization. WHO Director-General's opening remarks at the media briefing on COVID-19 - 11 March 2020. 2020, GENEBRA. Disponível em: www.who.int/dg/speeches/detail/who-director-general-s-opening-remarks-at-the-media-briefing-on-covid-19---11-march-2020. Acesso em: 10 sep. 2020.

6. World Health Organization. Global Map - WHO Coronavirus Disease (COVID-19) Dashboard. 2021, GENEBRA. Disponível em: https://covid19.who.int/. Acesso em: 16 mai. 2021.

7. Shi Z, Gewirtz AT. Together Forever: Bacterial–Viral Interactions in Infection and Immunity. Viruses. 2018 Mar; 10(3):122-130. https://doi.org/10.3390/v10030122.

8. Wojewodzic MW. Bacteriophages Could Be a Potential Game Changer in the Trajectory of Coronavirus Disease (COVID-19). Phage. 2020 Jun;1(2):60-65.http://dx.doi.org/10.1089/phage.2020.0014.

9. Moozhipurath RK, Kraft L, Skiera B. Evidence of protective role of Ultraviolet-B (UVB) radiation in reducing COVID-19 deaths. Sci Rep 10;2020 Oct;17705:1-10. https://doi.org/10.1038/s41598-020-74825-z.

10. Anderson RM, Heesterbeek H, Klinkenberg D, Hollingsworth T. How will country-based mitigation measures influence the course of the COVID-19 epidemic? The Lancet.2020 Mar;395(10228):931-934.http://dx.doi.org/10.1016/s0140-6736(20)30567-5.

11. Vitis R, Passiatore M, Perna A, Proietti L, Taccardo G. COVID-19 contagion and contamination through hands of trauma patients: what risks and what precautions?.

Journal Of Hospital Infection. 2020 Jun;105(2):354-355.http://dx.doi.org/10.1016/j.jhin.2020.03.037.

12. Gambardella C, Pagliuca R, Pomilla G, Gambardella A. COVID-19 risk contagion: Organization and procedures in a South Italy geriatric oncology ward. Journal Of Geriatric Oncology. 2020 Set;11(7):1187-1188.http://dx.doi.org/10.1016/j.jgo.2020.05.008.

13. Tufan ZK, Kayaaslan B. Crushing the curve, the role of national and international institutions and policy makers in COVID-19 pandemic. Turkish Journal Of Medical Sciences. 2020 Apr;50(1):495-508.http://dx.doi.org/10.3906/sag-2004-167.

14. Rothe C, Schunk M, Sothmann P, Bretzel G, Froeschl G, Wallrauch C, et al. Transmission of 2019-NCOV infection from an asymptomatic contact in Germany. New England Journal Of Medicine. 2020 Mar;382(10):970-971.http://dx.doi.org/10.1056/nejmc2001468.

15. Younes N, Al-Sadeq DW, AL-Jighefee H, Younes S, Al-Jamal O, Daas HI, et al. Challenges in Laboratory Diagnosis of the Novel Coronavirus SARS-CoV-2. Viruses. 2020 May;12(6):582. https://doi.org/10.3390/v12060582.

16. Kampf G, Todt D, Pfaender S, Steinmann E. Persistence of coronaviruses on inanimate surfaces and their inactivation with biocidal agents. Journal Of Hospital Infection. 2020 Mar;104(3):246-251. http://dx.doi.org/10.1016/j.jhin.2020.01.022.

17. Di Carlo P, Chiacchiaretta P, Sinjari B, Aruffo E, Stuppia L, De Laurenzi V, et al. Air and surface measurements of SARS-CoV-2 inside a bus during normal operation. 2020 Nov; PLoS ONE 15(11): e0235943. https://doi.org/10.1371/journal.pone.0235943.

18. Yabe T, Tsubouchi K, Fujiwara N, et al. Non-compulsory measures sufficiently reduced human mobility in Tokyo during the COVID-19 epidemic. Sci Rep 10. 2020 Oct;18053:1-9.https://doi.org/10.1038/s41598-020-75033-5.

19. Flaxman S, Mishra S, Gandy A, et al. Estimating the effects of non-pharmaceutical interventions on COVID-19 in Europe. Nature 584. 2020 Jun;257–261.https://doi.org/10.1038/s41586-020-2405-7

20. Bedford J, Enria D, Giesecke J, Heymann DL, Ihekweazu C, Kobinger G, Lane HC, Memish Z, Oh M, Sall AA, Schuchat A, Ungchusak K, Wieler LH. COVID-19: towards controlling of a pandemic. Lancet [Internet]. 2020 Mar;395(10229):1015–8. Available from: https://linkinghub.elsevier.com/retrieve/pii/S0140673620306735

21. Khan MH, Yadav H. Sanitization During and After COVID-19 Pandemic: A Short Review. Trans Indian Natl Acad Eng [Internet]. 2020 Nov 1; Available from: https://doi.org/10.1007/s41403-020-00177-9

22. Maurya D, Gohil MK, Sonawane U, Kumar D, Awasthi A, Prajapati AK, Kishnani K, Srivastava J, Age A, Pol R, Misra S, Sarin DR, Dube PK, Dwivedi V, Thakur A, Srivastava R, Shukla V, Ranjan R, Tiwari R, Patil AS, Agrawal P, Sinha A, Dubey M, Mittal R, Agarwal AK. Development of Autonomous Advanced Disinfection Tunnel to Tackle External Surface Disinfection of COVID-19 Virus in Public Places. Trans Indian Natl Acad Eng [Internet]. 2020 Jun 4;5(2):281–7. Available from: https://doi.org/10.1007/s41403-020-00141-7

23. Bhatia R. Need for integrated surveillance at human-animal interface for rapid detection & response to emerging coronavirus infections using One Health weapproach. Indian J Med Res. 2020 Feb & Mar;151(2 & 3):132-135.doi: 10.4103/ijmr.IJMR_623_20.

24. Henwood AF. Coronavirus disinfection in histopathology. Journal Of Histotechnology. 2020 Mar;43(2):102-104.http://dx.doi.org/10.1080/01478885.2020.1734718.

25. World Health Organization. Modes of transmission of virus causing COVID-19 : implications for IPC precaution recommendations. 2020, GENEBRA. Disponível em: https://www.who.int/news-room/commentaries/detail/modes-of-transmission-of-virus-causing-covid-19-implications-for-ipc-precaution-recommendations. Acesso em: 20 oct. 2020

26. Otter JA, Donskey C, Yezli S, Douthwaite S, Goldenberg SD, Weber DJ. Transmission of SARS and MERS coronaviruses and influenza virus in healthcare settings: the possible role of dry surface contamination. J Hosp Infect. 2016 Mar;92(3):235-50.doi:10.1016/j.jhin.2015.08.027.

27. Chan JF, Yuan S, Kok K, To KK, Chu H, Yang J, Xing F, Liu J, Yip CC, Poon RW. A familial cluster of pneumonia associated with the 2019 novel coronavirus indicating person-to-person transmission: a study of a family cluster. The Lancet. 2020 Feb;395(10223):514-523.http://dx.doi.org/10.1016/s0140-6736(20)30154-9.

28. Drosten C, Günther S, Preiser W, Werf SD, Brodt H, Becker S, Rabenau H, Panning M, Kolesnikova L, Fouchier RAM. Identification of a Novel Coronavirus in Patients with Severe Acute Respiratory Syndrome. New England Journal Of Medicine. 2003 May;348(20):1967-1976. http://dx.doi.org/10.1056/nejmoa030747.

29. Zaki AM, Van Boheemen S, Bestebroer TM, Osterhaus ADMe, Fouchier RAM. Isolation of a Novel Coronavirus from a Man with Pneumonia in Saudi Arabia. New England Journal Of Medicine. 2012 Nov;367(19):1814-1820.http://dx.doi.org/10.1056/nejmoa1211721.

30. Johns Hopkins University & Medicine. Coronavirus Resource Center - Global Map, 2021. Panorama geral dos casos de Covid 19 pelo mundo. Disponível em: https://coronavirus.jhu.edu/map.html. Acesso em: 16 mai. 2021.

31. Whitworth J. COVID-19: a fast evolving pandemic. Trans R Soc Trop Med Hyg. 2020 Apr;114(4):241-248.doi: 10.1093/trstmh/traa025.

32. Ning P, Shan D, Hong E, Liu L, Zhu Y, Cui R, Zhou Y, Wang B. Disinfection performance of chlorine dioxide gas at ultra-low concentrations and the decay rules under different environmental factors. Journal Of The Air & Waste Management Association. 2020 Jul;70(7):721-728.http://dx.doi.org/10.1080/10962247.2020.1769768.

33. Silva DF, Toledo Neto JL, Machado MF, Bochnia JR, Garcez AS, Foggiato AA. Effect of photodynamic therapy potentiated by ultrasonic chamber on decontamination of acrylic and titanium surfaces. Photodiagnosis And Photodynamic Therapy. 2019 Sep;27:345-353.http://dx.doi.org/10.1016/j.pdpdt.2019.06.011.

34. Dellinger EP. Prevention of Hospital-Acquired Infections. Surgical Infections. 2016 Aug;17(4):422-426.http://dx.doi.org/10.1089/sur.2016.048.

35. Cadnum JL, Jencson AL, Livingston SH, Li DF, Redmond SN, Pearlmutter B, Wilson BM, Donskey CJ. Evaluation of an electrostatic spray disinfectant technology for rapid decontamination of portable equipment and large open areas in the era of SARS-CoV-2. American Journal Of Infection Control. 2020 Aug;48(8):951-954.http://dx.doi.org/10.1016/j.ajic.2020.06.002.32.

36. World Health Organization. Prevention of Hospital-Acquired Infections: A Practical Guide. 2002, Genebra. Available at https://www.who.int/csr/resources/publications/whocdscsreph200212.pdf. Acesso em: 18 Sep. 2020.

37. Biswal M, Kanaujia R, Angrup A, Ray P, Mohan Singh S. Disinfection tunnels: potentially counterproductive in the context of a prolonged pandemic of COVID-19. Public Health [Internet]. 2020 Jun;183(January):48–9. Available from: https://linkinghub.elsevier.com/retrieve/pii/S0033350620301505

38. Mallhi TH, Khan YH, Alotaibi NH, Alzarea AI. Walkthrough Sanitization Gates for COVID-19: A Preventive Measure or Public Health Concern? Am J Trop Med Hyg [Internet]. 2020 Aug 5;103(2):581–2. Available from: http://www.ajtmh.org/content/journals/10.4269/ajtmh.20-0533

39. Brêda Mascarenhas LA, et al. Potential application for SARS-CoV-2 disinfection of novel technology developed for instant decontamination of personal protective equipment before the doffing step. Plos One, 2020. Available from: https://doi.org/10.1371/journal.pone.0250854

40. Brêda Mascarenhas LA, et al. Perception of professionals from different healthcare units regarding the use of spray technology for the instantaneous decontamination of personal protective equipment during the coronavirus disease pandemic. BioMed Research International, 2020 (submited).

41. Dancer SJ. Controlling Hospital-Acquired Infection: focus on the role of the environment and new technologies for decontamination. Clinical Microbiology Reviews. 2014 Out;27(4):665-690. http://dx.doi.org/10.1128/cmr.00020-14.

42. McDonnell G, Russell AD. Antiseptics and disinfectants: activity, action, and resistance. Clin Microbiol Rev. Jan 1999;12(1):147-79. doi: 10.1128/CMR.12.1.147.

43. Alp S. Bacterial resistance to antiseptics and disinfectants. Mikrobiyol Bul. 2007 Jan;41(1):155-61. PMID: 17427567.

44. Lin Q, Lim JYC, Xue K, Yew PYM, Owh C, Chee PL, Loh XJ. Sanitizing agents for virus inactivation and disinfection. View. 2020 May 24:e16. doi: 10.1002/viw2.16. PMCID: PMC7267133.

45. Sena NT, et al. In vitro antimicrobial activity of sodium hypochlorite and chlorhexidine against selected single-species biofilms. International Endodontic Journal. 2006 Nov;39(11):878-885. http://dx.doi.org/10.1111/j.1365-2591.2006.01161.x.

46. Sassone LM, Fidel RAS, Murad CF, Fidel SR, Hirata R. Antimicrobial activity of sodium hypochlorite and chlorhexidine by two different tests. Australian Endodontic Journal. 2008 Apr;34(1):19-24. http://dx.doi.org/10.1111/j.1747-4477.2007.00071.x.

47. Dellanno C, Vega Q, Boesenberg D. The antiviral action of common household disinfectants and antiseptics against murine hepatitis virus, a potential surrogate for SARS coronavirus. American Journal Of Infection Control. 2009 Oct;37(8):649-652. http://dx.doi.org/10.1016/j.ajic.2009.03.012.

48. Pappen FG, et al. Inhibition of Sodium Hypochlorite Antimicrobial Activity in the Presence of Bovine Serum Albumin. Journal Of Endodontics. 2010 Fev;36(2):268-271. http://dx.doi.org/10.1016/j.joen.2009.09.025.

49. Tirali RE, Bodur H, Sipahi B, Sungurtekin E. Evaluation of the antimicrobial activities of chlorhexidine gluconate, sodium hypochlorite and octenidine hydrochloridein vitro. Australian Endodontic Journal. 2010 Oct;39(1):15-18. http://dx.doi.org/10.1111/j.1747-4477.2010.00266.x.

50. Thorn RMS, Robinson GM, Reynolds DM. Comparative Antimicrobial Activities of Aerosolized Sodium Hypochlorite, Chlorine Dioxide, and Electrochemically Activated Solutions Evaluated Using a Novel Standardized Assay. Antimicrobial Agents And Chemotherapy. 2013 May;57(5):2216-2225. http://dx.doi.org/10.1128/aac.02589-12.

51. Arias-Moliz MT, et al. Antimicrobial Activity of a Sodium Hypochlorite/Etidronic Acid Irrigant Solution. Journal Of Endodontics. 2014 Dec;40(12):1999-2002. http://dx.doi.org/10.1016/j.joen.2014.07.031.

52. Zand V, Sadeghi M, Mojaddadi A. Antibacterial Efficacy of Different Concentrations of Sodium Hypochlorite Gel and Solution on Enterococcus faecalis Biofilm. Iranian Endodontic Journal.2016 Sep. http://dx.doi.org/10.22037/iej.2016.11.

53. Antas M, Szczotka-Bochniarz A, Woźniakowski G. Effective inactivation of porcine epidemic diarrhea virus on contaminated surgery masks by low-concentrated sodium hypochlorite dispersion. Pol J Vet Sci. Dec 2020;23(4):647-650. doi: 10.24425/pjvs.2020.135801.

54. Meyers C, et al. Ethanol and isopropanol inactivation of human coronavirus on hard surfaces. Journal Of Hospital Infection. 2021 Jan;107:45-49. http://dx.doi.org/10.1016/j.jhin.2020.09.026.

55. Joshi JR. COVSACK: an innovative portable isolated and safe COVID-19 sample collection kiosk with automatic disinfection. Trans Indian Natl. Acad. Eng. 2020 Jul;5:269–275. https://doi.org/10.1007/s41403-020-00139-1.

56. Mutuku JK, Hou W, Chen W. An Overview of Experiments and Numerical Simulations on Airflow and Aerosols Deposition in Human Airways and the Role of Bioaerosol Motion in COVID-19 Transmission. Aerosol And Air Quality Research. 2020;20(6):1172-1196. http://dx.doi.org/10.4209/aaqr.2020.04.0185.

57. Peng S, Chen Q, Liu E. The role of computational fluid dynamics tools on investigation of pathogen transmission: prevention and control. Science Of The Total Environment. 2020 Dec;746:142090. http://dx.doi.org/10.1016/j.scitotenv.2020.142090

58. Gao N, Niu J. Transient CFD simulation of the respiration process and inter-person exposure assessment. Building And Environment. 2006 Sep;41(9):1214-1222. http://dx.doi.org/10.1016/j.buildenv.2005.05.014.

59. Hariharan P, D'Souza GA, Horner M, Morrison TM, Malinauskas RA, Myers MR (2017) Use of the FDA nozzle model to illustrate validation techniques in computational fluid dynamics (CFD) simulations. PLoS ONE 12(6): e0178749. https://doi.org/10.1371/journal.pone.0178749.

2. REVISÃO BIBLIOGRÁFICA

2.1. Tecnologias de Desinfecção

A necessidade de promover melhorias nos processos de limpeza e desinfecção de superfícies ambientais vem crescendo em grande consenso entre as áreas. Apesar do empenho e acesso a tecnologias que atuam no controle de infecções, ao contrário das expectativas, seus riscos crescem a cada dia afetando cotidianamente a vida das pessoas. Essa situação é agravada pelo número crescente de pessoas susceptíveis a infecções [1]. O uso de soluções desinfetantes na descontaminação ambiental é, de certa forma, uma das ações que foram requeridas no combate às infecções por conta do crescente aumento de microrganismos multirresistentes aos tratamentos com antimicrobianos e associados às elevadas taxas de infecções nosocomiais [2].

Dessa forma, a desinfecção de superfícies foi incluída em várias políticas e recomendações nacionais e internacionais de combate às infecções ambientais. Em contraste com a higiene das mãos, atividade normalmente habitual no cotidiano, a opinião de que a desinfecção ambiental é importante começou recentemente a ganhar espaço [3], bem como as metodologias e tecnologias passíveis de auxiliar esse processo. Recentemente, com a pandemia do SARS-CoV-2, o desenvolvimento de câmaras/túneis de desinfecção foi um exemplo da rápida inovação em resposta à disseminação desse vírus pelo ambiente [4], que apesar de ser potencialmente transmitido através das vias aéreas, diversos estudos identificaram a sua potencial transmissão através de superfícies contaminadas [5]. As câmaras de desinfecção são equipamentos que possuem um ponto de entrada e saída, a câmara onde ocorre o processo de desinfecção, reservatório para o fornecimento de solvente (em caso de substâncias líquidas), alimentação elétrica, fornecimento de ar e compressor (normalmente não obrigatório) e um mecanismo de spray. Opções de iluminação, tomadas elétricas dentro do dispositivo, áudio/vídeo, scanners de temperatura e atomizadores químicos são apresentadas como características adicionais/opcionais a serem incluídas no dispositivo [4].

Vale ressaltar que, a pandemia trouxe a popularização do uso desses dispositivos para serem utilizados diretamente sobre pessoas, entretanto, o uso de tecnologias semelhantes já é aplicado em diversas áreas, para o controle de infecções microbianas em geral. Estudos anteriores demonstraram os benefícios do uso de dispositivos de luz ultravioleta para desinfecção de ambientes hospitalares [6], dispositivos portáteis com sistemas de pulverização para descontaminação de superfície [5], além das câmaras de desinfecção com diferentes agentes biocidas [7,8]. Dispositivos spray passaram a ser utilizados para a descontaminação de áreas poucos acessíveis, com o intuito de criar uma estratégia que pudesse melhorar a limpeza e desinfecção de grandes áreas, espaços de difícil acesso ou irregulares. No entanto, existe uma quantidade relativamente pequena de informação quanto a essa abordagem de limpeza e desinfecção [9]. Esses dispositivos normalmente se baseiam em sistemas de desinfecção por pulverização eletrostática, que transformam o líquido desinfetante em aerossóis e, em seguida, aplicam uma carga a cada gota de modo que sejam atraídas para as superfícies por meio de forças eletrostáticas maiores do que a gravidade [10]. Os fabricantes afirmam que podem ser usadas em uma variedade de tipos de instalações, como saúde, enfermagem, escolas, escritórios, instalações esportivas, para desinfecção de superfícies.

Na área de alimentos, por exemplo, câmaras de desinfecção por micro-ondas são comercializadas e utilizadas para a descontaminação de bens sensíveis, a exemplo de pescados, contribuindo para a redução de células vegetativas e o crescimento de biofilmes, problemas graves no controle de qualidade desses alimentos [11]. Outras tecnologias envolvendo a emissão de radiação ultravioleta são opções largamente utilizadas no ramo industrial. As lâmpadas UVC ou "lâmpadas germicidas" têm sido usadas por décadas na área de saúde e em outros ambientes para inativar bactérias (por exemplo, tuberculose) ou vírus no ar (dentro de dutos de ar à prova de luz) e para esterilização de água potável [12].

Estudos vem demonstrando que algumas dessas tecnologias são eficazes na inativação de patógenos, além disso diversos ensaios clínicos já demonstraram que o uso dessas tecnologias pode reduzir o número de infecções hospitalares [13], bem como de outros ambientes como indústrias, áreas públicas, entrada de shoppings e outros

comércios, entre outros. É válido ressaltar que o uso de nenhuma dessas estruturas, até então, possui aprovação para serem utilizadas diretamente sobre pessoas. Além disso, análises de custo benefício devem ser conduzidas já que existem diferenças substanciais entre os dispositivos e, dentro de cada tecnologia há várias opções comerciais (principalmente se tratando de dispositivos UV).

É importante destacar que a escolha do agente químico a ser aplicado nessas tecnologias é de suma importância, seja na aplicação direta ou para aplicação em superfícies de vestimentas, alimentos e outros. A escolha e aplicação desses agentes químicos deve ser baseada nas recomendações de seus fabricantes, bem como nos reportes de agências que fazem o alerta e controle de uso dessas substâncias, para que sejam evitados problemas de segurança e toxicidade [4].

No presente estudo, todos os experimentos foram realizados usando hipoclorito de sódio em concentrações de 0,25% como agente biocida [14]. O hipoclorito de sódio foi considerado um dos desinfetantes mais relevantes e prevalentes para a desinfecção de superfícies contra a SARS-CoV-2 [15].

2.2. Modelagem Computacional (CFD)

Nesta seção serão apresentadas as modelagens matemática e numérica utilizadas no presente estudo e as condições de contorno utilizadas para cada uma das geometrias simuladas, sendo abordadas as equações de continuidade e Navier-Stokes e apresentados os modelos numéricos de discretização e turbulência.

2.2.1. Modelagem Matemática

A modelagem de um escoamento é feita por meio da equação de conservação de massa (continuidade) e momento (Navier-Stokes). Ambas equações são apresentadas na forma diferencial e são obtidas a partir da dedução em um volume de controle infinitesimal. A partir da Lei da conservação de massa, na qual a massa do sistema não se altera, por ser uma quantidade fixa de massa, obtém-se a equação

diferencial da conservação da massa, também é chamada de equação da continuidade devido às considerações necessárias de massa específica e a velocidade serem funções contínuas. A equação de conservação de massa é apresentada a seguir, conforme Equação 1.

$$\frac{\partial \rho}{\partial t} + div(\rho \vec{u}) = 0 \quad (1)$$

onde t é o tempo; ρ é a densidade; $\vec{u}$ é o vetor velocidade.

As equações de Navier-Stokes são equações diferenciais da quantidade de movimento que originalmente descrevem um escoamento Newtoniano. As Equações 2, 3 e 4 são equações de Navier-Stokes nas três direções cartesianas.

$$\frac{\partial (\rho u)}{\partial t} + div(\rho u \vec{u}) = -\frac{\partial p}{\partial x} + div(\mu \, grad \, u) + S_{Mx} \quad (2)$$

$$\frac{\partial (\rho v)}{\partial t} + div(\rho v \vec{u}) = -\frac{\partial p}{\partial y} + div(\mu \, grad \, v) + S_{My} \quad (3)$$

$$\frac{\partial (\rho w)}{\partial t} + div(\rho w \vec{u}) = -\frac{\partial p}{\partial z} + div(\mu \, grad \, w) + S_{Mz} \quad (4)$$

onde t é o tempo; ρ é densidade; p é a pressão; x, y, e z são as três direções cartesianas; u, v e w são as velocidades nas direções x, y, e z, respectivamente; $\vec{u}$ é o vetor de velocidade tridimensional; μ é a viscosidade do fluido; S_{Mx}, S_{My}, e S_{Mz} são os termos de origem do momento nas direções x, y, e z, respectivamente.

Analisando o formato das Equações 2 a 4 é notória a semelhança entre elas. Substituindo as velocidades u, v e w por uma variável genérica ϕ, uma forma conservativa para todas as equações de escoamento, incluindo, por exemplo, temperatura pode ser escrita na forma da Equação 5:

$$\frac{\partial (\rho \phi)}{\partial t} + div(\rho \phi \vec{u}) = div(\Gamma \mathrm{grad} \phi) + S_{\phi} \quad (5)$$

onde t é o tempo; ρ é densidade; $\vec{u}$ é o vetor de velocidade; Γ é o coeficiente de difusão e S_ϕ é o termo fonte para a variável genérica.

Os termos presentes na Equação 5 e também nas Equações 2 a 4 podem ser interpretados da seguinte forma:

Taxa de crescimento de ϕ do elemento fluido.	+	Quantidade de ϕ que sai do elemento fluido (advecção).	=	Taxa de incremento de ϕ devido à difusão.	+	Taxa de incremento de ϕ devido a fontes.

2.2.2. Modelagem Numérica

Problemas fluidodinâmicos são desenvolvidos numericamente a partir da solução das equações de Navier-Stokes entretanto, para obter solução dessas equações, uma abordagem numérica deve ser adotada. Desta forma, um método numérico pode ser utilizado para resolver aproximações algébricas das equações de Navier-Stokes.

No presente trabalho, foi utilizado o programa ANSYS CFX 17.1 para obtenção das soluções numéricas.

A seguir serão apresentados o método de discretização e o modelo de turbulência utilizados no presente trabalho. A aplicação desses modelos ocorre na etapa de pré-processamento, onde serão utilizados para discretizar a geometria na forma temporal e espacial e, posteriormente, solucionar numericamente o sistema.

2.2.2.1. Método dos Volumes Finitos

O Método dos Volumes Finitos (MVF) é utilizado neste trabalho e consiste na integração das equações governantes diretamente no domínio físico, seguindo as três etapas a seguir:

- Uma malha computacional é gerada dividindo o domínio contínuo em volumes de controles discretos;
- As equações governantes são integradas nos volumes de controle individuais desenvolvendo as equações algébricas das variáveis discretas dependentes, como por exemplo, temperatura e velocidade;
- Por fim, as equações discretas são linearizadas e resolvidas em um sistema de equações lineares produzindo valores atualizados das variáveis independentes.

A integração das equações diferenciais será apresentada para um caso unidimensional e em regime permanente da equação de transporte (Equação 5) para uma propriedade genérica ϕ, sendo os resultados dessa integração estendidos para os casos bidimensional e tridimensional. Eliminando os termos transiente e convectivo da equação de transporte, temos a Equação 6.

$$div(\Gamma \mathrm{grad}\phi) + S_\phi = 0 \tag{6}$$

Para facilitar o entendimento da utilização do MVF, o domínio unidimensional é dividido em volumes de controle em torno dos pontos W, P e E. O volume de controle é formado entorno do ponto P, conforme apresentado na Figura 4.

Figura 4: Domínio unidimensional para aplicação do MVF [16].

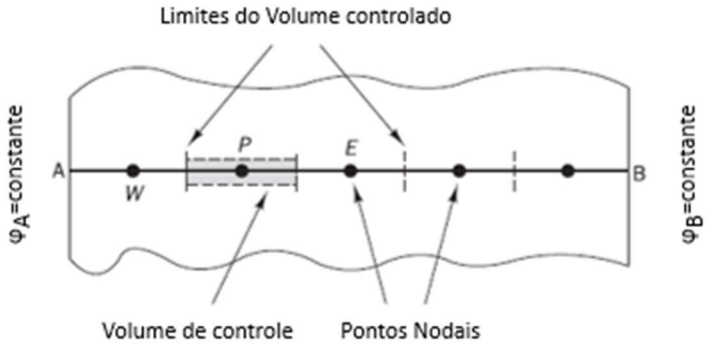

Considerando o domínio definido na Figura 4, o sistema é governado pela Equação 7.

$$\frac{d}{dx}\left(\Gamma\frac{d\phi}{dx}\right)+S=0 \tag{7}$$

onde Γ é o coeficiente de difusão e S é o termo fonte.

Na Figura 5 são apresentados um ponto nodal geral P e seus vizinhos W e E, sendo W o ponto a oeste de P e E o ponto a leste de P em uma geometria unidimensional. Adicionalmente, é possível determinar as faces do volume de controle sendo w sua face a oeste e sua face a leste sendo e. As distâncias entre os pontos WP e PE podem ser identificados como δX_{WP} e δX_{PE} respectivamente. A largura total do volume de controle é expressa por $\Delta X = \delta X_{we}$, sendo esta a soma das distâncias entre a face w e o ponto P e entre o ponto P e a face e são apresentadas como δX_{wP} e δX_{Pe}, respectivamente.

Figura 5: Definições e distâncias num domínio unidimensional [14].

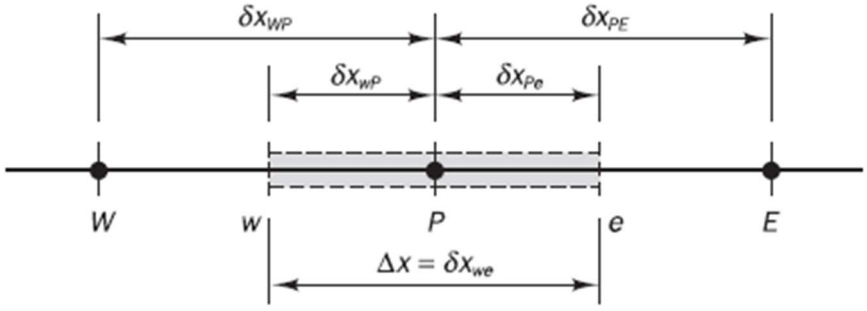

Um passo importante do MVF é a integração das equações governantes sobre um volume de controle para obter uma equação discretizada, nesse caso, para o ponto nodal P. Considerando a integração da Equação 8 no volume de controle, teremos:

$$\int_{\Delta V}\frac{d}{dx}\left(\Gamma\frac{d\phi}{dx}\right)dV+\int_{\Delta V}SdV=\left(\Gamma A\frac{d\phi}{dx}\right)_e-\left(\Gamma A\frac{d\phi}{dx}\right)_w+\bar{S}\Delta V=0 \tag{8}$$

onde A é a área da seção transversal da face do volume de controle, ΔV é o volume e e $\bar{S}$ é o valor médio da fonte S_ϕ sobre o volume de controle.

A forma discretizada das derivadas da Equação 8 podem ser obtidas, conforme Equações 9 e 10:

$$\left(\Gamma A \frac{d\phi}{dx}\right)_e = \Gamma_e A_e \left(\frac{\phi_E - \phi_P}{\delta x_{WP}}\right) \tag{9}$$

$$\left(\Gamma A \frac{d\phi}{dx}\right)_w = \Gamma_w A_w \left(\frac{\phi_P - \phi_W}{\delta x_{WP}}\right) \tag{10}$$

Na prática o termo fonte S pode ser uma função da variável dependente. Nesses casos, o método de volume finito aproxima o termo fonte por meio de uma forma linear [16], conforme Equação 11.

$$\bar{S}\Delta V = S_u + S_P \phi_P \tag{11}$$

Substituindo as Equações 9, 10 e 11 na Equação 8 obtemos a equação algébrica discretizada (Equação 12).

$$\left(\frac{\Gamma_e}{\delta x_{PE}} A_e + \frac{\Gamma_w}{\delta x_{WP}} A_w - S_P\right)\phi_P = \left(\frac{\Gamma_w}{\delta x_{WP}} A_w\right)\phi_W + \left(\frac{\Gamma_e}{\delta x_{PE}} A_e\right)\phi_E + S_u \tag{12}$$

Os coeficientes da Equação 12 podem ser identificados algebricamente, conforme Equação 13.

$$a_P \phi_P = a_W \phi_W + a_E \phi_E + S_u \tag{13}$$

onde

$$a_W = \frac{\Gamma_w A_W}{\delta x_{WP}} \tag{14}$$

$$a_E = \frac{\Gamma_e A_E}{\delta x_{PE}} \tag{15}$$

$$a_P = a_W + a_E - S_P \quad (16)$$

A Equação 12 discretizada é montada para cada ponto nodal para a solução do problema. Para volumes de controle que são adjacentes aos contornos do domínio, as equações são modificadas para incorporar as condições de contorno. O ANSYS CFX utiliza uma fatoração LU incompleta para resolver o sistema de equações algébricas lineares e assim obter a solução do escoamento estudado. O mesmo método é utilizado com sucesso em diversas aplicações em CFD [17–19].

2.2.2.2. Modelos de Turbulência

Flutuações instantâneas de velocidade e grandezas escalares como temperatura, caracterizam o fluxo turbulento e devido a essas flutuações, a turbulência contribui significativamente no transporte de momento, calor e massa [20]. Devido a sua natureza aleatória, o fluxo turbulento impede uma definição do movimento das partículas de um fluido. Desta forma, a velocidade, como apresentada na Figura 6 é decomposta em um valor médio constante U com uma componente flutuante $u'(t)$, conforme Equação 17, chamada de decomposição de Reynolds [16].

Figura 6: Variação da velocidade ao longo do tempo em um escoamento turbulento [16].

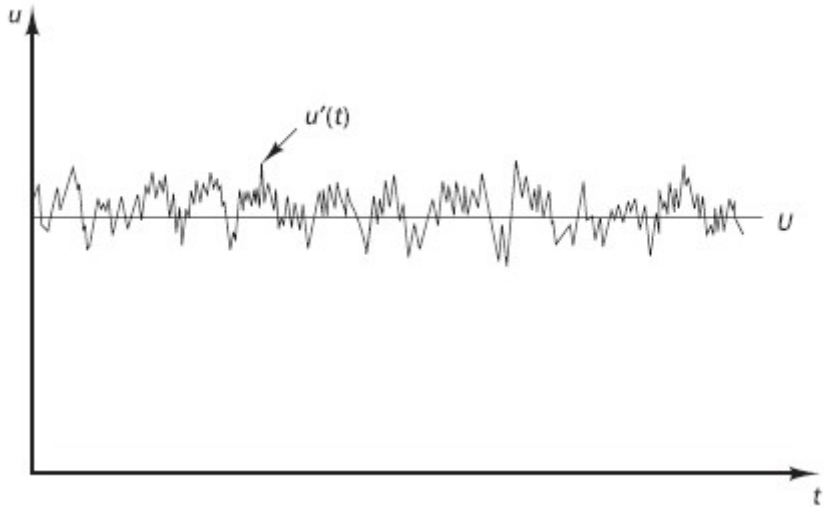

$$u(t) = U + u'(t) \tag{17}$$

Segundo Souza *et al.* [21], na maioria dos estudos de escoamento de fluidos ter conhecimento do comportamento médio do escoamento é suficiente. Entretanto, Reynolds [22], sugeriu que o escoamento instantâneo fosse separado em uma componente média e outra componente flutuante e inseridas nas equações das flutuações médias de Navier-Stokes, conforme Equações 18, 19 e 20. Esse conjunto de equações é chamado de Equações de Reynolds Average Navier-Stokes (RANS).

$$\frac{\partial(\rho u)}{\partial t} + div(\rho u\vec{u}) = -\frac{\partial p}{\partial x} + div(\mu\ grad\ u) + \left[-\frac{\partial\left(\rho\overline{u'^2}\right)}{\partial x} - \frac{\partial(\rho\overline{v'u'})}{\partial y} - \frac{\partial(\rho\overline{w'u'})}{\partial z}\right] + S_{Mx} \tag{18}$$

$$\frac{\partial(\rho v)}{\partial t} + div(\rho v\vec{u}) = -\frac{\partial p}{\partial y} + div(\mu\ grad\ v) + \left[-\frac{\partial(\rho\overline{u'v'})}{\partial x} - \frac{\partial\left(\rho\overline{v'^2}\right)}{\partial y} - \frac{\partial(\rho\overline{v'w'})}{\partial z}\right] + S_{My} \tag{19}$$

$$\frac{\partial(\rho w)}{\partial t} + div(\rho w\vec{u}) = -\frac{\partial p}{\partial z} + div(\mu\ grad\ w) + \left[-\frac{\partial(\rho\overline{u'w'})}{\partial x} - \frac{\partial(\rho\overline{v'w'})}{\partial y} - \frac{\partial\left(\rho\overline{w'^2}\right)}{\partial z}\right] + S_{Mz} \tag{20}$$

onde t é o tempo; ρ é densidade; p é a pressão; x, y, e z são as três direções cartesianas; u, v e w são as velocidades médias e u′, v′ e w′ são as flutuações das velocidades nas direções x, y, e z, respectivamente; $\vec{u}$ é o vetor de velocidade tridimensional; μ é a viscosidade do fluido; e S_{Mx}, S_{My} e S_{Mz} são os termos de origem do momento nas direções x, y, e z, respectivamente.

Da mesma forma que foi gerada a Equação 5, substituindo as velocidades u, v e w por uma variável genérica ϕ, uma forma conservativa para todas as equações RANS, incluindo, por exemplo, velocidade em uma dada direção pode ser escrita na forma da Equação 21, equação de transporte escalar.

$$\frac{\partial(\rho\phi)}{\partial t} + div(\rho\phi\vec{u}) = div(\Gamma\ grad\ \phi) + \left[-\frac{\partial(\rho\overline{u'\varphi'})}{\partial x} - \frac{\partial(\rho\overline{v'\varphi'})}{\partial y} - \frac{\partial(\rho\overline{w'\varphi'})}{\partial z}\right] + S_{\phi} \tag{21}$$

onde t é o tempo; ρ é densidade; $\vec{u}$ é o vetor de velocidade; Γ é o coeficiente de difusão; φ é uma variável escalar e S_ϕ é o termo fonte para a variável genérica.

O tratamento estatístico da turbulência por meio das equações supracitadas acrescenta termos desconhecidos que contêm o produto de quantidades flutuantes no tempo, agindo como esforços adicionais no fluido. Esses termos, chamados de tensores de Reynolds, composto por três tesões normais e três tensões de cisalhamento, não são fáceis de serem encontrados diretamente e, por conta disso, se tornam variáveis a serem resolvidas. Essas tensões são esforços turbulentos e precisam ser modelados por equações adicionais para o sistema de equações resultantes ser determinado.

Existe, atualmente, uma gama de modelos de turbulência desenvolvidos e aplicados em simulação numérica. Entretanto, não existe um modelo que seja o mais adequado para todos os tipos de escoamento. Desta forma, se faz necessário analisar as condições sensíveis ao escoamento a ser simulado e a partir disso, escolher o modelo que melhor descreva a turbulência desse escoamento.

Os trabalhos correlatos apresentados na sessão 2.3 deste documento encontram-se algumas aplicações de modelos de turbulência. Os trabalhos de Asgari B e Amani E [32], Pinilla JA, Asuaje M e Ratkovich N [35], Zhang H et al. [36] e Bede KM, Kalata W e Schick RJ [38] utilizaram o modelo k – ε. Já, Ishak et al. [34] e Delele et al. [37] utilizaram o modelo SST k – ω. Hariharan et al. [31] utilizaram os três modelos k – ε, k – ω e SST k – ω. No presente estudo foi utilizado o modelo de turbulência SST k – ω, por ser o modelo que melhor descreve a turbulência do escoamento estudado. Para um melhor entendimento da escolha desse modelo de turbulência, a seguir será feita uma breve explanação do y^+, variável de extrema importância em simulações de escoamentos turbulentos.

Na Figura 7 é ilustrada a localização do y^+ do escoamento característico em uma superfície plana e, de forma associativa, podemos identificar essa localização também em um escoamento interno, a exemplo de um tubo.

Figura 7: Localização do y+ em uma superfície plana [23].

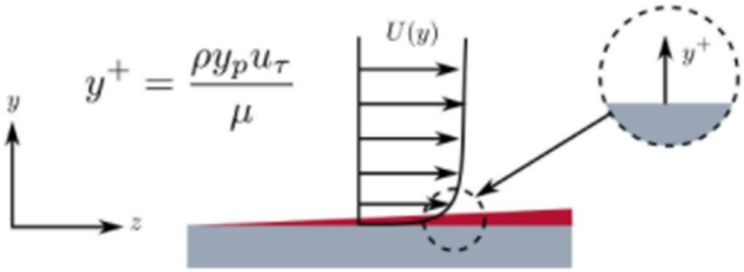

A Figura 8 apresenta o perfil de velocidade em região muito próxima a uma superfície sólida, onde é obtido o y^+, uma relação adimensional para a velocidade e distância normal à parede da superfície sólida. As três camadas ilustradas na Figura 8 fazem parte da lei de parede, sendo a primeira camada (subcamada viscosa) muito fina, com $y^+ = 5$ [24], região onde os efeitos viscosos são predominantes. A segunda camada (camada de transição) região onde tanto o efeito viscoso quanto o turbulento são importantes [21], com y^+ variando entre 5 e 30. Por fim, a terceira camada (camada logarítmica) região onde os efeitos de turbulência são mais influentes, com valores de y^+ acima de 30 [24].

Figura 8: Perfil de velocidade junto a uma superfície sólida [21].

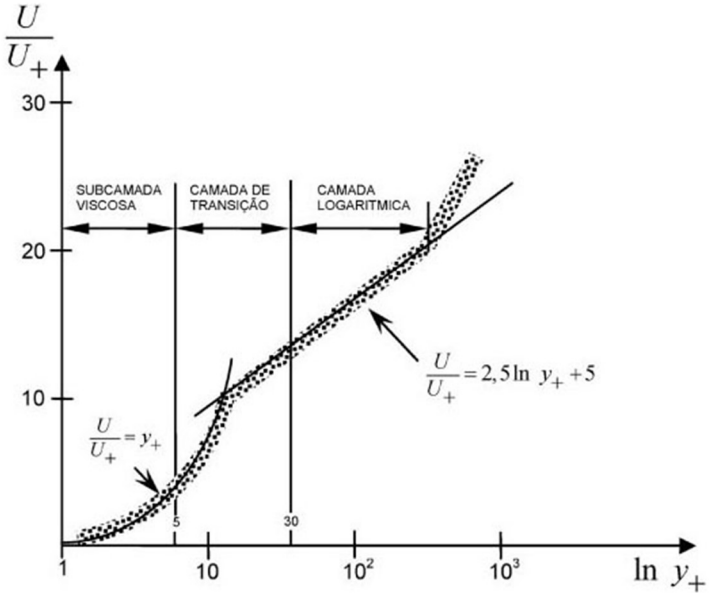

Em uma região próxima de uma superfície sólida, Prandtl observou características importantes referente ao escoamento do fluido sobre esta superfície e criou a hipótese de que o comprimento de mistura nesta região é proporcional à distância normal à parede, conforme Equação 22.

$$l_m = \kappa * y \tag{22}$$

onde y é a distância perpendicular à parede e κ é a constante de Von Kármán, igual a 0,4.

A subcamada viscosa da camada limite turbulenta é caracterizada pela condição de nenhum deslizamento, onde a velocidade do fluido é nula próximo à parede sólida. Desta forma, integrando a equação da tensão de cisalhamento na superfície, de acordo com a lei da viscosidade de Newton, temos que o perfil de velocidade é dado por:

$$u = \frac{\tau_0}{\rho v} y \tag{23}$$

onde τ_0 é a tensão de cisalhamento na superfície.

A velocidade de atrito é uma importante relação no estudo da camada limite e é expressa da seguinte forma:

$$u_* = \sqrt{\frac{\tau_0}{\rho}} \tag{24}$$

Dividindo a Equação 23 pela Equação 24, teremos a seguinte relação:

$$\frac{u}{u_*} = \frac{\sqrt{\tau_0 / \rho}}{v} y = y^+ \tag{25}$$

Obtendo assim, a equação para obtenção do valor de y^+.

Na subcamada turbulenta da camada limite é possível obter uma equação para o perfil da velocidade, que pode ser descrita da seguinte maneira:

$$\frac{u}{u_*} = \frac{1}{k} * \ln y^+ + C \tag{26}$$

onde k = 0,4 e C = 5. C é uma constante de integração cujo o valor foi obtido experimentalmente por Kundu & Cohen [24]. Substituindo os valores é possível notar que a Equação 26 é igual a equação da subcamada turbulenta presente na Figura 8.

A camada de transição é de difícil determinação, sendo assim, não possui uma equação que determine o comportamento da sua curva característica. Desta forma, dependendo do tratamento numérico dado à camada limite, os modelos de turbulência têm diferentes faixas adequadas para os valores de y^+. O modelo k – ε padrão, por exemplo, requer um valor y^+ na parede entre aproximadamente 30 a 300. De acordo com Salim e Cheah [20] para valores y^+ abaixo de 30, o modelo de turbulência k – ε não é adequado, sendo o modelo SST k – ω mais adequado, por se tratar de um modelo híbrido entre o k – ε e k – ω [25]. Na Equação 27 é representado o modelo matemático do y^+.

$$y^+ = \frac{y u_*}{\nu} \tag{27}$$

onde u_* é a velocidade de fricção, y é a distância absoluta da parede e v é a velocidade cinemática.

Como o modelo utilizado SST k – ω é uma combinação das melhores características dos modelos k – ε e k – ω, ou seja, se ajusta automaticamente a melhor alternativa para calcular a turbulência de acordo com a região do fluído a qual está sendo aplicado esse modelo de turbulência. A seguir serão apresentados os modelos de turbulência k – ε, k – ω e SST k – ω.

2.2.2.2.1. Modelo k – ε

Jones e Launder [26] desenvolveram o modelo k – ε baseado no conceito de viscosidade turbulenta (μ_t), no qual os termos de tensões de Reynolds são tidos como proporcionais a uma viscosidade cinemática, de forma análoga ao conceito original de viscosidade. Estes termos são contabilizados, conforme Equação 28.

$$-\rho\overline{u_a u_b} = \mu_t\left(\frac{\partial u_a}{\partial x_b} + \frac{\partial u_b}{\partial x_a}\right) - \frac{2}{3}\delta_{ab}\left(\rho k + \mu_t \sum_{c=1}^{3}\frac{\partial u_c}{\partial x_c}\right) \tag{28}$$

onde,

$$\delta_{ab} = \begin{cases} 0\ se\ a\ \neq b \\ \\ 1\ se\ a = b \end{cases} \tag{29}$$

O segundo termo do lado direto da Equação 20 é uma adequação para torná-la válida para o cálculo de tensões normais.

Nesse modelo, o k é considerado a energia cinética turbulenta e ε a dissipação turbulenta. A viscosidade turbulenta (μ_t) é dependente, no modelo em questão, destes dois parâmetros como mostra a Equação 30.

$$\mu_t = \rho C_\mu \frac{k^2}{\varepsilon} \tag{30}$$

onde C_μ é uma constante.

Os valores de k e ε são encontrados diretamente a partir das suas equações diferenciais 31 e 32.

$$\frac{\partial(\rho \mathrm{k})}{\partial t} + \mathrm{div}(\rho \mathrm{k}\vec{u}) = \mathrm{div}\left[\left(\nu + \frac{\mu_t}{\sigma_\mathrm{k}}\right)\mathrm{grad\ k}\right] + P_\mathrm{k} - \rho\varepsilon \tag{31}$$

$$\frac{\partial(\rho\varepsilon)}{\partial t} + \mathrm{div}(\rho\varepsilon\vec{u}) = \mathrm{div}\left[\left(\nu + \frac{\mu_t}{\sigma_\varepsilon}\right)\mathrm{grad}\ \varepsilon\right] + \frac{\varepsilon}{k}(C_{\varepsilon 1}P_\mathrm{k} - C_{\varepsilon 2}\rho\varepsilon) \tag{32}$$

onde $C_{\varepsilon 1}$, $C_{\varepsilon 2}$, σ_{k} e σ_{ε} são constantes do modelo de turbulência e P_{κ} é a produção de turbulência devido a forças viscosas. P_{κ} é modelado de acordo com a Equação 33.

$$P_{\mathrm{k}} = \sum_{a=1}^{3}\sum_{b=1}^{3}\sum_{C=1}^{3}\left[\mu_t\left(\frac{\partial u_a}{\partial x_b}+\frac{\partial u_b}{\partial x_a}\right)\frac{\partial u}{\partial x_b}-\frac{2}{3}\frac{\partial u_c}{\partial x_c}\left(3\mu_t\frac{\partial u_c}{\partial x_c}+\rho\mathrm{k}\right)\right] \tag{33}$$

As constantes do modelo proposto por Launder e Sharma [27] são apresentadas na Tabela 2.

Tabela 2: Constantes do modelo k – ε [27].

Constante	Valor
$C_{\varepsilon 1}$	1,44
$C_{\varepsilon 2}$	1,92
σ_k	1,0
σ_{ε}	1,3
C_{μ}	0,09

2.2.2.2.2. Modelo k – ω

Wilcox [28] desenvolveu o modelo k – ω também baseado no conceito de viscosidade turbulenta (μ_t), e suas tensões de Reynolds calculadas pelas Equações 18 a 20.

Nesse modelo, o k é considerado a energia cinética turbulenta e ω frequência turbulenta e sua viscosidade turbulenta é calculada através da Equação 34.

$$\mu_t = \rho\frac{k}{\omega} \tag{34}$$

Os valores de k e ω são encontrados diretamente a partir das suas equações diferenciais 35 e 36.

$$\frac{\partial(\rho k)}{\partial t} + \text{div}(\rho k \vec{u}) = \text{div}\left[\left(\nu + \frac{\mu_t}{\sigma_k}\right)\text{grad k}\right] + P_k - \beta' \rho k \omega \quad (35)$$

$$\frac{\partial(\rho \omega)}{\partial t} + \text{div}(\rho \omega \vec{u}) = \text{div}\left[\left(\nu + \frac{\mu_t}{\sigma_\omega}\right)\text{grad } \omega\right] + \alpha \frac{\omega}{k} P_k - \beta \rho \omega^2 \quad (36)$$

onde β', α, β, σ_k e σ_ω são constantes do modelo e P_k é a produção de turbulência devido a forças viscosas. P_k é modelado de forma semelhante ao modelo k – ε, através da Equação 33.

As constantes do modelo proposto por Wilcox [28] são apresentadas na Tabela 3.

Tabela 3: Constantes do modelo k – ω [28].

Constante	Valor
β'	$^{9}/_{100}$
α	$^{5}/_{9}$
β	$^{3}/_{40}$
σ_k	$^{1}/_{2}$
σ_ω	$^{1}/_{2}$

2.2.2.2.3. Modelo SST k – ω (Shear Stress Transport)

Menter [29] elaborou o modelo SST k – ω fazendo a união da modelagem k – ω para as regiões próximas às superfícies e k – ε para as regiões mais distantes da parede. Para esta combinação foi utilizado o modelo k – ω de Wilcox [28], conforme Equações 37 e 38, e realizada uma transformação do modelo k – ε em uma formulação k – ω, conforme Equações 39 e 40.

$$\frac{\partial(\rho k)}{\partial t} + \text{div}(\rho k \vec{u}) = \text{div}\left[\left(\nu + \frac{\mu_t}{\sigma_{k1}}\right)\text{grad k}\right] + P_k - \beta' \rho k \omega \quad (37)$$

$$\frac{\partial(\rho \omega)}{\partial t} + \text{div}(\rho \omega \vec{u}) = \text{div}\left[\left(\nu + \frac{\mu_t}{\sigma_{\omega 1}}\right)\text{grad } \omega\right] + \alpha_1 \frac{\omega}{k} P_k - \beta_1 \rho \omega^2 \quad (38)$$

$$\frac{\partial(\rho\omega)}{\partial t} + \mathrm{div}(\rho\omega\vec{u}) = \mathrm{div}\left[\left(\nu + \frac{\mu_t}{\sigma_{\omega 1}}\right)\mathrm{grad}\ \omega\right] + \alpha_1 \frac{\omega}{k} P_k - \beta_1 \rho\omega^2 \quad (39)$$

$$\frac{\partial(\rho\omega)}{\partial t} + \mathrm{div}(\rho\omega\vec{u}) = \mathrm{div}\left[\left(\nu + \frac{\mu_t}{\sigma_{\omega 2}}\right)\mathrm{grad}\ \omega\right] + 2\rho\frac{1}{\sigma_{\omega 2}\omega}\sum_{a=1}^{3}\left(\frac{\partial k}{\partial x_a}\frac{\partial \omega}{\partial x_a}\right) + \alpha_2 \frac{\omega}{k} P_k - \beta_2 \rho\omega^2 \quad (40)$$

As constantes do modelo proposto por Menter [29] são apresentadas na Tabela 4.

Tabela 4: Constantes do modelo SST k – ω [29].

Constante	Valor
β'	0,09
α_1	0,31
β_1	0,075
σ_{k1}	0,85
$\sigma_{\omega 1}$	0,5
α_2	0,44
β_2	0,0828
σ_{k2}	1
$\sigma_{\omega 2}$	0,856

O modelo k – ω é multiplicado por uma função de mistura F_1 o modelo k – ε transformado é multiplicado por $(1 - F_1)$, e os produtos são então somados nas Equações 41 e 42.

$$\frac{\partial(\rho k)}{\partial t} + \mathrm{div}(\rho k\vec{u}) = \mathrm{div}\left[\left(\nu + \frac{\mu_t}{\sigma_{k3}}\right)\mathrm{grad}\ \mathrm{k}\right] + P_k - \beta'\rho k\omega \quad (41)$$

$$\frac{\partial(\rho\omega)}{\partial t} + \mathrm{div}(\rho\omega\vec{u}) = \mathrm{div}\left[\left(\nu + \frac{\mu_t}{\sigma_{\omega 3}}\right)\mathrm{grad}\ \omega\right] + 2\rho\frac{1}{\sigma_{\omega 2}\omega}\sum_{a=1}^{3}\left(\frac{\partial k}{\partial x_a}\frac{\partial \omega}{\partial x_a}\right) + \alpha_3 \frac{\omega}{k} P_k - \beta_3 \rho\omega^2 \quad (42)$$

onde, β' e $\sigma_{\omega 2}$ são constantes que têm os mesmos valores indicados na Tabela 3. As constantes do modelo SST k – ω que possuem o índice "3" são encontrados por meio das constantes exibidas na Tabela 3 com o auxílio da Equação 43.

$$\phi_3 = F_1\phi_1 + (1 - F_1)\phi_2 \tag{43}$$

onde ϕ é uma constante, podendo ser qualquer uma das seguintes constantes: σ_k, σ_ω, α ou β.

A função de mistura F_1 presente na Equação 43 é definida pela Equação 44.

$$F_1 = \tanh(arg_1^4) \tag{44}$$

onde arg_1 é obtida pela Equação 45.

$$arg_1 = min\left[max\left(\frac{\sqrt{\kappa}}{\beta'\omega y_p}; \frac{500\upsilon}{y_p^2\omega}\right); \frac{4\rho\kappa}{CD_{\kappa\omega}\sigma_{\omega 2}y_p^2}\right] \tag{45}$$

Na Equação 45, y_p é a distância à parede mais próxima e o termo $CD_{\kappa\omega}$ é definido pela Equação 46.

$$CD_{\kappa\omega} = max\left(2\rho\frac{1}{\sigma_{\omega 2}}\sum_{a=1}^{3}\left(\frac{\partial\kappa}{\partial x_a}\frac{\partial\omega}{\partial x_a}\right); 1{,}0X10^{-10}\right) \tag{46}$$

No modelo SST k – ω apresentado por Menter [29] a modelagem da viscosidade turbulenta não é idêntica àquela proposta por Wilcox [28] no modelo k – ω. Para o modelo SST k – ω utiliza-se o conceito de viscosidade cinemática turbulenta υ_t, fornecida pela Equação 47.

$$\upsilon_t = {}^{\mu_t}/_{\rho} \tag{47}$$

A viscosidade cinemática turbulenta é então obtida pela Equação 48.

$$\upsilon_t = \frac{a_1 k}{max(a_1\omega; SF_2)} \tag{48}$$

onde S é a taxa de deformação e F_2 é dada pela Equação 49.

$$F_2 = \tanh(arg_2^2) \tag{49}$$

sendo arg_2 dado pela Equação 50.

$$arg_2 = \left[max\left(\frac{\sqrt{\kappa}}{\beta' \omega y_p}; \frac{500\upsilon}{y_p^2 \omega}\right)\right] \tag{50}$$

2.3. Trabalhos Correlatos

Com base em simulações CFD, Joshi [30] desenvolveu uma câmara para realização de testes RT-PCR em pacientes para detecção do novo coronavírus, onde o paciente é quem entra na câmara e após a coleta, é realizada a desinfecção da mesma por meio de aspersão de agente biocida, reduzindo, segundo o autor, o uso de EPIs pelos profissionais de saúde que realizam o teste. No entanto, não foi apresentada a metodologia utilizada nas simulações CFD como por exemplo, o método de discretização e modelo de turbulência. As propriedades do agente biocida utilizadas nas simulações foram as mesmas da água. Na Figura 9 são apresentadas imagens de simulação CFD da câmara.

Figura 9: Simulação CFD da câmara e posições de bicos de pulverização (a), após aspersão em tempos de 1, 3 e 12 segundos [30].

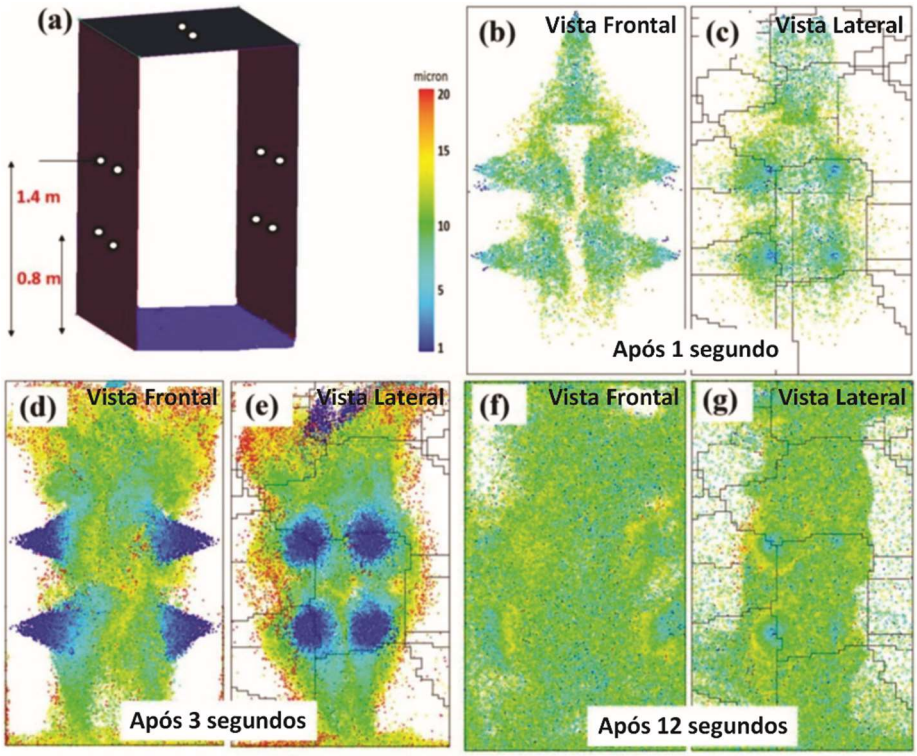

Hariharan et al. [31] realizaram ensaios experimentais e simulações CFD utilizando volumes finitos e aplicaram modelos de turbulência SST $k-\omega$, $k-\omega$ e $k-\varepsilon$ em um modelo de bico da Food and Drug Administration (FDA) com objetivo de ilustrar técnicas de validação de simulações CFD. Os resultados apresentaram que o modelo SST $k-\omega$ foi o que mais se aproximou dos resultados experimentais, conforme Figura 10.

Figura 10: Comparação de erro dos modelos de turbulência e experimental [31].

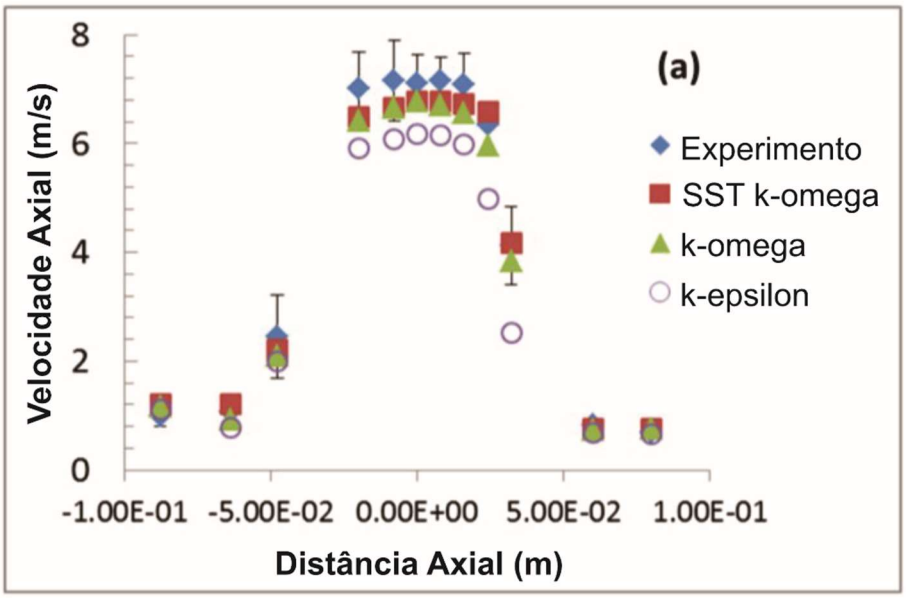

Asgari, B. e Amani, E. [32] desenvolveram um modelo computacional apropriado para avaliar a interação entre spray e parede utilizando volumes finitos com uma abordagem Euleriana para o meio contínuo (fase gasosa) e Lagrangeana para o meio disperso (gotas do spray) e modelo de turbulência $k-\varepsilon$. Eles também aplicaram coeficientes normal de restituição, para avaliar a parcela de gotas respingadas.

Fathinia, F., Khiadani, M., e Al-Abdeli Y.M. [33] realizaram investigações experimentais e matemáticas para avaliação do ângulo de pulverização e tamanhos de gotas de um sistema de dessalinização por evaporação flash. As medições de ângulo de pulverização e tamanhos de gotas foram realizadas por meio de capturas de imagens utilizando uma câmara de alta velocidade acoplada a um microscópio de longa distância, onde as imagens foram tratadas e em seguida calculados os ângulos de formação do spray e tamanhos de gotas. A Figura 11 apresenta uma imagem do ângulo formado pelo spray na saída do bico.

Figura 11: Medição de ângulo (α) do spray a partir da captura de imagem [33].

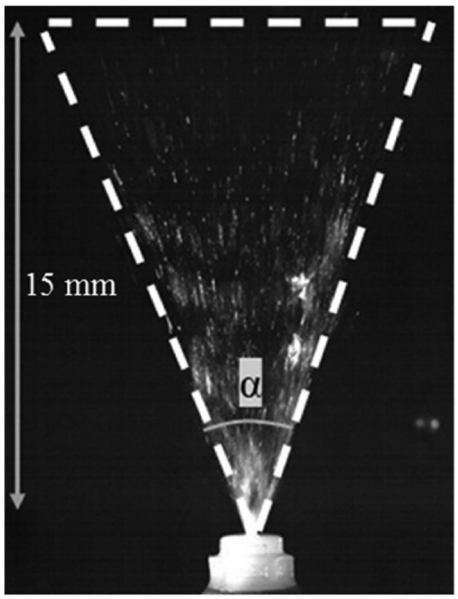

Ishak et al. [34] realizaram simulações CFD aplicando um modelo de fase discreta (DFM) para estudar o injetor de combustível processo de cavitação e a característica de macro spray de três tipos diferentes de formato de bico de spray com mistura de diesel e biocombustível híbrido para várias pressões de injeção e contrapressões. O escoamento multifásico foi descrito utilizando o modelo de mistura, que considerou que as fases de vapor e líquido foram misturadas uniformemente. Para uma interação de duas vias, a fase contínua foi calculada baseado no modelo Euleriano, enquanto as trajetórias das partículas foram calculadas com base no resultado de o fluxo contínuo. O modelo SST k – ω foi escolhido por ter vantagens para problemas de camada limite na fronteira, além de ser mais preciso e robusto em comparação com outros modelos de turbulência.

Pinilla, J.A., Asuaje, M. e Ratkovich, N. [35] realizaram simulações CFD para representar os fenômenos de resfriamento evaporativo usando o sistema de nebulização. Os modelos físicos da fase contínua (ar) e da fase dispersa (gotas de água) foram simulados de acordo com o modelo de Lagrange e aplicado o modelo de turbulência k – ε. Os resultados foram comparados com as mesmas variáveis retiradas dos dados experimentais do túnel de vento e considerados semelhantes no que diz respeito ao comportamento da temperatura e da umidade relativa, concluindo que os

resultados obtidos na simulação foram próximos aos reportados experimentalmente com diferenças de 3 a 6%.

Zhang H. et al. [36] realizaram simulações CFD para avaliar a influência do ângulo e velocidade de injeção de bicos nebulizadores na perda de carga do duto de entrada de uma turbina a gás. Baseada em um fluxo de duas fases, as simulações foram realizadas por uma abordagem Euleriana-Lagrageana, sendo o ar definido como fase contínua e a gota de água como fase dispersa. O modelo de turbulência aplicado foi o k – ε. Além disso, para se obter a distribuição do diâmetro das gotas, os pesquisadores aplicaram a função de distribuição de Rosin-Rammler.

Delele et al. [37] realizaram simulações CFD baseadas em um modelo de fluxo multifásico Euleriano-Lagrageano para avaliar o desempenho de um sistema de nebulização de fungicida em ambiente de armazenamento de frutas com variação de taxa de circulação de ar. Os erros relativos médios gerais das simulações em comparação aos valores medidos foram menores para o modelo de turbulência SST k – ω, sendo este utilizado no estudo. Além disso, as paredes foram consideradas como no-slip, desprezando a possibilidade de re-arrastamento e ressalto de partículas em contato com as paredes.

Bede, K.M., Kalata, W. e Schick, R.J. [38] realizaram ensaios experimentais e simulações CFD de um spray em múltiplos ângulos de injeção utilizando volume de fluido (VOF) com uma abordagem lagrangeana para rastreamento da partícula (gotas de água) e modelo de turbulência k – ε. Além disso, aplicaram a função de Rosin-Rammler para gerar a distribuição do tamanho de gotas do spray.

REFERÊNCIAS

1. D Bloomfield SF. Importance of disinfection as a means of prevention in our changing world hygiene and the home. GMS Krankenhhyg Interdiszip [Internet]. 2007 Sep 13;2(1):Doc25. Available from: http://www.ncbi.nlm.nih.gov/pubmed/20200686%0Ahttp://www.pubmedcentral.nih.gov/articlerender.fcgi?artid=PMC2831500

2. Communication from the Commission to the European Parliament and the Council. Action plan against the rising threats from antimicrobial resistance. Brussels: European Commission; 2011.

3. Gebel J, Exner M, French G, Chartier Y, Christiansen B, Gemein S, Goroncy-Bermes P, Hartemann P, Heudorf U, Kramer A, Maillard J-Y, Oltmanns P, Rotter M, Sonntag H-G. The role of surface disinfection in infection prevention. GMS Hyg Infect Control. 2013;8(1):Doc10.

4. Wickramatillake A, Kurukularatne C. SARS-CoV-2 human disinfection chambers: A critical analysis. Occup Med (Chic Ill). 2020;70(5):330–4.

5. Cadnum JL, Jencson AL, Livingston SH, Li DF, Redmond SN, Pearlmutter B, Wilson BM, Donskey CJ. Evaluation of an electrostatic spray disinfectant technology for rapid decontamination of portable equipment and large open areas in the era of SARS-CoV-2. Am J Infect Control. 2020 Aug 1;48(8):951–4.

6. Dellinger EP. Prevention of Hospital-Acquired Infections. Surg Infect (Larchmt) [Internet]. 2016 Aug;17(4):422–6. Available from: https://www.liebertpub.com/doi/10.1089/sur.2016.048

7. Silva DF, Toledo Neto JL, Machado MF, Bochnia JR, Garcez AS, Foggiato AA. Effect of photodynamic therapy potentiated by ultrasonic chamber on decontamination of acrylic and titanium surfaces. Photodiagnosis Photodyn Ther [Internet]. 2019 Sep;27(July):345–53. Available from: https://linkinghub.elsevier.com/retrieve/pii/S1572100019301462

8. Ishikawa S, Ueno S, Mitsui M, Matsumura Y, Hatsuoka T. Construction of Its Evaluation System in Originally Designed Test-Chamber System and Sporicidal Activity of Aerosolized Hypochlorite Solution to Bacillus subtilis Spores. Biocontrol Sci [Internet]. 2019 [cited 2020 Sep 25];24(1):57–65. Available from: https://www.jstage.jst.go.jp/article/bio/24/1/24_57/_article

9. World Health Organization. Water, sanitation, hygiene, and waste management for SARS-CoV-2, the virus that causes COVID-19. Interim guidance. 2020.

10. The Clorox Company. Clorox Professional Announces Clorox ® Total 360 TM System [Internet]. 2017 [cited 2020 Sep 12]. Available from:

https://s21.q4cdn.com/507168367/files/doc_news/Clorox-Professional-Announces-Clorox-Total-360-System.pdf

11. Weisstechnik. Microwave Disinfection Chambers [Internet]. Available from: https://www.weiss-technik.com/fileadmin/Redakteur/Mediathek/Broschueren/WeissTechnik/Waermetechnik/weisstechnik-Microwave-Disinfection-Chamber-EN.pdf

12. International Commission on non-ionizing radiation protection. UVC LAMPS and SARS-COV-2 [Internet]. Available from: https://www.icnirp.org/en/activities/news/news-article/sars-cov-2-and-uvc-lamps.html

13. Weber DJ, Kanamori H, Rutala WA. 'No touch' technologies for environmental decontamination. Curr Opin Infect Dis [Internet]. 2016 Aug 1 [cited 2020 Sep 25];29(4):424–31. Available from: http://journals.lww.com/00001432-201608000-00016

14. World Health Organization. Water, sanitation, hygiene, and waste management for SARS-CoV-2, the virus that causes COVID-19: Interim guidance. 29 July 2020. In: Genebra [Internet]. 2020 [cited 22 Sep 2020]. Available: https://www.who.int/publications/i/item/water-sanitation-hygiene-and-wastemanagement-for-the-covid-19-virus-interim-guidance

15. Kampf G. Potential role of inanimate surfaces for the spread of coronaviruses and their inactivation with disinfectant agents. Infect Prev Pract. 2020; 2: 100044. https://doi.org/10.1016/j.infpip.2020.100044

16. Versteeg HK, Malalasekera W. An Introduction to Computational Fluid Dynamics. 2. ed. London: Pearson Education Limited, 2007. 503 p.

17. Birken P et al. Preconditioner updates applied to CFD model problems. Applied Numerical Mathematics, 2008.

18. Kovenya V. et al. On some approaches to solve CFD problems. Computer & Fluids, 2001.

19. Sidlof P, Horacek J, RIDKY V. Parallel CFD simulation of flow in a 3D model of vibrating human vocal folds. Computer & Fluids, 2012.

20. Salim SM, Cheah SC. Wall y+ strategy for dealing with wall-bounded turbulent flows. Int. MultiConf. Eng. Comput. Sci. (IMECS). v. 2., p. 1-6, 2009.

21. Souza JFA et al. Uma revisão sobre a turbulência e sua modelagem. Revista Brasileira de Geofísica, [s.l.], v. 29, n. 1, p. 21-41, mar. 2011. FapUNIFESP (SciELO). http://dx.doi.org/10.1590/s0102-261x2011000100002.

22. Reynolds O. IV. On the dynamical theory of incompressible viscous fluids and the determination of the criterion. Philosophical Transactions Of The Royal Society Of London. (A.), [S.L.], v. 186, p. 123-164, 31 dez. 1895. The Royal Society. http://dx.doi.org/10.1098/rsta.1895.0004.

23. Incropera FP et al. Fundamentos de Transferência de Calor e de Massa. Rio de Janeiro: Ltc, 2014.

24. Kundu PK, Cohen IM. Fluid Mechanics. 2. ed. San Diego: Academic Press, 2002. 730 p.

25. Menter FR. Review of the shear-stress transport turbulence model experience from an industrial perspective. International Journal Of Computational Fluid Dynamics. 2009 Apr;23(4):305-316.http://dx.doi.org/10.1080/10618560902773387.71.

26. Jones WP, Launder BE. The Prediction of Laminarization with a two-equation Model of Turbulence. International Journal of Heat and Mass Transfer, 1972.

27. Launder BE, Sharma BI. Application of the energy-dissipation model of turbulence to the calculation of flow near a spinning disc. Letters In Heat And Mass Transfer. 1974 Nov;1(2):131-137.http://dx.doi.org/10.1016/0094-4548(74)90150-7.

28. Wilcox DC. Reassessment of the scale-determining equation for advanced turbulence models. Aiaa Journal, [s.l.], v. 26, n. 11, p. 1299-1310, nov. 1988. American Institute of Aeronautics and Astronautics (AIAA). http://dx.doi.org/10.2514/3.10041.

29. Menter FR. "Two-Equation Eddy-Viscosity Turbulence Models for Engineering Applications," AIAA Journal, Vol. 32, No. 8, August 1994, pp. 1598-1605.

30. Joshi JR. COVSACK: an innovative portable isolated and safe COVID-19 sample collection kiosk with automatic disinfection. Trans Indian Natl. Acad. Eng. 2020 Jul;5:269–275. https://doi.org/10.1007/s41403-020-00139-1.

31. Hariharan P, D'Souza GA, Horner M, Morrison TM, Malinauskas RA, Myers MR (2017) Use of the FDA nozzle model to illustrate validation techniques in computational fluid dynamics (CFD) simulations. PLoS ONE 12(6): e0178749. https://doi.org/10.1371/journal.pone.0178749.

32. Asgari B, Amani E. An improved spray-wall interaction model for Eulerian-Lagrangian simulation of liquid sprays. International Journal Of Multiphase Flow. 2021 Jan;134:103487.http://dx.doi.org/10.1016/j.ijmultiphaseflow.2020.103487.

33. Fathinia F, Khiadani M, Al-abdeli YM. Experimental and mathematical investigations of spray angle and droplet sizes of a flash evaporation desalination system. Powder Technology. 2019 Oct;355:542-551. http://dx.doi.org/10.1016/j.powtec.2019.07.081.

34. Ishak MHH, Ismail F, Mat SC, Abdullah MZ, Aziz M A; Idroas M Y. Numerical Analysis of Nozzle Flow and Spray Characteristics from Different Nozzles Using Diesel and Biofuel Blends. Energies. 2019 Jan;12(2):281. http://dx.doi.org/10.3390/en12020281.

35. Pinilla JA, Asuaje M, Ratkovich N. Study of a fogging system using a computational fluid dynamics simulation. Applied Thermal Engineering. 2015 Mar;96:228-239.http://dx.doi.org/10.1016/j.applthermaleng.2015.10.117.

36. Zhang H, Luo M, Pan X, Zheng Q. Numerical analysis of gas turbine inlet fogging nozzle manifold resistance. Proceedings Of The Institution Of Mechanical Engineers, Part A: Journal of Power and Energy. 2015 Nov;230(1):63-75. http://dx.doi.org/10.1177/0957650915616279.

37. Delele MA, Vorstermans B, Creemers P, Tsige AA, Tijskens E, Schenk A, Opara UL, Nicolai BM, Verboven P. Investigating the performance of thermonebulisation fungicide fogging system for loaded fruit storage room using CFD model. Journal of Food Rngineering. 2012 Mar;109(1):87-97. https://doi.org/10.1016/j.jfoodeng.2011.09.030.

38. Bade K, Kalata W, Schick R. Experimental and Computational Study of a Spray at Multiple Injection Angles. ILASS Americas, 22nd Annual Conference on Liquid Atomization and Spray Systems. 2021 May.

3. ARTIGO I

Potential application of novel technology developed for instant decontamination of personal protective equipment before the doffing step

Artigo publicado em **PloS ONE** 16(6): e0250854, 2021.

Luís Alberto Breda Mascarenhas[1]; Bruna. Aparecida Souza Machado[1,2*]; Leticia de Alencar Pereira Rodrigues[1]; Katharine Valéria Saraiva Hodel[1]; Alex Álisson Bandeira Santos[2]; Paulo Roberto Freitas Neves[2]; Leone Peter Correia da Silva Andrade[1]; Milena Botelho Soares[1,3]; Jailson Bittencourt de Andrade[1] e Roberto Badaró[1]

[1]SENAI CIMATEC, SENAI Institute of Innovation (ISI) in Health Advanced Systems (CIMATEC ISI SAS), University Center SENAI/CIMATEC, Salvador, Bahia, Brazil
[2]SENAI CIMATEC, National Service of Industrial Learning – SENAI, Computational Modeling and Industrial Technology, University Center SENAI/CIMATEC, Salvador, Bahia, Brazil
[3]Gonçalo Moniz Institute, Oswaldo Cruz Foundation (IGM-FIOCRUZ/BA), Salvador 40296-710, Bahia, Brazil

DOI: 10.1371/journal.pone.0250854

Neste artigo foi avaliado, por meio de ensaios experimentais, a eficácia de uma câmara de desinfecção desenvolvida para descontaminação de superfícies de EPIs. Hipoclorito de sódio 0,25% foi utilizado como agente biocida e os EPIs, contaminados com microrganismos vivos foram expostos ao agente biocida em dois tempos de exposição. Os resultados mostraram que a tecnologia desenvolvida pode ser uma alternativa para controle da biocarga evitando a contaminação de diversos microrganismos, incluindo o SARS-CoV-2.

Por ser um trabalho interdisciplinar, o artigo contou com o apoio de algumas áreas do SENAI CIMATEC, sendo: Área de Eficiência Energética, contribuiu para o projeto e desenvolvimento da câmara de desinfecção, metodologia e realização de ensaios experimentais. Instituto SENAI de Inovação em Sistemas Avançados em Saúde, contribuiu com a metodologia, ensaios experimentais e avaliação da eficácia da tecnologia na inativação de microrganismos vivos. No final do artigo são apresentadas as contribuições da cada um dos autores no desenvolvimento do trabalho.

PLOS ONE

RESEARCH ARTICLE

Potential application of novel technology developed for instant decontamination of personal protective equipment before the doffing step

Luís Alberto Brêda Mascarenhas[1☯], Bruna Aparecida Souza Machado[1,2☯*], Leticia de Alencar Pereira Rodrigues[1‡], Katharine Valéria Saraiva Hodel[1‡], Alex Álisson Bandeira Santos[2‡], Paulo Roberto Freitas Neves[2‡], Leone Peter Correia da Silva Andrade[1‡], Milena Botelho Soares[1,3‡], Jailson Bittencourt de Andrade[1‡], Roberto Badaró[1‡]

1 SENAI CIMATEC, SENAI Institute of Innovation (ISI) in Health Advanced Systems (CIMATEC ISI SAS), University Center SENAI/CIMATEC, Salvador, Bahia, Brazil, **2** SENAI CIMATEC, National Service of Industrial Learning–SENAI, Computational Modeling and Industrial Technology, University Center SENAI/CIMATEC, Salvador, Bahia, Brazil, **3** Gonçalo Moniz Institute, Oswaldo Cruz Foundation (IGM-FIOCRUZ/BA), Salvador, Bahia, Brazil

☯ These authors contributed equally to this work.
‡ LAPR, KVSH, AÁBS, PRFN, LPCSA, MBS, JBA and RB also contributed equally to this work.
* brunam@fieb.org.br, brunamachado17@hotmail.com

Citation: Brêda Mascarenhas LA, Machado BAS, Rodrigues LdAP, Saraiva Hodel KV, Bandeira Santos AÁ, Freitas Neves PR, et al. (2021) Potential application of novel technology developed for instant decontamination of personal protective equipment before the doffing step. PLoS ONE 16(6): e0250854. https://doi.org/10.1371/journal.pone.0250854

Editor: Amitava Mukherjee, VIT University, INDIA

Received: September 27, 2020

Accepted: February 2, 2021

Published: June 4, 2021

Data Availability Statement: All relevant data are within the paper and its Supporting Information files.

Funding: The author(s) received no specific funding for this work.

Competing interests: The authors have declared that no competing interests exist.

Abstract

The use of personal protective equipment (PPE) has been considered the most effective way to avoid the contamination of healthcare workers by different microorganisms, including SARS-CoV-2. A spray disinfection technology (chamber) was developed, and its efficacy in instant decontamination of previously contaminated surfaces was evaluated in two exposure times. Seven test microorganisms were prepared and inoculated on the surface of seven types of PPE (respirator mask, face shield, shoe, glove, cap, safety glasses and lab coat). The tests were performed on previously contaminated PPE using a manikin with a motion device for exposure to the chamber with biocidal agent (sodium hypochlorite) for 10 and 30s. In 96.93% of the experimental conditions analyzed, the percentage reduction was >99% (the number of viable cells found on the surface ranged from $4.3x10^6$ to <10 CFU/mL). The samples of *E. faecalis* collected from the glove showed the lowest percentages reduction, with 86.000 and 86.500% for exposure times of 10 and 30 s, respectively. The $\log_{10}$ reduction values varied between 0.85 $\log_{10}$ (*E. faecalis* at 30 s in glove surface) and 9.69 $\log_{10}$ (*E. coli* at 10 and 30 s in lab coat surface). In general, *E. coli*, *S. aureus*, *C. freundii*, *P. mirabilis*, *C. albicans* and *C. parapsilosis* showed susceptibility to the biocidal agent under the tested conditions, with >99% reduction after 10 and 30s, while *E. faecalis* and *P. aeruginosa* showed a lower susceptibility. The 30s exposure time was more effective for the inactivation of the tested microorganisms. The results show that the spray disinfection technology has the potential for instant decontamination of PPE, which can contribute to an additional barrier for infection control of healthcare workers in the hospital environment.

Introduction

Contaminated surfaces are a potential source for the spread of many bacterial and fungal pathogens [1]. These microorganisms can be considered important vectors for the dissemination of diseases and, consequently, the increase in mortality and morbidity rates, causing overload of the health system worldwide [2]. There is currently growing concern that the environment may be an underestimated source for the spread of emerging viruses, including of the influenza virus [3], Ebola virus [4], and coronaviruses, especially the severe acute respiratory syndrome named SARS-CoV-2 [5]. SARS-CoV-2 is the causative agent of novel coronavirus 2019 disease (COVID-19) which was isolated and identified for the first time in humans in the city of Wuhan, Hubei Province, China [6]. Based on evidence of an increasing incidence of infections [7] and the possibility of transmission by asymptomatic carriers [8], it was demonstrated that SARS-CoV-2 can be effectively transmitted between humans through droplets (aerosols) or direct contact with contaminated surfaces, which facilitated its rapid spread worldwide [9, 10].

Healthcare workers (HCWs) are one of the most vulnerable populations to microbial contamination, mainly because they work in close physical contact with patients [11]. This vulnerability was demonstrated at times of emergency in health systems, such as during the outbreak caused by SARS-CoV [12], Ebola virus [13] and currently with SARS-CoV-2 [14], where a high rate of infection among HCWs has been reported. The high prevalence of COVID-19 among HCWs is mainly associated with the execution of the procedures involved in airway management for oxygen supplementation of many patients with severe COVID-19 pneumonia presenting with pronounced arterial hypoxemia (major generators of aerosol) [12, 15], which increases the viral load in which these professionals are in contact [16, 17]. The risk of viral transmission to HCWs has been a concern since the beginning of the outbreak in China, where more than 3,300 HCWs were infected, with a mortality rate of 1.1% [18]. In Europe, approximately 20% of HCWs were infected by SARS-CoV-2 in Italy and 26% in Spain, the two epicenters of the disease in the European continent between March and April [19, 20]. In Brazil, currently considered the epicenter of the disease in Latin America [21], data from the Ministry of Health indicate that at least 257,156 HCWs were infected by SARS-CoV-2 by August of this year [22].

The use of personal protective equipment (PPE) by HCWs has been considered the most effective way to avoid contamination by different microorganisms of high epidemiological concern [23–25], including SARS-CoV-2 [26], as they have the ability to act as a barrier to pathogens [27]. Studies have shown that the use of PPE and actions to decontaminate their surfaces are crucial to reduce the infection rate among HCWs in direct contact with patients diagnosed with COVID-19 and other contagious diseases [23, 28]. The step of PPE removal (doffing) by HCWs can be thus considered critical since there may be contact between the contaminated surface of the PPE and the HCWs, leading to an increased chance of self-contamination through the mucous membranes of the nose, eyes or mouth [29]. Therefore, this step should be performed following well-established biosafety protocols [30], It has been demonstrated that doffing PPE is among others an important risk factor associated with HCWs contamination with SARS-CoV-2 [31].

Several devices with different technologies have been developed for the inactivation or reduction of bioburden on surfaces and environments [1], and the use of such devices has gained popularity for presenting a response to the global demand created for the control of possible environmental surfaces contamination [32]. Examples include devices with ultraviolet-C (UV-C) or xenon UV light for disinfection of hospital environments [33, 34], portable equipment with a disinfectant spraying system [35] or hospital air disinfection systems [36]

and disinfection chambers [37]. Faced with increased production and demand, health regulatory agencies recommend that studies be presented to prove the performance of these devices in the face of decontamination effectiveness [38, 39]. Although there are few studies demonstrating the efficacy of disinfection chambers [40], their use becomes interesting for the decontamination of surfaces, including personal protective closes and equipment (PPE), since it is not mandatory that the contaminated material undergoes to manual cleaning mainly at the moment before the doffing step for previous elimination of the microorganisms [37]. Thus, disinfection chambers can be a practical alternative for bioburden control in environments with a high rate of pathogenic microorganisms, such as hospitals. In addition, the disinfection chambers can help mitigate the possibility of an accident self-contamination of the HCWs during the processing of hand manipulation of the disposable PPEs.

Different disinfecting agents have been studied and suggested to act in these devices as biocidal agents against different pathogens of hospital importance (such SARS-CoV-2, multidrug-resistant bacteria and fungi). Examples include physical agents such as UV light [41] and chemical agents such as alcoholic solutions [5, 42], quaternary ammonium compounds [43, 44], ozone gas [45] and sodium hypochlorite [46]. Sodium hypochlorite is one of the most well-known and used biocidal agents worldwide due to its broad-spectrum microbicidal properties [47]. Compared with other chlorine-containing biocides, the use of sodium hypochlorite is characterized by a relatively lower toxicity when in contact with mucous membranes, the equipment required for its synthesis are simpler, its handling is safer, and its operation and preparation costs are lower, which makes its use feasible in hospitals [48]. In addition, the use of sodium hypochlorite is recommended by the World Health Organization (WHO) for the disinfection of environmental surfaces related to health care in the context of COVID-19, in concentrations between 0.1 and 0.5% (1000 and 5000 ppm, respectively) [49].

Despite being a promising alternative, especially considering the current situation, there are still few reports in the literature on the efficacy of disinfection chambers and/or devices using sodium hypochlorite as a biocidal agent for reducing or inactivating the burden of different pathogens on contaminated surfaces, more specifically for PPE, and on its potential use in emergency and public health situations. [38, 50, 51]. The use of disinfection chambers in controlled environments, such as hospitals and health units, could help to reduce the risk of self-contamination by health workers during the doffing step, since the instantaneously dispersed solution could significantly reduce the pathogens present on surfaces and contribute to greater safety of these HCWs self-contamination. Nevertheless, this approach has not yet been reported by any earlier study.

Through the use of the disinfection chamber it is possible to decontaminate the surfaces of all PPEs used in clinical practice at the same time, making the doffing step safer for the HCWs. This can be considered an advantage over the PPE disinfection technologies mentioned in the literature [52–54], since the proposed decontamination processes do not reduce the risk of self-contamination. Indeed, the objective of this study was to develop a disinfection chamber for instantaneous dispersion of a biocidal solution (0.25% sodium hypochlorite) and to determine its efficacy on previously contaminated surfaces at different exposure times, aiming at its possible application as an additional barrier against pathogens, such as SARS-CoV-2, to protect HCWs during the withdraw procedure prior PPE disposal.

Materials and methods

Fig 1 shows the general scheme of the method applied in this study to evaluate the efficacy of the chamber for instant disinfection of the surfaces of seven PPE previously contaminated with different microorganisms and subjected to different exposure times to the biocidal agent

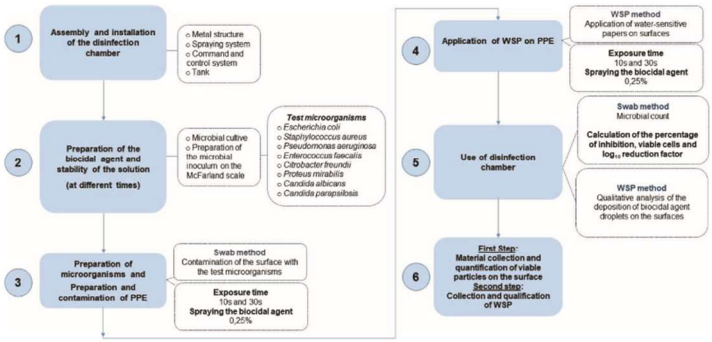

Fig 1. Schematic illustrating the method used in this study to evaluate the spray disinfection technology for instant decontamination of personal protective equipment.

https://doi.org/10.1371/journal.pone.0250854.g001

(0.25% sodium hypochlorite). To evaluate the efficacy of the disinfection process, tests were performed in two distinct steps with quantitative and qualitative analyses using a manikin that moved through a linear and rotary motion system to simulate the passage of an individual in a hospital environment (before the doffing step), an environment well known for presenting a high burden of infectious agents [55].

Development and installation of the disinfection chamber

The chamber consisted of a modular framework constructed of aluminum and carbon steel, with dimensions of 240 x 150 x 250 cm (height x depth x width), with an open entrance and exit. The design of the disinfection chamber allows the framework to be easily transported, installed and uninstalled. The nebulization system for the chamber comprised six nebulizer nozzles (Senninger, USA) installed on the inner side and top of the chamber to promote a better homogeneity in the spraying of the biocide agent. In addition, a water filter, a submerged pump and a 1-m^3 storage tank (1000 L capacity) with lid, with flow rate of 10 L/h were used to complete the system. The command and control system was installed by means of an electrical panel with voltage of 220 V, was responsible for the activation and operation of the entire system and contained a sensor for the activation of the nebulizers.

Biocidal agent: Preparation and stability analysis

The biocidal agent (bleach) was prepared at a concentration of 0.25% [49, 56] by diluting an initial solution with 2.38% active chlorine [57]. A total volume of 1,000 L was prepared directly in the storage tank of the chamber for the experiments. All experiments to evaluate the disinfection potential of PPE were performed during the first three days after preparation of the biocidal agent (bleach). The stability of the biocidal agent (0.25% sodium hypochlorite) was evaluated on days 0, 3, 6, 9, 13 and 20 by determining the percentage of active chlorine present in the solution and through pH analysis. The use of the biocide agent in the concentration of 0.25% was based on the WHO recommendation for the disinfection of environmental surfaces, which ranges from 0.1 to 0.5% [49]. Thus, an intermediate concentration was chosen. The amount of active chlorine was evaluated by iodometric titration [58], and the pH was determined through the hydrogen ionic activity using a standard electrode (pH meter, Mettler-Toledo). The analyses were performed in triplicates.

Experimental standard strains

The standard reference strains used in this study were *Escherichia coli* (ATCC 8739), *Staphylococcus aureus* (ATCC 6538), *Pseudomonas aeruginosa* (ATCC 27853), *Enterococcus faecalis* (ATCC 29212), *Citrobacter freundii* (ATCC 43864), *Proteus mirabilis* (ATCC 29906), *Candida albicans* (ATCC 18804) and *Candida parapsilosis* (ATCC 22019), which were obtained from Microbiologics (St. Cloud, Minnesota) or from the Culture Collection of the Institute of Health Sciences, Federal University of Bahia (Universidade Federal da Bahia–UFBA), located in Salvador, Brazil. The selection of test strains was based on studies of microorganisms commonly causing nosocomial infections, as well as on the recommendations of regulatory agencies for evaluating the efficacy of chemical disinfectants [57, 59–65]. The suspensions of the test microorganisms were prepared by transferring cells from the pure culture to plates containing 15–20 mL of plate count agar: agar (9 g/L); dextrose (1 g/L); tryptone (5.0 g/L) and yeast extract (2.5 g/L). To evaluate the disinfection profile in the chamber against the test microorganisms, the inocula were prepared by suspending 1–5 colonies in 5 mL of 0.85% saline solution and the turbidity was adjusted to McFarland No. 0.5 tube [66].

Preparation of study surfaces (PPE)

The PPE items used to evaluate the effectiveness of the disinfection chamber were selected according to the recommendations for prevention and control of the spread of SARS-CoV-2 and other infectious agents transmitted mainly by aerosols in health services (Table 1) [24, 67, 68]. To ensure the sterility of the surface of the selected items before contamination with the standard strains, the items were exposed to UV light for 40 minutes using a laminar flow (model LA2000T, LOGEN) after being sanitized with 70% ethanol [69]. Surface samples from each item were collected using sterile swabs, and their contents were seeded in nutrient agar (37˚C for 24 hours) to confirm sterility.

Assay for evaluation and distribution of the biocidal agent for spray disinfection during exposure in the chamber

The assays for evaluating the disinfection potential of the biocidal agent in the chamber developed in this study were based on the method used to monitor viable particles on surfaces [70, 71] and qualitative analysis of the biocidal agent distribution on the surfaces [72]. The disinfection process was performed by spraying the biocidal agent (0.25% sodium hypochlorite) in the chamber using a suitably dressed manikin with a motion system that allowed the manikin to pass through the chamber automatically and to perform a 360˚ turn, for 10 and 30 s of exposure. The manikin was chosen so that there would be a simulation closer to what would be the use of the disinfection chamber by healthcare workers in nosocomial environment. In the first

Table 1. Items used to evaluate the efficacy of instantaneous spraying of biocidal agent (0.25% sodium hypochlorite) in a disinfection chamber against the test microorganisms.

Selected item	Brand	Composition	Surface type
Respirator face mask	Air Safety	Polypropylene	Porous
Professional shoe	Soft Works	Ethylene vinyl acetate	Nonporous
Procedure glove	Supermax	Nitrile (nitrile)	Porous
Disposable Cap	Descarpack	Polypropylene	Porous
Face shield	CIMATEC	Polycarbonate	Nonporous
Safety glasses	Carbography	Polycarbonate	Nonporous
Disposable lab coat (apron)	Jarc Smart Products	Polypropylene and Polyethylene	Porous

https://doi.org/10.1371/journal.pone.0250854.t001

step, the surfaces were contaminated using a sterile swab immersed in the test tube containing the test microorganism.

Previously demarcated areas of 30 cm^2 [70] were used for contamination, with the right side used for the control (without exposure to the biocidal agent by spraying, in other words, these surfaces were sampled before the manikin (and PPE) was decontaminated) and the left side used for each test microorganism (Fig 2). The surface of the contaminated item was sampled with a swab immersed in 10 mL of buffered peptone water (Swab-Samplers - 3M, USA), and its content was used to analyze the number of viable particles on the surface for the control and after exposure to the disinfection chamber. For the control test, swabbing for microorganism collection was performed immediately after contamination; for the exposure tests to the biocidal agent, after 10 and 30 s. The control surfaces of each PPE analyzed were associated with both exposure experiments (10 and 30 s exposure). The antimicrobial action of sodium hypochlorite was neutralized by sodium thiosulphate [73, 74]. Sterile PPE items were used for each experiment, with a new item used for each microorganism or exposure time. In the second step, water-sensitive papers (WSP) (76x26 mm and 19.76 cm^2 area; Syngenta) were labeled from 1 to 6 and applied to the left side of the manikin (Fig 2) for exposure to the biocidal agent using the same exposure times and contamination sites of the first experiment. After each experiment, the papers were immediately stored in a desiccator with silica gel, and then images were recorded for qualitative analysis (observation of the paper color profile) of the deposition of biocidal agent on the surfaces of the PPE items.

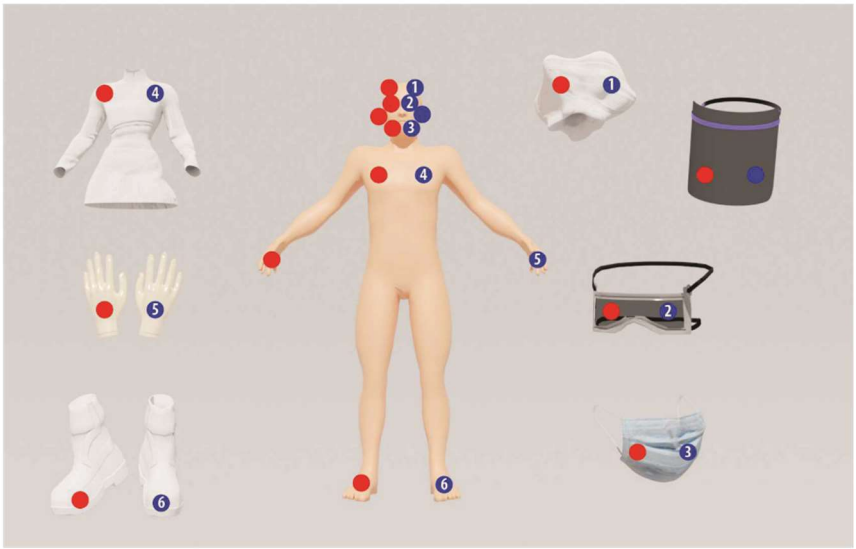

Fig 2. Demarcated areas for contamination by the test microorganisms for evaluation of the potential of instantaneous disinfection by the spray biocidal agent (0.25% sodium hypochlorite). The red circles represent the inoculation area (30 cm^2) used as control (right side), the blue circles represent the inoculation area (30 cm^2) used as test (left side), and the numbers in the blue circles represent the positions of the water-sensitive papers for each experiment: (1) cap; (2) safety glasses; (3) respirator face mask; (4) lab coat; (5) glove; and (6) shoe. For the control, the surface of the items was swabbed for microorganism collection immediately after surface contamination, while for the tests, the surfaces were swabbed after predetermined exposure times to the biocidal agent.

https://doi.org/10.1371/journal.pone.0250854.g002

Monitoring of viable particles on the surface

Viable microorganisms in the swabbed samples were determined using a nutrient agar culture method specific for each type of microorganism, which were quantified from their growth in the plate [75]. The tests were performed immediately after the swabbed samples were collected. The samples were vigorously shaken to extract the microorganisms from the swab and release them into the saline solution so that they could be serially diluted (10^{-1} to 10^{-8}). The dilutions were inoculated into the specific culture media and incubated according to the type of method. For *E. coli*, *P. mirabilis* and *C. freundii*, the VRBA count method was used; for *P. aeruginosa*, *S. aureus*, *C. albicans* and *C. parapsilosis*, the count of the total number of mesophilic microorganisms; and *E. faecalis* were counted by the EPA (US Environmental Protection Agency) method [70, 76, 77]. After quantification of the colonies under an optical microscope (Nikon Instruments), the results were expressed as $\log_{10}$ CFU/mL and CFU/cm^2. The number of CFUs was determined after incubation, and the number of CFUs per milliliter was calculated. The logarithmic scale ($\log_{10}$) reduction factor was calculated using the formula RF = $\log_{10}$ (A) —$\log_{10}$ (B) (where A is the number of colonies recovered from the unexposed (control) surfaces and B is the number of colonies recovered from the exposed (test) surfaces) [56, 78]. The decimal percentage reduction in CFU/mL was calculated using the formula %R = [(A—B)/A] * 100 [79].

Statistical analysis

Statistical analysis was performed using GraphPad Prism 8 (San Diego, CA, USA), where analysis of variance and Student's t-test were used to compare the means of the two groups (10 and 30 s), according to each test condition (microorganism x PPE item), with significance level of $p < 0.05$. Principal component analysis (PCA) was performed using PAST version 3.26 (Oslo, Norway) with the means of the logarithmic reductions of each test condition to obtain the correlation between the analyzed variables (PPE–cap, safety glasses, respirator face mask, lab coat, glove, shoe and face shield–or surface type).

Results

Table 2 shows the results for the number of viable cells (CFU/mL and CFU/cm^2), the logarithmic reduction factor ($\log_{10}$) of each assay compared to the respective control (without exposure to the biocidal agent), and the percentage reduction (%) after exposure to the biocidal agent in the disinfection chamber for 10 and 30 s for each test microorganism and for each individual PPE item evaluated in this study. Fig 3 shows the graphs of the logarithmic reduction ($\log_{10}$) of each test microorganism per individual PPE item.

In total, 147 experimental conditions were studied, considering the two exposure times for each test microorganism (n = 98) and control (n = 49), as well as for the seven different types of PPE evaluated. In general, there was a significant reduction in the investigated microorganisms after exposure of the previously contaminated items in the disinfection chamber, regardless of the item, which demonstrated the efficacy of the biocidal agent spraying system for instantaneous disinfection of PPE for some of the microorganisms evaluated. In addition, the results showed that at 10 and 30 s, there was only a significant difference in the microbial load reduction factor during exposure of the biocidal agent to the microorganisms *E. faecalis* and *P. aeruginosa* ($p > 0.05$). In this case, the exposure time of 30 s was more efficient for the inactivation of the studied microorganisms in terms of $\log_{10}$ and percentage reduction for all studied PPE (Table 2 and Fig 3).

A percentage reduction of >99% was determined for 96.93% (n = 95) of the tested conditions when compared to the control, while a percentage reduction of between 86.00–99% was

Table 2. Result of the number of viable cells in CFU/mL and their equivalent number in (CFU/cm^{2}), log$_{10}$ reduction factor (mean ± standard deviation) and percentage reduction for the microorganisms studied at 10 and 30 s of exposure to the biocidal agent in the disinfection chamber (results obtained from the comparative analysis with the control without exposure to the biocidal agent).

Test microorganisms	Exposure conditions	Personal Protection Equipment													
		Cap		Safety glasses		Respirator face mask		Lab coat		Glove		Shoe		Face shield	
		Log$_{10}$ and (% reduction)	Number of viable cells in CFU/ mL and (CFU/cm^{2})	Log$_{10}$ and (% reduction)	Number of viable cells in CFU/ mL and (CFU/cm^{2})	Log$_{10}$ and (% reduction)	Number of viable cells in CFU/ mL and (CFU/cm^{2})	Log$_{10}$ and (% reduction)	Number of viable cells in CFU/ mL and (CFU/cm^{2})	Log$_{10}$ and (% reduction)	Number of viable cells in CFU/ mL and (CFU/cm^{2})	Log$_{10}$ and (% reduction)	Number of viable cells in CFU/ mL and (CFU/cm^{2})	Log$_{10}$ and (% reduction)	Number of viable cells in CFU/ mL and (CFU/cm^{2})
E. faecalis	Control	7.78±0.05	6.0x10^{7} (2.0x10^{6})	7.77±0.02	5.9x10^{7} (2.0x10^{6})	8.72±0.01	5.3x10^{8} (1.8x10^{7})	8.74±0.02	5.5x10^{8} (1.8x10^{7})	4.30±0.03	2.0x10^{4} (6.7x10^{2})	8.76±0.01	5.7x10^{8} (1.9x10^{7})	7.61±0.03	4.1x10^{7} (1.4x10^{6})
	10 s	3.36^{g}±0.08 (>99%)	2.6x10^{4} (8.7x10^{2})	3.45^{g}±0.03 (>99%)	2.1x10^{4} (7.0x10^{2})	1.96^{g}±0.02 (98.906%)	5.8x10^{6} (1.9x10^{6})	4.96^{f}±0.06 (>99%)	6.0x10^{3} (2.0x10^{2})	0.87^{g}±0.10 (86.500%)	2.7x10^{3} (9.0x10^{1})	4.79^{f}±0.01 (>99%)	9.2x10^{3} (3.1x10^{2})	4.06^{f}±0.05 (>99%)	3.6x10^{3} (1.2x10^{2})
	30 s	4.00^{f}±0.05 (>99%)	6.0x10^{3} (2.0x10^{2})	3.79^{f}±0.02 (>99%)	9.6x10^{3} (3,2x10^{2})	2.09^{f}±0.03 (>99%)	4.3x10^{6} (1.4x10^{5})	5.42^{e}±0.06 (>99%)	2.1x10^{3} (7.0x10^{1})	0.85^{g}±0.0 (86.000%)	2.8x10^{3} (9.3x10^{1})	5.08^{e}±0.03 (>99%)	4.7x10^{3} (1.6x10^{2})	4.15^{e}±0.09 (>99%)	2.9x10^{3} (9.7x10^{1})
P. aeruginosa	Control	8.66±0.04	4.6x10^{8} (1.5x10^{7})	8.66±0.03	4.6x10^{8} (1,5x10^{7})	8.72±0.02	5.3x10^{8} (1.8x10^{7})	8.84±0.01	6.9x10^{8} (2.3x10^{7})	8.74±0.03	5.5x10^{8} (1.8x10^{7})	8.77±0.02	5.9x10^{8} (2.0x10^{7})	8.82±0.05	6.6x10^{8} (2.2x10^{7})
	10 s	2.78^{i}±0.04 (>99%)	7.7x10^{5} (2,6x10^{4})	2.81^{h}±0.04 (>99%)	7.2x10^{5} (2,4x10^{4})	2.92^{e}±0.04 (>99%)	6.4x10^{5} (2.1x10^{4})	8.84^{b}±0.01 (>99%)	<10 (<0.33)	8.74^{b}±0.03 (>99%)	<10 (<0.33)	2.89^{h}±0.04 (>99%)	7.6x10^{5} (2.5x10^{4})	8.82^{b}±0.05 (>99%)	<10 (<0.33)
	30 s	2.80^{h}±0.05 (>99%)	7.3x10^{5} (2.4x10^{4})	2.76^{i}±0.03 (>99%)	8.0x10^{5} (2,7x10^{4})	2.93^{e}±0.05 (>99%)	6.2x10^{5} (2.1x10^{4})	8.84^{b}±0.01 (>99%)	<10 (<0.33)	8.74^{b}±0.03 (>99%)	<10 (<0.33)	8.77^{b}±0.02 (>99%)	<10 (<0.33)	8.82^{b}±0.05 (>99%)	<10 (<0.33)
C. freundii and *P. mirabilis*	Control	8.26±0.03	1.8x10^{8} (6.0x10^{6})	8.26±0.09	1.8x10^{8} (6,0x10^{6})	8.28±0.06	1.9x10^{8} (6.3x10^{6})	8.26±0.02	1.8x10^{8} (6.0x10^{6})	8.26±0.01	1.8x10^{8} (6.0x10^{6})	8.28±0.03	1.9x10^{8} (6.3x10^{6})	8.23±0.07	1.7x10^{8} (5,7x10^{6})
	10 s	8.26^{b}±0.03 (>99%)	<10 (<0.33)	8.26^{b}±0.09 (>99%)	<10 (<0.33)	8.28^{b}±0.06 (>99%)	<10 (<0.33)	8.26^{c}±0.02 (>99%)	<10 (<0.33)	8.26^{c}±0.01 (>99%)	<10 (<0.33)	8.28^{c}±0.03 (>99%)	<10 (<0.33)	8.23^{c}±0.07 (>99%)	<10 (<0.33)
	30 s	8.26^{b}±0.03 (>99%)	<10 (<0.33)	8.26^{b}±0.09 (>99%)	<10 (<0.33)	8.28^{b}±0.06 (>99%)	<10 (<0.33)	8.26^{c}±0.02 (>99%)	<10 (<0.33)	8.26^{c}±0.01 (>99%)	<10 (<0.33)	8.28^{c}±0.03 (>99%)	<10 (<0.33)	8.23^{c}±0.07 (>99%)	<10 (<0.33)
E. coli	Control	9.56±0.02	3.6x10^{9} (1.2x10^{8})	9.58±0.02	3.8x10^{9} (1,3x10^{8})	9.61±0.04	4.1x10^{9} (1.4x10^{8})	9.69±0.04	4.9x10^{9} (1.6x10^{8})	9.72±0.02	5.3x10^{9} (1.8x10^{8})	9.59±0.05	3.9x10^{9} (1.3x10^{8})	9.65±0.05	4.5x10^{9} (1.5x10^{8})
	10 s	9.56^{a}±0.02 (>99%)	<10 (<0.33)	9.58^{a}±0.02 (>99%)	<10 (<0.33)	9.61^{a}±0.04 (>99%)	<10 (<0.33)	9.69^{a}±0.04 (>99%)	<10 (<0.33)	9.72^{a}±0.02 (>99%)	<10 (<0.33)	9.59^{a}±0.05 (>99%)	<10 (<0.33)	9.65^{a}±0.05 (>99%)	<10 (<0.33)
	30 s	9.56^{a}±0.02 (>99%)	<10 (<0.33)	9.58^{a}±0.02 (>99%)	<10 (<0.33)	9.61^{a}±0.04 (>99%)	<10 (<0.33)	9.69^{a}±0.04 (>99%)	<10 (<0.33)	9.72^{a}±0.02 (>99%)	<10 (<0.33)	9.59^{a}±0.05 (>99%)	<10 (<0.33)	9.65^{a}±0.05 (>99%)	<10 (<0.33)
S. aureus	Control	7.57±0.01	3.7x10^{7} (1.2x10^{6})	7.63±0.03	4.3x10^{7} (1.3x10^{6})	7.54±0.03	3.5x10^{7} (1.2x10^{6})	7.60±0.02	4.0x10^{7} (1.3x10^{6})	7.43±0.05	2.7x10^{7} (9.0x10^{5})	7.59±0.05	3.9x10^{7} (1.3x10^{6})	7.32±0.06	2.1x10^{7} (7x10^{5})
	10 s	7.57^{c}±0.01 (>99%)	<10 (<0.33)	7.63^{c}±0.03 (>99%)	<10 (<0.33)	7.54^{c}±0.03 (>99%)	<10 (<0.33)	7.60^{d}±0.02 (>99%)	<10 (<0.33)	7.43^{d}±0.05 (>99%)	<10 (<0.33)	7.59^{d}±0.05 (>99%)	<10 (<0.33)	7.32^{d}±0.06 (>99%)	<10 (<0.33)
	30 s	7.57^{c}±0.01 (>99%)	<10 (<0.33)	7.63^{c}±0.03 (>99%)	<10 (<0.33)	7.54^{c}±0.03 (>99%)	<10 (<0.33)	7.60^{d}±0.02 (>99%)	<10 (<0.33)	7.43^{d}±0.05 (>99%)	<10 (<0.33)	7.59^{d}±0.05 (>99%)	<10 (<0.33)	7.32^{d}±0.06 (>99%)	<10 (<0.33)
C. albicans	Control	4.40±0.05	2.5x10^{4} (8.3x10^{2})	5.00±0.06	1.0x10^{5} (3.3x10^{3})	4.00±0.06	1.0x10^{4} (3.3x10^{2})	4.60±0.03	4.0x10^{4} (1.3x10^{6})	4.54±0.05	3.5x10^{4} (1.2x10^{3})	4.30±0.03	2.0x10^{4} (6.8x10^{2})	4.08±0.05	1.2x10^{4} (4.0x10^{2})
	10 s	4.40^{d}±0.05 (>99%)	<10 (<0.33)	5.00^{e}±0.06 (>99%)	<10 (<0.33)	4.00^{d}±0.06 (>99%)	<10 (<0.33)	4.60^{g}±0.03 (>99%)	<10 (<0.33)	4.54^{e}±0.05 (>99%)	<10 (<0.33)	4.30^{g}±0.03 (>99%)	<10 (<0.33)	4.08^{f}±0.05 (>99%)	<10 (<0.33)
	30 s	4.40^{d}±0.05 (>99%)	<10 (<0.33)	5.00^{e}±0.06 (>99%)	<10 (<0.33)	4.00^{d}±0.04 (>99%)	<10 (<0.33)	4.60^{g}±0.03 (>99%)	<10 (<0.33)	4.54^{e}±0.05 (>99%)	<10 (<0.33)	4.30^{g}±0.03 (>99%)	<10 (<0.33)	4.08^{f}±0.05 (>99%)	<10 (<0.33)

(*Continued*)

Table 2. (Continued)

Test microorganisms	Exposure conditions	Personal Protection Equipment													
		Cap		Safety glasses		Respirator face mask		Lab coat		Glove		Shoe		Face shield	
		Log_{10} and (% reduction)	Number of viable cells in CFU/mL and (CFU/cm^2)	Log_{10} and (% reduction)	Number of viable cells in CFU/mL and (CFU/cm^2)	Log_{10} and (% reduction)	Number of viable cells in CFU/mL and (CFU/cm^2)	Log_{10} and (% reduction)	Number of viable cells in CFU/mL and (CFU/cm^2)	Log_{10} and (% reduction)	Number of viable cells in CFU/mL and (CFU/cm^2)	Log_{10} and (% reduction)	Number of viable cells in CFU/mL and (CFU/cm^2)	Log_{10} and (% reduction)	Number of viable cells in CFU/mL and (CFU/cm^2)
C. parapsilosis	Control	4.18±0.04	$1.5x10^4$ ($5x10^2$)	5.48±0.04	$3.0x10^5$ ($1.0x10^4$)	4.00±0.04	$1.0x10^4$ ($3.3x10^2$)	4.30±0.03	$2.0x10^4$ ($6.8x10^2$)	4.20±0.08	$1.6x10^4$ ($5.3x10^2$)	4.30±0.06	$2.0x10^4$ ($6.8x10^2$)	4.18±0.07	$1.5x10^4$ ($5.0x10^2$)
	10 s	4.18^{c}±0.04 (>99%)	<10 (<0.33)	5.48^{d}±0.04 (>99%)	<10 (<0.33)	4.00^{d}±0.04 (>99%)	<10 (<0.33)	4.30^{h}±0.03 (>99%)	<10 (<0.33)	4.20^{f}±0.08 (>99%)	<10 (<0.33)	4.30^{g}±0.06 (>99%)	<10 (<0.33)	4.18^{c}±0.07 (>99%)	<10 (<0.33)
	30 s	4.18^{c}±0.04 (>99%)	<10 (<0.33)	5.48^{d}±0.04 (>99%)	<10 (<0.33)	4.00^{d}±0.04 (>99%)	<10 (<0.33)	4.30^{h}±0.03 (>99%)	<10 (<0.33)	4.20^{f}±0.08 (>99%)	<10 (<0.33)	4.30^{g}±0.06 (>99%)	<10 (<0.33)	4.18^{c}±0.07 (>99%)	<10 (<0.33)

https://doi.org/10.1371/journal.pone.0250854.t002

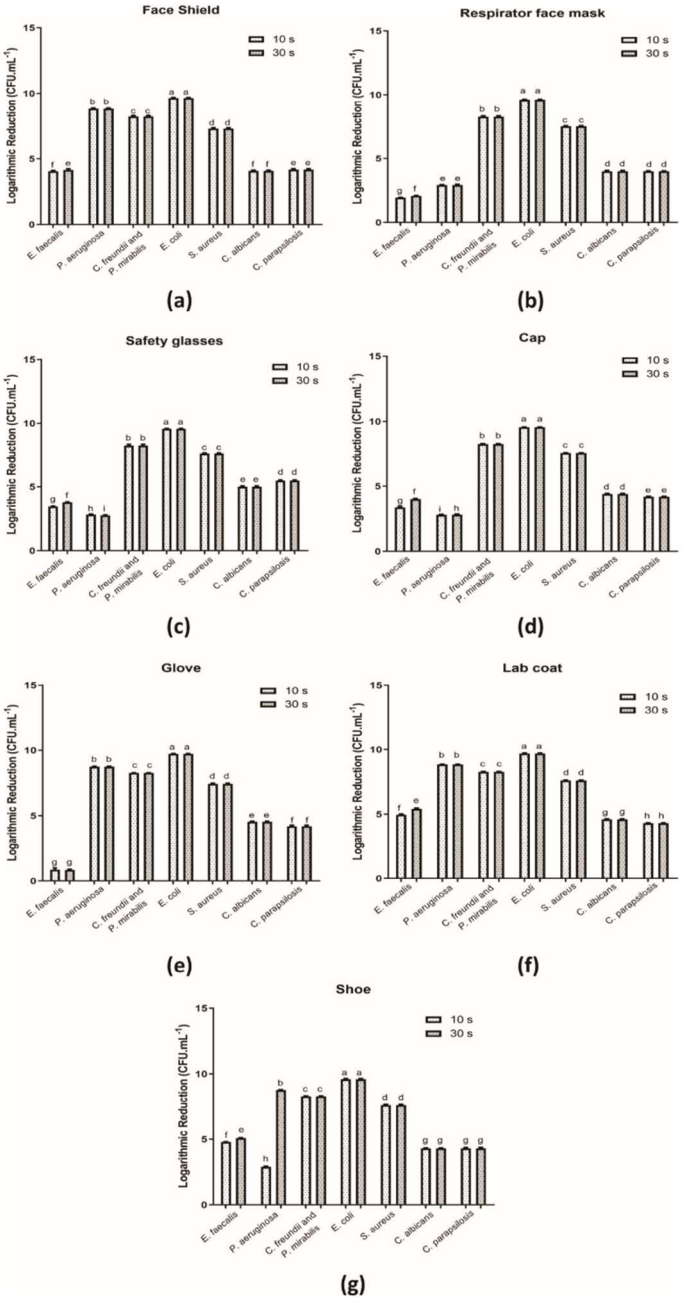
Face Shield
Respirator face mask
Safety glasses
Cap
Glove
Lab coat
Shoe
10 s
30 s
Logarithmic Reduction (CFU.mL-1)
E. faecalis
P. aeruginosa
C. freundii and P. mirabilis
E. coli
S. aureus
C. albicans
C. parapsilosis
(a)
(b)
(c)
(d)
(e)
(f)
(g)

Fig 3. Logarithmic reduction of the analyzed test microorganisms after exposure to the biocidal agent for 10 and 30 s according to the PPE item: (a) face shield; (b) respirator face mask; (c) safety glasses; (d) cap; (e) glove (f) lab coat and (g) shoe. Bars followed by the same letters are not significantly different at $p < 0.05$ according to Student's t test with 95% confidence.

https://doi.org/10.1371/journal.pone.0250854.g003

found for 3.07% (n = 3) of the tested conditions. The lowest percentage reductions identified were 86.500 and 86.000% for the test with *E. faecalis* when the glove was evaluated at exposure times of 10 and 30 s, respectively. In general, the exposure time of 10 s to 0.25% sodium hypochlorite under the investigated conditions effectively reduced the microbial load by >99% for all investigated microorganisms, except for *E. faecalis*. For these microorganism, percentage reduction >99% at 10 s and 30 s of exposure was identified for all PPE, except for the glove and respirator face mask. It is noteworthy that the results related to the percentage reduction for the exposure time of 30 s were similar to the time of 10 s, except for *E. faecalis* (Table 2).

The percentage reduction is also reflected in the total number of viable cells, where 78.57% (n = 77) of the analyzed conditions corresponded to <10 CFU/mL or <0.33 CFU/cm^2 at 10 and 30 s of exposure to spraying of 0.25% sodium hypochlorite. In general, there was a reduction in the number of viable cells for all analyzed conditions when compared to the results found for the control group. The resistance to the biocidal agent under the investigated conditions of the microorganisms *E. faecalis* and *P. aeruginosa* was demonstrated in this parameter, since they were the only ones that showed viable cells in the concentration >10 CFU/mL or >0.33 CFU/cm^2 after the disinfection process in the chamber, with the exception of samples of *P. aeruginosa* collected from the face shield, glove and lab coat, at exposure times of 10 and 30 s, in addition to the shoe after 30 s of exposure. The exposure time of 10 s was able to reduce the number of viable cells for <10 CFU/mL or <0.33 CFU/cm^2 in 38 experimental conditions, while for the time of 30 s, this reduction occurred in 39 experimental conditions. The differences related to the recovery of microorganisms may be associated with resistance to the biocidal agent under the conditions tested, as well as the inoculum concentration.

Fig 3 shows that *E. coli* was the microorganism with the highest $\log_{10}$ reduction values, regardless of the analyzed experimental condition (PPE item/surface and exposure time), with values >9 $\log_{10}$. The microorganisms *S. aureus*, *C. albicans*, *C. parapsilosis*, *C. freundii* and *P. mirabilis* showed the same $\log_{10}$ reduction at the tested exposure times, without significant difference regardless of the surface analyzed. It is important to highlight that for *Candida* species the $\log_{10}$ reduction value was lower than the bacterial species and this effect may be due to the lower initial inoculum used. With regard to the PPE items, the lab coat showed the highest $\log_{10}$ reduction values, varying between 4.30 $\log_{10}$ (*C. parapsilosis* at 10 and 30 s) and 9.69 $\log_{10}$ (*E. coli* at 10 and 30 s). The surface of the glove was the only one in which the $\log_{10}$ reduction of *E. faecalis* was similar ($p > 0.05$) at the exposure times of 10 and 30 s, with 0.87 and 0.85 $\log_{10}$, respectively, and was the lowest when compared to the reduction in the other analyzed surface.

Fig 4 shows the results of the PCA applied to the different study variables, which in this study were related to the type of PPE (cap, safety glasses, respirator face mask, lab coat, glove, shoe and face shield). In PCA, the clustering of the samples defines the structure of the data through graphs of scores and loadings whose axes are principal components (PC) on which the data is projected. The scores provide the composition of the PCs in relation to the samples, while loadings provide that same composition in relation to the variables. The total variance of principal component 1, mainly influenced by the respirator face mask, was 78.31% and that of principal component 2, mainly influenced by the glove, was 16.01%, totaling 94.32% (Fig 4A). The graph of the principal components shows that the microorganisms *E. faecalis* and *P. aeruginosa* were the only ones for which the samples from the 10 and 30 s exposure times did not

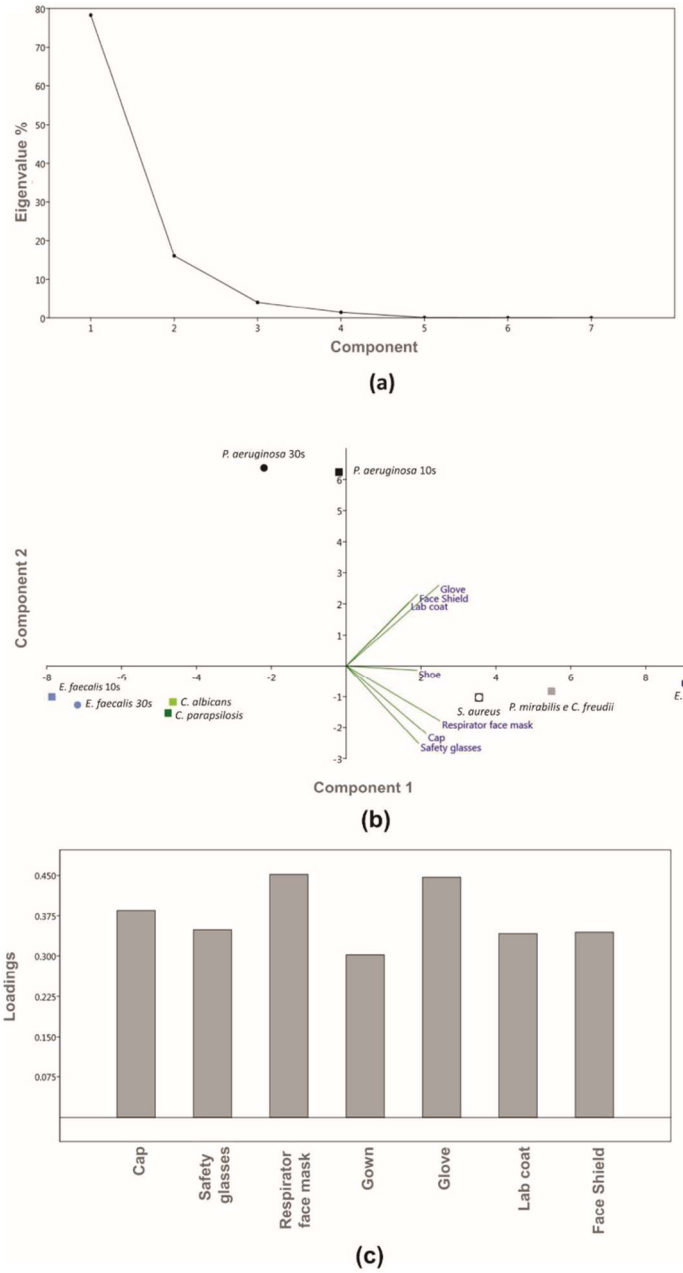

Fig 4. Principal component analysis of the samples of the test microorganisms analyzed at 10 and 30 s: (a) cumulative variance according to the quantity of components (PPE–cap, safety glasses, respirator face mask, lab coat, glove, shoe

and face shield—or surface type) (%); (b) graph of scores of principal components 1 (respirator face mask) and 2 (glove) and (c) graph of variable loadings of principal component 1.

https://doi.org/10.1371/journal.pone.0250854.g004

overlap (Fig 4B). In addition, the graph shows the formation of clusters for all tested microorganisms at different exposure times. Clustering is important because it can indicate similar behavior among the samples evaluated according to the study variables. Note that the only analyzed fungi (*C. albicans* and *C. parapsilosis*) formed a cluster in the lower left quadrant, as well as the samples from 10 and 30 s of *E. faecalis*, having no influence on the type of surface/item tested. However, the microorganisms *S. aureus*, *E. coli*, *C. freundii* and *P. mirabilis* clustered together in the lower right quadrant, being influenced by the type of surface/item tested (safety glasses, cap, respirator face mask and shoe), indicating that these microorganisms had similar behavior at the evaluated experimental conditions.

P. aeruginosa was the only microorganism whose samples from 10 and 30 s were allocated in the upper right quadrant, not being influenced by the main analyzed variable, the PPE item. Note also that there was no negative correlation between the porous and nonporous surface variables for principal component 1, where all PPE correlated positively with each other (Fig 4c). Thus, from the PCA analysis, it is observed that the type of microorganism analyzed influenced the results, since there was formation of clusters. In addition, even for the microorganisms that did not have overlapping values for the exposure times of 10 and 30 s, the behavior in response to the variables was similar since they remained in the same quadrant.

Fig 5 shows images of WSP discoloration due to the absorption of sodium hypochlorite droplets sprayed in the disinfection chamber after 10 and 30 s of exposure. Each image was

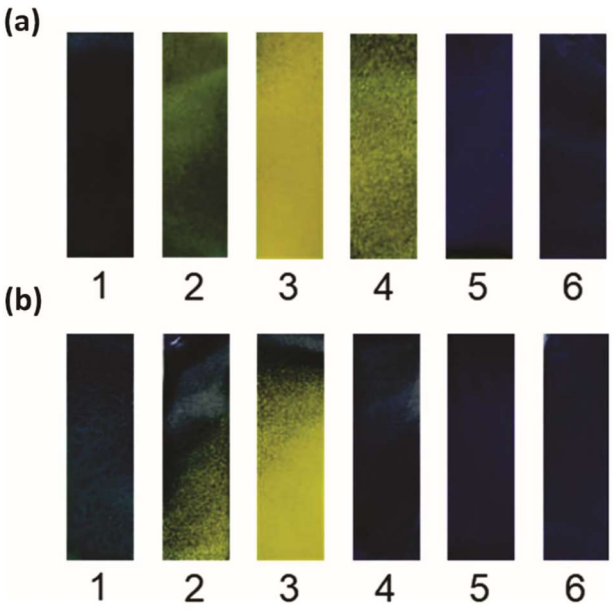

Fig 5. Discoloration of the WSPs exposed to spraying of the biocidal agent in the disinfection chamber in the study areas: (a) WSPs collected after 10 s of exposure; (b) WSPs collected after 30 s of exposure. WSPs position: (1) cap; (2) safety glasses; (3) respirator face mask; (4) lab coat; (5) glove; and (6) shoe. Blue areas represent the deposition of the biocidal agent, while yellow areas indicate no deposition.

https://doi.org/10.1371/journal.pone.0250854.g005

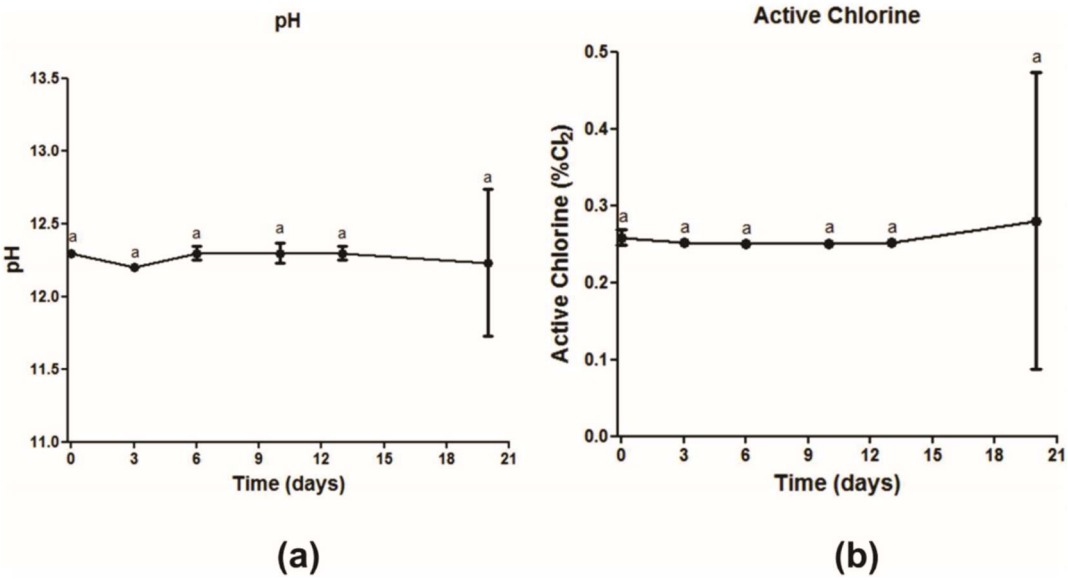

Fig 6. Stability analysis of sodium hypochlorite on days 0, 3, 6, 10, 13 and 20: (a) pH analysis and (b) percentage of active chlorine. There was no significant difference at $p < 0.05$ between values followed by the same letter according to Student's t test with 95% confidence.

https://doi.org/10.1371/journal.pone.0250854.g006

observed ex situ after the WSPs were removed from the study surface areas (positions 1 to 6—Fig 2). In general, there was good dispersion of the biocidal agent across the study area when using the disinfection chamber composed of the six nebulizer nozzles. The areas of the WSP with bluish tones show that there was deposition of the biocidal agent during the passage of the manikin through the disinfection chamber, while areas with yellowish tones indicate the absence of deposition of the studied agent.

In general, when comparing the distribution of the biocidal agent at the investigated exposure times, similar good deposition coverage of the agent on the WSPs was observed, which may be associated with the $\log_{10}$ reduction profile of the studied microorganisms, where the exposure time to the biocidal agent had no significant influence on the reduction factor (except for *E. faecalis* and *P. aeruginosa*) (Table 2 and Fig 3). Thus, the amount of biocidal agent that reaches the study areas during the 10 s exposure would be sufficient to inactivate most of the investigated microorganisms. Qualitatively, greater deposition is observed in some points of the WSPs for the time of 30 s and this may explain the greater efficacy of the longer exposure time for the two most resistant microorganisms (*E. faecalis* and *P. aeruginosa*). In addition, the lower deposition of the biocidal agent on the respirator face mask (area 3), indicated by the yellowish tone, may have interfered with the reduction efficiency of these microorganisms.

Fig 6 and S1 Table shows the results obtained for the stability analysis of the biocidal agent at a concentration of 0.25% by determining the pH (Fig 6A) and the percentage of active chlorine (Fig 6B). The results showed that the sodium hypochlorite solution was stable over the evaluated period, with no significant difference ($p > 0.05$) between the means determined for the pH and for the active chlorine concentration (%). These results demonstrate the viability of using the sodium hypochlorite solution with adequate active chlorine concentration

(0.25%) for at least 20 days for application in the disinfection chamber, with maintenance of its disinfectant capacity.

Discussion

In this study we demonstrated the high rates of microbial load reduction after exposure to the sodium hypochlorite biocidal agent used in the personal protective closes and equipment (PPE) disinfection chamber at the two analyzed times (10 and 30 s) regardless of the type of surface/PPE item investigated. Some studies [80, 81] and standards [79, 82] indicate that disinfection methods with $\geq 5 \log_{10}$ CFU reduction are considered effective and, consequently, appropriate for clinical use, which reinforces the importance of our results for the instant disinfection of PPE, especially during the SARS-CoV-2 pandemic. This logarithmic reduction implies the elimination of 99.999% of the microbial load [79, 82]. Considering these values as a reference, the microorganisms *P. aeruginosa* and *E. faecalis* showed the lowest sensitivity to sodium hypochlorite under the tested conditions (for some PPE items) when compared to the other microorganisms, although the results were quite satisfactory in relation to the reduction factor found for these bacteria under the studied conditions.

There are reports in the literature on the resistance of *P. aeruginosa* and *E. faecalis* to sodium hypochlorite at concentrations <0.3% and <0.22%, respectively [83, 84]. This mechanism may be associated with the bacterial ability to remove or discharge the charge of hypochlorous acid (HClO), which is a strong oxidizing agent that damages the permeability of the bacterial cell wall and its genetic material [85]. However, Lineback et al. [86] showed that the use of sodium hypochlorite at a concentration of 1.312% against *P. aeruginosa* was more effective than quaternary ammonium, while Yoo et al. [87] reported that this biocidal agent at 0.031% showed activity against clinical isolates of *E. faecalis*. In this study, the concentration of 0.25% of sodium hypochlorite was effective in reducing the load >99% for *P. aeruginosa* and ≥86.000% for *E. faecalis*.

Regarding the analyzed fungal strains, the percentage reduction value was >99% and the number of viable cell was <10 CFU/mL or <0.33 CFU/cm^2 for all experimental conditions, indicating that *C. albicans* and *C. parapsilosis* are sensitive to sodium hypochlorite under the tested conditions, which shows that spraying of the biocidal agent may be an effective alternative for the inactivation of these microorganisms when compared to other methods [62]. Infections caused by *Candida* species are classified as one of the main contaminants in the hospital environment because these pathogens can lead to systemic infection [88]. Although *C. albicans* is still the species most frequently isolated from nosocomial fungal infections [89], cases associated with *C. parapsilosis* have increased significantly in recent years [90] due to the resistance of *Candida* species to antifungals and disinfectants [91]. Thus, it is important to note that spraying systems have been used to control bioburden in nosocomial environments, especially for combating multidrug-resistant strains [81].

The study by Ishikawa et al. [37] demonstrated that the efficacy of a small disinfection chamber using a spray system with 5.00% sodium hypochlorite solution for the inactivation of *Bacillus subtilis* spores. The authors reported that the disinfection system used is a "test chamber", which does not have the physical structure for the passage of a person, being able only to perform the sporicidal effect in a small area [37]. However, unlike Ishikawa et al. [37] work, our study demonstrates the efficacy of a spray system (disinfection chamber) containing sodium hypochlorite for the instant disinfection of different PPE items (at 10 or 30 s) against *Candida* species and Gram-positive and Gram-negative bacteria on different types of surfaces at the same time. The efficacy demonstrated by the biocide agent in the concentration of 0.25% against the microorganisms tested suggests that new studies can be conducted using a

lower concentration of the chemical agent, such as 0.1%, which is also in the concentration range recommended by WHO for the disinfection of environmental surfaces [49].

Hospital infections are caused by factors such as environmental contamination, frequent handling of contaminated material, and the ability of microorganisms to survive for prolonged periods on different types of surfaces [1, 92]. Within the hospital environment, sodium hypochlorite is the most widely used disinfectant because it has broad-spectrum antimicrobial activity, considering Gram-positive and Gram-negative bacteria and fungi [83] as well as demonstrated virucidal activity [93]. Köhler et al. [94] showed that sodium hypochlorite effectively reduced the concentration of multidrug-resistant Gram-positive bacteria (*Pseudomonas*, *Acinetobacter* and *Klebsiella*) after exposure times of 1 to 15 min, longer exposure time than those studied in this work. Regarding the activity against viral agents, It has been demonstrated that sodium hypochlorite in concentrations between 0.01 and 0.5% is capable of inactivating the SARS-CoV-1 on stainless steel surfaces [95, 96]. In addition, Ma et al. [97] showed that instant hand hygiene using disinfecting wipes containing 0.05 or 0.25% active chlorine removed 96.62% and 99.98%, of the influenza virus, respectively, which causes avian influenza. The authors also point out that, although they have not tested with SARS-CoV-2, hand cleaning with the disinfecting wipes can help to control the spread of COVID-19. Similarly to the study by Ma et al. [97], one limitation of our study was not to use SARS-CoV-2 as a test microorganism. However, based on the promising results identified in this study, which showed that the biocide capacity of sodium hypochlorite was maintained under the conditions tested, the evaluated concentration of 0.25% has the potential for disinfecting surfaces contaminated by different microorganisms and can be extrapolated to enveloped viruses based on results in the literature, being a potential agent against SARS-CoV-2. The choice of evaluating different bacteria and fungi as biological indicators stemmed from the need to accelerate the confirmation of the disinfectant action of the proposed technology, since some of these microorganisms are resilient compared to viruses [98], have a relatively faster growth and can be manipulated in laboratory environments with a lower level of biosafety.

Other studies have already demonstrated the effect of different biocidal agents against the microorganisms tested in this study, showing that the efficacy of the disinfection process varies with the type of disinfectant [99, 100] or according to the application method used [101, 102]. There are few reports in the scientific literature on the efficacy of PPE decontamination after exposure to pathogens, as was analyzed in this study. Among them, Lemmer et al. [103] showed that disinfection with 2% peracetic acid with 0.2% surfactant through a spray system was able to inactivate *B. thuringiensis* spores in high density polyethylene protective coveralls after 5 min of exposure. Compared to our study, sodium hypochlorite was more effective than peracetic acid because the exposure time required was shorter to reduce the microbial load on the surface, considering the polyethylene surface and other analyzed materials. In addition, the instantaneous decontamination demonstrated by the results obtained in 10 and 30 s exposure times shows the potential of the disinfection chamber application in places with intense or moderate people flow, such as the exits of intensive care units and wards in hospitals. In addition, reducing the microbial load on the surface of PPE can help reduce the risks associated with handling and exposure to biomedical waste, an important source of environmental contamination [104].

The results also suggest that the use of sodium hypochlorite may be recommended due to the stability of its solution in terms of pH and concentration of active chlorine over the 20 days, since the exchange or replacement of the biocide agent solution does not need to be performed, for example, on a daily basis. The dissociation of NaOCl into HOCl-, its main active agent, is pH-dependent [105]. Thus, it is important that the solution remains stable so that the levels of the active agent do not decrease. The critical issue raised by health authorities'

agencies are sodium hypochlorite toxicity when in contact with mucous membranes and may lead to tissue damage or allergic reactions [106, 107]. Therefore, we are aware of the possibility of episodes of clinical toxicity caused by the sodium hypochlorite, especially in persons that are known to be allergic to bleaches, and that this can be considered as a limitation of the study. In addition, we re-emphasized that the disinfection chamber with 0.25% sodium hypochlorite be used only by fully trained workers (considering its installation, the preparation of the biocide agent in the correct concentration, and for its correct use), thus promoting an effective disinfection process against bacteria and potential emerging pathogens, such as SARS-CoV-2, that is safe for users.

The use of the proposed disinfection technology becomes an attractive alternative, especially for middle-income countries such as Brazil [38]. This occurs due to factors such as the material used in the chamber framework, which are widely used in the industry for the manufacture of different items, its modular design that allows scalable production as well as the low-cost of sodium hypochlorite. These factors can make production cheaper and facilitate transport and installation in different health facilities. In addition, the results obtained related to WPS showed that the nebulizer nozzles disposition promoted a satisfactory spraying of the biocide agent.

Indeed, disinfection chamber could be considered as an interesting disinfection technology for use in emerging countries, since it can improve the control cases of nosocomial infection in those places that usually have the most overloaded health systems.

Conclusions

The disinfection chamber proved to be a potential technology for the rapid and effective disinfection of the surface of PPE, regardless of the evaluated item, routinely used by HCWs for protection against infectious agents. The spraying system with the biocidal agent was effective in reduce the microbial load, where the percentage reduction equal to >99% and, consequently, bringing the number of viable cells to <10 CFU/mL and <0.33 CFU/cm^2 after exposure times of 10 and 30 s in 96.93% of the experimental conditions analyzed. The lowest percentages reduction were found for the sample of *E. faecalis* collected from the glove, where the values obtained were 86.000 and 86.500% for the exposition of 10 and 30 s, respectively, while the highest amount of viable cells was found for *P. aeruginosa* sample at 10 s in the cap, with 7.7x10^5 CFU/mL or 2.6x10^4 CFU/cm^2. The $\log_{10}$ reduction values varied between 0.85 $\log_{10}$ (*E. faecalis* at 30 s in glove surface) and 9.69 $\log_{10}$ (*E. coli* at 10 and 30 s in lab coat surface).

Thus, the bacterial species *E. coli*, *S. aureus*, *C. freundii* and *P. mirabilis* and the fungi *C. albicans* and *C. parapsilosis* showed susceptibility to 0.25% sodium hypochlorite under the evaluated experimental conditions independent of the exposure time or PPE item evaluated, while the microorganism *E. faecalis* was less susceptible to the biocidal agent under the tested conditions. In general, a 30-s exposure time was more efficient in reducing the investigated microbial load.

The results of this study show that the disinfection chamber with 0.25% sodium hypochlorite may be an alternative to control the bioburden in nosocomial environments, especially to prevent the self-contamination of HCWs in the doffing step. The importance of the use of the chamber by properly attired HCWs is also emphasized in order to avoid direct contact with the tested biocidal agent. In addition, because this is a novel study, these results may contribute to the development and safe use of disinfection equipment in environments where the environmental bioburden must be controlled. It is also important to highlight that the experimental design of the study was carried out in order to have a simulation of how the disinfection

chamber would be used by HCW in the nosocomial environment. Thus, the manipulation of viral strains would not be appropriate in the conditions tested, since the handling of these microorganisms requires a laboratory environment with a higher level of biosafety. However, although virucidal efficacy was not directly determined, the chamber may be an alternative to reduce the contamination rates among HCWs in front of different types of emerging microorganisms, reducing the impacts in the area of public health.

Supporting information

S1 Fig. Image of the disinfection chamber: Spray disinfection technology for instant decontamination of personal protective equipment.
(DOCX)

S2 Fig. Images of the manikin suitably dressed with PPEs used to simulate the use of the disinfection chamber by healthcare workers in nosocomial environments.
(DOCX)

S1 Table. Raw data of stability of sodium hypochlorite regarding pH and active chlorine analysis (mean ± standard deviation).
(DOCX)

Acknowledgments

The authors thank Bahia Department of Health (Secretaria de Saúde do Estado da Bahia–SESAB), Directorate of Sanitary and Environmental Surveillance of Bahia (Diretoria de Vigilância Sanitária e Ambiental do Estado da Bahia–DIVISA BA) and Hospital Espanhol of Salvador (COVID-19 Campaign Hospital).

Author Contributions

Conceptualization: Luís Alberto Brêda Mascarenhas, Bruna Aparecida Souza Machado, Leone Peter Correia da Silva Andrade, Jailson Bittencourt de Andrade, Roberto Badaró.

Data curation: Luís Alberto Brêda Mascarenhas, Bruna Aparecida Souza Machado, Paulo Roberto Freitas Neves, Jailson Bittencourt de Andrade, Roberto Badaró.

Formal analysis: Luís Alberto Brêda Mascarenhas, Bruna Aparecida Souza Machado, Leticia de Alencar Pereira Rodrigues, Alex Álisson Bandeira Santos, Paulo Roberto Freitas Neves, Milena Botelho Soares, Roberto Badaró.

Investigation: Luís Alberto Brêda Mascarenhas, Bruna Aparecida Souza Machado, Leticia de Alencar Pereira Rodrigues, Alex Álisson Bandeira Santos, Leone Peter Correia da Silva Andrade, Milena Botelho Soares, Roberto Badaró.

Methodology: Luís Alberto Brêda Mascarenhas, Bruna Aparecida Souza Machado, Leticia de Alencar Pereira Rodrigues, Katharine Valéria Saraiva Hodel, Alex Álisson Bandeira Santos, Paulo Roberto Freitas Neves, Leone Peter Correia da Silva Andrade, Jailson Bittencourt de Andrade, Roberto Badaró.

Project administration: Luís Alberto Brêda Mascarenhas, Bruna Aparecida Souza Machado, Leone Peter Correia da Silva Andrade, Jailson Bittencourt de Andrade, Roberto Badaró.

Software: Katharine Valéria Saraiva Hodel.

Supervision: Luís Alberto Brêda Mascarenhas, Bruna Aparecida Souza Machado, Leone Peter Correia da Silva Andrade, Roberto Badaró.

Validation: Luís Alberto Brêda Mascarenhas, Bruna Aparecida Souza Machado, Alex Álisson Bandeira Santos, Paulo Roberto Freitas Neves, Leone Peter Correia da Silva Andrade, Milena Botelho Soares, Jailson Bittencourt de Andrade, Roberto Badaró.

Visualization: Luís Alberto Brêda Mascarenhas, Bruna Aparecida Souza Machado, Leone Peter Correia da Silva Andrade, Roberto Badaró.

Writing – original draft: Luís Alberto Brêda Mascarenhas, Bruna Aparecida Souza Machado, Katharine Valéria Saraiva Hodel, Alex Álisson Bandeira Santos, Leone Peter Correia da Silva Andrade, Milena Botelho Soares, Jailson Bittencourt de Andrade, Roberto Badaró.

References

1. Weber DJ, Kanamori H, Rutala WA. "No touch" technologies for environmental decontamination: Focus on ultraviolet devices and hydrogen peroxide systems. Curr Opin Infect Dis. 2016; 29: 424–431. https://doi.org/10.1097/QCO.0000000000000284 PMID: 27257798
2. Ferrara P, Albano L. COVID-19 and healthcare systems: What should we do next? Public Health. 2020; 185: 1–2. https://doi.org/10.1016/j.puhe.2020.05.014 PMID: 32502747
3. Chowdhury S, Azziz-Baumgartner E, Kile JC, Hoque MA, Rahman MZ, Hossain ME, et al. Association of biosecurity and hygiene practices with environmental contamination with influenza a viruses in live bird markets, Bangladesh. Emerg Infect Dis. 2020; 26: 2087–2096. https://doi.org/10.3201/eid2609.191029 PMID: 32818393
4. Cutts TA, Robertson C, Theriault SS, Nims RW, Kasloff SB, Rubino JR, et al. Efficacy of microbicides for inactivation of Ebola–Makona virus on a non-porous surface: a targeted hygiene intervention for reducing virus spread. Sci Rep. 2020; 10: 1–9. https://doi.org/10.1038/s41598-019-56847-4 PMID: 31913322
5. Kratzel A, Todt D, V'kovski P, Steiner S, Gultom M, Thao TTN, et al. Inactivation of Severe Acute Respiratory Syndrome Coronavirus 2 by WHO-Recommended Hand Rub Formulations and Alcohols. Emerg Infect Dis. 2020; 26. https://doi.org/10.3201/eid2607.200915 PMID: 32284092
6. Lu H, Stratton CW, Tang Y. Outbreak of pneumonia of unknown etiology in Wuhan, China: The mystery and the miracle. J Med Virol. 2020; 92: 401–402. https://doi.org/10.1002/jmv.25678 PMID: 31950516
7. Munster VJ, Koopmans M, van Doremalen N, van Riel D, de Wit E. A Novel Coronavirus Emerging in China—Key Questions for Impact Assessment. N Engl J Med. 2020; 382: 692–694. https://doi.org/10.1056/NEJMp2000929 PMID: 31978293
8. Yin S, Peng Y, Ren Y, Hu M, Tang L, Xiang Z, et al. The implications of preliminary screening and diagnosis: Clinical characteristics of 33 mild patients with SARS-CoV-2 infection in Hunan, China. J Clin Virol. 2020; 128: 104397. https://doi.org/10.1016/j.jcv.2020.104397 PMID: 32388472
9. Rothe C, Schunk M, Sothmann P, Bretzel G, Froeschl G, Wallrauch C, et al. Transmission of 2019-nCoV Infection from an Asymptomatic Contact in Germany. N Engl J Med. 2020; 382: 970–971. https://doi.org/10.1056/NEJMc2001468 PMID: 32003551
10. Liu Y, Ning Z, Chen Y, Guo M, Liu Y, Gali NK, et al. Aerodynamic analysis of SARS-CoV-2 in two Wuhan hospitals. Nature. 2020; 582: 557–560. https://doi.org/10.1038/s41586-020-2271-3 PMID: 32340022
11. Adams JG, Walls RM. Supporting the Health Care Workforce during the COVID-19 Global Epidemic. JAMA—J Am Med Assoc. 2020; 323: 1439–1440. https://doi.org/10.1001/jama.2020.3972 PMID: 32163102
12. Tran K, Cimon K, Severn M, Pessoa-Silva CL, Conly J. Aerosol Generating Procedures and Risk of Transmission of Acute Respiratory Infections to Healthcare Workers: A Systematic Review. Semple MG, editor. PLoS One. 2012; 7: e35797. https://doi.org/10.1371/journal.pone.0035797 PMID: 22563403
13. James PB, Wardle J, Steel A, Adams J, Bah AJ, Bai P, et al. Providing healthcare to Ebola survivors: A qualitative exploratory investigation of healthcare providers ' views and experiences in Sierra Leone Providing healthcare to Ebola survivors: A qualitative exploratory investigation of healthcare providers ' v. Glob Public Health. 2020; 0: 1–16. https://doi.org/10.1080/17441692.2020.1762105 PMID: 32379008

14. Wei J-T, Liu Z-D, Fan Z-W, Zhao L, Cao W-C. Epidemiology of and Risk Factors for COVID-19 Infection among Health Care Workers: A Multi-Centre Comparative Study. Int J Environ Res Public Health. 2020; 17: 7149. https://doi.org/10.3390/ijerph17197149 PMID: 33003634

15. Dhont S, Derom E, Van Braeckel E, Depuydt P, Lambrecht BN. The pathophysiology of "happy" hypoxemia in COVID-19. Respir Res. 2020; 21: 198. https://doi.org/10.1186/s12931-020-01462-5 PMID: 32723327

16. Lai X, Wang M, Qin C, Tan L, Ran L, Chen D, et al. Coronavirus Disease 2019 (COVID-2019) Infection Among Health Care Workers and Implications for Prevention Measures in a Tertiary Hospital in Wuhan, China. JAMA Netw Open. 2020; 3: e209666. https://doi.org/10.1001/jamanetworkopen.2020.9666 PMID: 32437575

17. Nissen K, Krambrich J, Akaberi D, Hoffman T, Ling J, Lundkvist Å, et al. Long-distance airborne dispersal of SARS-CoV-2 in COVID-19 wards. Sci Rep. 2020; 10: 19589. https://doi.org/10.1038/s41598-020-76442-2 PMID: 33177563

18. Wang J, Zhou M, Liu F. Reasons for healthcare workers becoming infected with novel coronavirus disease 2019 (COVID-19) in China. J Hosp Infect. 2020; 105: 100–101. https://doi.org/10.1016/j.jhin.2020.03.002 PMID: 32147406

19. Felice C, Luca G, Tanna D, Zanus G, Grossi U. Impact of COVID-19 Outbreak on Healthcare Workers in Italy: Results from a National E-Survey. J Community Health. 2020 [cited 7 Jun 2020]. https://doi.org/10.1007/s10900-020-00845-5 PMID: 32440724

20. Kursumovic E, Lennane S, Cook TM. Deaths in healthcare workers due to COVID-19: the need for robust data and analysis. Anaesthesia. 2020; 5–8. https://doi.org/10.1111/anae.15116 PMID: 32397005

21. Marson FAL, Ortega MM. COVID-19 in Brazil. Pulmonology. 2020. https://doi.org/10.1016/j.pulmoe.2020.04.008 PMID: 32371054

22. Ministério da Saúde do Brasil. Coronavírus Brasil. 2020 [cited 16 Sep 2020]. Available: https://covid.saude.gov.br/

23. Suen LKP, Guo YP, Tong DWK, Leung PHM, Lung D, Ng MSP, et al. Self-contamination during doffing of personal protective equipment by healthcare workers to prevent Ebola transmission. Antimicrob Resist Infect Control. 2018; 7: 157. https://doi.org/10.1186/s13756-018-0433-y PMID: 30607244

24. Tellier R, Li Y, Cowling BJ, Tang JW. Recognition of aerosol transmission of infectious agents: a commentary. BMC Infect Dis. 2019; 19: 1–9. https://doi.org/10.1186/s12879-018-3567-x PMID: 30606108

25. Jones RM, Bleasdale SC, Maita D, Brosseau LM. A systematic risk-based strategy to select personal protective equipment for infectious diseases. Am J Infect Control. 2020; 48: 46–51. https://doi.org/10.1016/j.ajic.2019.06.023 PMID: 31358421

26. Cinar P, Kubal T, Freifeld A, Mishra A, Shulman L, Bachman J, et al. Safety at the Time of the COVID-19 Pandemic: How to Keep our Oncology Patients and Healthcare Workers Safe. J Natl Compr Canc Netw. 2020; 18: 1–6. https://doi.org/10.6004/jnccn.2020.0003 PMID: 31910382

27. Visnovsky LD, Zhang Y, Leecaster MK, Safdar N, Barko L, Haroldsen C, et al. Effectiveness of a multisite personal protective equipment (PPE)-free zone intervention in acute care. Infect Control Hosp Epidemiol. 2019; 40: 761–766. https://doi.org/10.1017/ice.2019.111 PMID: 31172904

28. Korth J, Wilde B, Dolff S, Anastasiou OE, Krawczyk A, Jahn M, et al. SARS-CoV-2-specific antibody detection in healthcare workers in Germany with direct contact to COVID-19 patients. J Clin Virol. 2020; 128: 104437. https://doi.org/10.1016/j.jcv.2020.104437 PMID: 32434708

29. Muñoz-Leyva F, Niazi AU. Common breaches in biosafety during donning and doffing of protective personal equipment used in the care of COVID-19 patients. Can J Anaesth. 2020; 67: 900–901. https://doi.org/10.1007/s12630-020-01648-x PMID: 32291630

30. Thadathilankal-Jess, Karin H, Hellmuth W. Donning and doffing of personal protective equipment (PPE) for angiography during the COVID-19 crisis. Eur Heart J. 2020; 41: 1786–1787. https://doi.org/10.1093/eurheartj/ehaa283 PMID: 32282025

31. Karim N, Afroj S, Lloyd K, Clarke Oaten L, Andreeva D V, Carr C, et al. Sustainable Personal Protective Clothing for Healthcare Applications: A Review. ACS Nano. 2020; acsnano.0c05537. https://doi.org/10.1021/acsnano.0c05537 PMID: 32866368

32. Wickramatillake A, Kurukularatne C. SARS-CoV-2 human disinfection chambers: a critical analysis. Occup Med (Chic Ill). 2020 [cited 6 Jun 2020]. https://doi.org/10.1093/occmed/kqaa078 PMID: 32372076

33. Gardam M, McGeer A, Mertz D. Portable ultraviolet light surface-disinfecting devices for prevention of hospital-acquired infections: A health technology assessment. Ont Health Technol Assess Ser. 2018; 18: 1–73.

34. El Haddad L, Ghantoji SS, Stibich M, Fleming JB, Segal C, Ware KM, et al. Evaluation of a pulsed xenon ultraviolet disinfection system to decrease bacterial contamination in operating rooms. BMC Infect Dis. 2017; 17. https://doi.org/10.1186/s12879-017-2792-z PMID: 29017457

35. Cadnum JL, Jencson AL, Livingston SH, Li D, Redmond SN, Pearlmutter B, et al. Evaluation of an Electrostatic Spray Disinfectant Technology for Rapid Decontamination of Portable Equipment and Large Open Areas in the Era of SARS-CoV-2. Am J Infect Control. 2020. https://doi.org/10.1016/j.ajic.2020.06.002 PMID: 32522608

36. Verhougstraete M, Reynolds K. Use of a portable air disinfecting system to remove seeded coliphage in hospital rooms. Am J Infect Control. 2016; 44: 714–715. https://doi.org/10.1016/j.ajic.2015.12.025 PMID: 26905789

37. Ishikawa S, Ueno S, Mitsui M, Matsumura Y, Hatsuoka T. Construction of its evaluation system in originally designed test-chamber system and sporicidal activity of aerosolized hypochlorite solution to bacillus subtilis spores. Biocontrol Sci. 2019; 24: 57–65. https://doi.org/10.4265/bio.24.57 PMID: 30880314

38. Anvisa. NOTA TÉCNICA No 38/2020/SEI/COSAN/GHCOS/DIRE3/ANVISA. Brasília; 2020 [cited 5 Aug 2020] pp. 1–5. Available: https://sei.anvisa.gov.br/sei/controlador.php?acao=documento_imprimir_web&acao_origem=arvore_visualizar&id_documento=1118935&infra_sis. . .1/5

39. FDA. Enforcement Policy for Sterilizers, Disinfectant Devices, and Air Purifiers During the Coronavirus Disease 2019 (COVID-19) Public Health Emergency Guidance for Industry and Food and Drug Administration Staff Preface Public Comment. In: FDA [Internet]. Mar 2020 [cited 16 Nov 2020] pp. 1–14. Available: https://www.fda.gov/regulatory-information/search-fda-guidance-documents.

40. Biswal M, Kanaujia R, Angrup A, Ray P, Mohan Singh S. Disinfection tunnels: potentially counterproductive in the context of a prolonged pandemic of COVID-19. Public Health. Elsevier B.V.; 2020. pp. 48–49. https://doi.org/10.1016/j.puhe.2020.04.045 PMID: 32422441

41. Keil SD, Ragan I, Yonemura S, Hartson L, Dart NK, Bowen R. Inactivation of severe acute respiratory syndrome coronavirus 2 in plasma and platelet products using a riboflavin and ultraviolet light-based photochemical treatment. Vox Sang. 2020; vox.12937. https://doi.org/10.1111/vox.12937 PMID: 32311760

42. Aboualizadeh E, Bumah V V., Masson-Meyers DS, Eells JT, Hirschmugl CJ, Enwemeka CS. Understanding the antimicrobial activity of selected disinfectants against methicillin-resistant Staphylococcus aureus (MRSA). Gupta V, editor. PLoS One. 2017; 12: e0186375. https://doi.org/10.1371/journal.pone.0186375 PMID: 29036196

43. Schrank CL, Minbiole KPC, Wuest WM. Are Quaternary Ammonium Compounds, the Workhorse Disinfectants, Effective against Severe Acute Respiratory Syndrome-Coronavirus-2? ACS Infect Dis. 2020; 1–5. https://doi.org/10.1021/acsinfecdis.0c00265 PMID: 32412231

44. Chapuis A, Amoureux L, Bador J, Gavalas A, Siebor E, Chrétien M-L, et al. Outbreak of Extended-Spectrum Beta-Lactamase Producing Enterobacter cloacae with High MICs of Quaternary Ammonium Compounds in a Hematology Ward Associated with Contaminated Sinks. Front Microbiol. 2016; 7: 1070. https://doi.org/10.3389/fmicb.2016.01070 PMID: 27462306

45. Libonati A, Di Taranto V, Mea A, Montemurro E, Gallusi G, Angotti V, et al. Clinical antibacterial effectiveness Healozone Technology after incomplete caries removal. Eur J Paediatr Dent. 2019; 20: 73–78. https://doi.org/10.23804/ejpd.2019.20.01.14 PMID: 30919649

46. Henwood AF. Coronavirus disinfection in histopathology. J Histotechnol. 2020; 43: 102–104. https://doi.org/10.1080/01478885.2020.1734718 PMID: 32116147

47. Röhner E, Jacob B, Böhle S, Rohe S, Löffler B, Matziolis G, et al. Sodium hypochlorite is more effective than chlorhexidine for eradication of bacterial biofilm of staphylococci and Pseudomonas aeruginosa. Sport Traumatol Arthrosc. 2020 [cited 8 Jun 2020]. https://doi.org/10.1007/s00167-020-05887-9 PMID: 32034427

48. Wang J, Shen J, Ye D, Yan X, Zhang Y, Yang W, et al. Disinfection technology of hospital wastes and wastewater: Suggestions for disinfection strategy during coronavirus Disease 2019 (COVID-19) pandemic in China. Environ Pollut. 2020; 262: 114665. https://doi.org/10.1016/j.envpol.2020.114665 PMID: 32443202

49. WHO. Cleaning and Disinfection of Environmental Surfaces in the context of COVID-19. Geneva; 2020 [cited 30 Aug 2020] p. 7. Available: https://apps.who.int/iris/rest/bitstreams/1277966/retrieve

50. OPAS. O uso de túneis e outras tecnologias para desinfecção de humanos usando aspersão de produtos químicos ou radiação UV-C. 2020 [cited 30 Aug 2020] pp. 1–3. Available: https://iris.paho.org/handle/10665.2/52243

51. WHO. Coronavirus disease (COVID-19) Situation Report-115. In: World Health Organization [Internet]. 14 May 2020 [cited 13 Nov 2020] pp. 1–19. https://doi.org/10.1016/j.ajic.2019.01.014

52. Yim W, Cheng D, Patel S, Kui R, Meng YS, Jokerst J. Assessment of N95 and K95 respirator decontamination: fiber integrity, filtration efficiency, and dipole charge density. medRxiv. 2020 [cited 11 Nov 2020]. https://doi.org/10.1101/2020.07.07.20148551 PMID: 32676621

53. Mantlo E, Rhodes T, Boutros J, Patterson-Fortin L, Evans A, Paessler S, et al. In vitro efficacy of a copper iodine complex PPE disinfectant for SARS-CoV-2 inactivation. F1000Research. 2020; 9: 1–10. https://doi.org/10.12688/f1000research.24651.2 PMID: 33123349

54. Saini V, Sikri K, Dhingra Batra S, Kalra P, Gautam K. Development of a highly effective low-cost vaporized hydrogen peroxide-based method for disinfection of personal protective equipment for their selective reuse during pandemics. Gut Pathog. 2020; 12: 1–11. https://doi.org/10.1186/s13099-019-0341-6 PMID: 31911822

55. Drohan SE, Levin SA, Grenfell BT, Laxminarayan R. Incentivizing hospital infection control. Proc Natl Acad Sci U S A. 2019; 116: 6221–6225. https://doi.org/10.1073/pnas.1812231116 PMID: 30858309

56. Suchomel M, Lenhardt A, Kampf G, Grisold A. Enterococcus hirae, Enterococcus faecium and Enterococcus faecalis show different sensitivities to typical biocidal agents used for disinfection. J Hosp Infect. 2019; 103: 435–440. https://doi.org/10.1016/j.jhin.2019.08.014 PMID: 31449920

57. Gottardi W, Nagl M. Chlorine covers on living bacteria: the initial step in antimicrobial action of active chlorine compounds. J Antimicrob Chemother. 2005; 55: 475–482. https://doi.org/10.1093/jac/dki054 PMID: 15761074

58. Jackson DS, Crockett DF, Wolnik KA. The indirect detection of bleach (sodium hypochlorite) in beverages as evidence of product tampering. J Forensic Sci. 2006; 51: 827–831. https://doi.org/10.1111/j.1556-4029.2006.00160.x PMID: 16882227

59. Vandini A, Temmerman R, Frabetti A, Caselli E, Antonioli P, Balboni PG, et al. Hard Surface Biocontrol in Hospitals Using Microbial-Based Cleaning Products. PLoS One. 2014; 9: e108598. https://doi.org/10.1371/journal.pone.0108598 PMID: 25259528

60. Pereira SSP, de Oliveira HM, Turrini RNT, Lacerda RA. Disinfection with sodium hypochlorite in hospital environmental surfaces in the reduction of contamination and infection prevention: A systematic review. Rev da Esc Enferm. 2015; 49: 675–681. https://doi.org/10.1590/S0080-623420150000400020 PMID: 26353107

61. Choudhury GK, Chitumalla R, Manual L, Rajalbandi SK, Chauhan MS, Talukdar P. Disinfectant efficacy of 0.525% sodium hypochlorite and Epimax on alginate impression material. J Contemp Dent Pract. 2018; 19: 113–116. https://doi.org/10.5005/jp-journals-10024-2222 PMID: 29358546

62. Cai L, Wang H, Liang L, Wang G, Xu X, Wang H. Response of Formed-Biofilm of *Enterobacter cloacae*, *Klebsiella oxytoca*, and *Citrobacter freundii* to Chlorite-Based Disinfectants. J Food Sci. 2018; 83: 1326–1332. https://doi.org/10.1111/1750-3841.14149 PMID: 29668034

63. Centers for Disease Control and Prevention. Chemical Disinfectants |Guideline for Disinfection and Sterilization in Healthcare Facilities. 2008 [cited 5 Jun 2020]. Available: https://www.cdc.gov/infectioncontrol/guidelines/disinfection/disinfection-methods/chemical.html

64. Pires RH, De Fátima Da Silva J, Martins CHG, Almeida AMF, Soares CP, Mendes-Giannini MJS. Effectiveness of disinfectants used in hemodialysis against both Candida orthopsilosis and C. parapsilosis sensu stricto biofilms. Antimicrob Agents Chemother. 2013; 57: 2417–2421. https://doi.org/10.1128/AAC.01308-12 PMID: 23478969

65. Ba KT, Kang Bsc J, Ba KJ, Kyle AM. Evaluation of the antimicrobial efficacy and skin safety of a novel color additive in combination with chlorine disinfectants. Am J Infect Control. 2018; 46: 1254–1261. https://doi.org/10.1016/j.ajic.2018.04.223 PMID: 29803593

66. NCCLS. M44-A2 Method for Antifungal Disk Diffusion Susceptibility Testing of Yeasts; Approved Guideline-Second Edition. 2009. Available: www.clsi.org.

67. World Health Organization (WHO). Severe Acute Respiratory Infections Treatment Centre. 2020; 1–50.

68. Godoy G. Facial protection for healthcare workers during pandemics: a scoping review. BMJ Glob Heal. 2020; 5: 2553. https://doi.org/10.1136/bmjgh-2020-002553 PMID: 32371574

69. André CB, Santos A Dos, Pfeifer CS, Giannini M, Girotto EM, Ferracane JL. Evaluation of three different decontamination techniques on biofilm formation, and on physical and chemical properties of resin composites. J Biomed Mater Res B Appl Biomater. 2018; 106: 945–953. https://doi.org/10.1002/jbm.b.33907 PMID: 28440891

70. Anvisa. Brazilian Pharmacopoeia. 2019 [cited 9 Sep 2020] pp. 1–874. Available: http://portal.anvisa.gov.br/farmacopeia-brasileira

71. WHO. Environmental Monitoring of Clean Rooms in Vaccine Manufacturing Facilities Points to consider for manufacturers of human vaccines. 2012. Available: https://www.who.int/immunization_

standards/vaccine_quality/env_monitoring/en/#:~:text=Environmental Monitoring of Clean Rooms in Vaccine Manufacturing Facilities—Points,to submit vaccines for prequalification

72. Nishida K, Ishii M, Tsushima S, Hirai S. Detection of water vapor in cathode gas diffusion layer of polymer electrolyte fuel cell using water sensitive paper. J Power Sources. 2012; 199: 155–160. https://doi.org/10.1016/j.jpowsour.2011.10.026

73. Bansal N, Sinha I, Virdi JS. Virulence plasmid (pYV)-associated susceptibility of Yersinia enterocolitica to chlorine and heavy metals. J Appl Microbiol. 2000; 89: 663–667. https://doi.org/10.1046/j.1365-2672.2000.01164.x PMID: 11054171

74. Bagattini M, Buonocore R, Giannouli M, Mattiacci D, Bellopede R, Grimaldi N, et al. Effect of treatment with an overheated dry-saturated steam vapour disinfection system on multidrug and extensively drug-resistant nosocomial pathogens and comparison with sodium hypochlorite activity. BMC Res Notes. 2015; 8: 551. https://doi.org/10.1186/s13104-015-1534-9 PMID: 26452549

75. Sato-Boku A, Nagano K, Hasegawa Y, Kamimura Y, Sento Y, So MH, et al. Comparison of disinfection effect between benzalkonium chloride and povidone iodine in nasotracheal intubation: A randomized trial. BMC Anesthesiol. 2019; 19: 1–8. https://doi.org/10.1186/s12871-018-0673-7 PMID: 30611197

76. Kornacki JL, Gurtler JB, Stawick BA. Enterobacteriaceae, Coliforms, and Escherichia coli as Quality and Safety Indicators. 5th ed. In: Salfinger Y, Tortorello M Lou, editors. Compendium of Methods for the Microbiological Examination of Foods. 5th ed. Washington D.C: American Public Health Association; 2015. https://doi.org/10.2105/mbef.0222.014

77. U.S. Environmental Protection Agency. Method 1600: Enterococci in Water by Membrane Filtration Using membrane-Enterococcus Indoxyl-B-D-Glucoside Agar (mEI). EPA 821-R-02–022. Washington DC; 2002.

78. De Vries T, Hamilton M. Estimating the Antimicrobial Log Reduction: Part 1. Quantitative Assays. Quant Microbiol. 1999; 1: 29–45. https://doi.org/10.1023/A:1010072226737

79. CEN-European Committee for Standardization. EN 14561:2006: Chemical Disinfectants and Antiseptics. Quantitative Carrier Test for the Evaluation of Bactericidal Activity for Instruments Used in the Medical Area. Test Method and Requirements (Phase 2, Step 2). Brussels:; 2006. Available: https://www.sis.se/en/produkter/health-care-technology/sterilization-and-disinfection/disinfectants-and-antiseptics/ssen145612006/

80. Guridi A, Sevillano E, Fuente I de la, Mateo E, Eraso E, Quindós G. Disinfectant activity of a portable ultraviolet c equipment. Int J Environ Res Public Health. 2019; 16. https://doi.org/10.3390/ijerph16234747 PMID: 31783593

81. Kenters N, Huijskens EGW, de Wit SCJ, van Rosmalen J, Voss A. Effectiveness of cleaning-disinfection wipes and sprays against multidrug-resistant outbreak strains. Am J Infect Control. 2017; 45: e69–e73. https://doi.org/10.1016/j.ajic.2017.04.290 PMID: 28571980

82. CEN–European Committee for Standardization. EN 14562:2006—Chemical disinfectants and antiseptics. Quantitative carrier test for the evaluation of fungicidal or yeasticidal activity for instruments used in the medical area. Test method and requirements (phase 2, step 2)–BSI British Standards. Brussels; 2006. Available: https://shop.bsigroup.com/ProductDetail/?pid=000000000030137934

83. Kawamura M, Fujimura S, Tokuda K, Aoyagi T, Endo S, Kanamori H, et al. Mutant selection window of disinfectants for Staphylococcus aureus and Pseudomonas aeruginosa. J Glob Antimicrob Resist. 2019; 17: 316–320. https://doi.org/10.1016/j.jgar.2019.01.015 PMID: 30684653

84. Rizzotti L, Rossi F, Torriani S. Biocide and antibiotic resistance of Enterococcus faecalis and Enterococcus faecium isolated from the swine meat chain. Food Microbiol. 2016; 60: 160–164. https://doi.org/10.1016/j.fm.2016.07.009 PMID: 27554158

85. Fukuzaki S. Mechanisms of Actions of Sodium Hypochlorite in Cleaning and Disinfection Processes. Biocontrol Sci. 2006; 11: 147–157. https://doi.org/10.4265/bio.11.147 PMID: 17190269

86. Lineback CB, Nkemngong CA, Wu ST, Li X, Teska PJ, Oliver HF. Hydrogen peroxide and sodium hypochlorite disinfectants are more effective against Staphylococcus aureus and Pseudomonas aeruginosa biofilms than quaternary ammonium compounds. Antimicrob Resist Infect Control. 2018; 7: 1–7. https://doi.org/10.1186/s13756-017-0291-z PMID: 29312658

87. Yoo A, Rossi-Fedele G, Kidd SP, Rogers AH, Zilm PS. Association between Extracellular Material and Biofilm Formation in Response to Sodium Hypochlorite by Clinical Isolates of Enterococcus faecalis. J Endod. 2018; 44: 269–273. https://doi.org/10.1016/j.joen.2017.08.025 PMID: 29208399

88. Dadar M, Tiwari R, Karthik K, Chakraborty S, Shahali Y, Dhama K. Candida albicans—Biology, molecular characterization, pathogenicity, and advances in diagnosis and control–An update. Microb Pathog. 2018; 117: 128–138. https://doi.org/10.1016/j.micpath.2018.02.028 PMID: 29454824

89. Medeiros MAP, de Melo APV, de Oliveira Bento A, de Souza LBFC, de Assis Bezerra Neto F, Garcia JBL, et al. Epidemiology and prognostic factors of nosocomial candidemia in Northeast Brazil: A six-

year retrospective study. PLoS One. 2019; 14. https://doi.org/10.1371/journal.pone.0221033 PMID: 31437188

90. Tóth R, Nosek J, Mora-Montes HM, Gabaldon T, Bliss JM, Nosanchuk JD, et al. Candida parapsilosis: From genes to the bedside. Clin Microbiol Rev. 2019; 32: 1–38. https://doi.org/10.1128/CMR.00111-18 PMID: 30814115

91. Kumar JA, Eilertson B, Cadnum JL, Whitlow CS, Jencson AL, Safdar N, et al. Environmental Contamination with Candida Species in Multiple Hospitals Including a Tertiary Care Hospital with a Candida auris Outbreak. Pathog Immun. 2019; 4: 260–270. https://doi.org/10.20411/pai.v4i2.291 PMID: 31768483

92. Adams CE, Dancer SJ. Dynamic Transmission of Staphylococcus Aureus in the Intensive Care Unit. Int J Environ Res Public Health. 2020; 17: 2109. https://doi.org/10.3390/ijerph17062109 PMID: 32235764

93. Jeong MI, Park SY, Ha S Do. Effects of sodium hypochlorite and peroxyacetic acid on the inactivation of murine norovirus-1 in Chinese cabbage and green onion. Lwt. 2018; 96: 663–670. https://doi.org/10.1016/j.lwt.2018.06.019

94. Köhler AT, Rodloff AC, Labahn M, Reinhardt M, Truyen U, Speck S. Efficacy of sodium hypochlorite against multidrug-resistant Gram-negative bacteria. J Hosp Infect. 2018; 100: e40–e46. https://doi.org/10.1016/j.jhin.2018.07.017 PMID: 30026008

95. Sattar SA, Springthorpe VS, Karim Y, Loro P. Chemical disinfection of non-porous inanimate surfaces experimentally contaminated with four human pathogenic viruses. Epidemiol Infect. 1989; 102: 493–505. https://doi.org/10.1017/s0950268800030211 PMID: 2737256

96. Kampf G, Todt D, Pfaender S, Steinmann E. Persistence of coronaviruses on inanimate surfaces and their inactivation with biocidal agents. J Hosp Infect. 2020; 104: 246–251. https://doi.org/10.1016/j.jhin.2020.01.022 PMID: 32035997

97. Ma Q-X, Shan H, Zhang H-L, Li G-M, Yang R-M, Chen J-M. Potential utilities of mask-wearing and instant hand hygiene for fighting SARS-CoV-2. J Med Virol. 2020. https://doi.org/10.1002/jmv.25805 PMID: 32232986

98. Wolfe MK, Gallandat K, Daniels K, Desmarais AM, Scheinman P, Lantagne D. Handwashing and Ebola virus disease outbreaks: A randomized comparison of soap, hand sanitizer, and 0.05% chlorine solutions on the inactivation and removal of model organisms Phi6 and E. coli from hands and persistence in rinse water. PLoS One. 2017; 12: e0172734. https://doi.org/10.1371/journal.pone.0172734 PMID: 28231311

99. Cadnum JL, Shaikh AA, Piedrahita CT, Sankar T, Jencson AL, Larkin EL, et al. Effectiveness of disinfectants against candida auris and other candida species. Infect Control Hosp Epidemiol. 2017; 38: 1240–1243. https://doi.org/10.1017/ice.2017.162 PMID: 28793937

100. Montagna MT, Triggiano F, Barbuti G, Bartolomeo N, De Giglio O, Diella G, et al. Study on the in vitro activity of five disinfectants against Nosocomial bacteria. Int J Environ Res Public Health. 2019; 16. https://doi.org/10.3390/ijerph16111895 PMID: 31146343

101. Bonyadi Z, Mirzaee M, Ejtehadi MM, Mokhtari M. The bactericidal effect of simultaneous titanium oxide on common hospital bacteria. Environ Monit Assess. 2017; 189: 1–4. https://doi.org/10.1007/s10661-017-6049-5 PMID: 28623574

102. Fu L, Le T, Liu Z, Wang L, Guo H, Yang J, et al. Different efficacies of common disinfection methods against candida auris and other candida species. J Infect Public Health. 2020; 13: 730–736. https://doi.org/10.1016/j.jiph.2020.01.008 PMID: 32005617

103. Lemmer K, Pauli G, Howaldt S, Schwebke I, Mielke M, Grunow R. Decontamination of personal protective equipment. Heal Secur. 2019; 17: 200–212. https://doi.org/10.1089/hs.2019.0005 PMID: 31173501

104. Ilyas S, Srivastava RR, Kim H. Disinfection technology and strategies for COVID-19 hospital and biomedical waste management. Sci Total Environ. 2020; 749. https://doi.org/10.1016/j.scitotenv.2020.141652 PMID: 32822917

105. Diomedi Pacheco A, Chacón E, Delpiano L, Hervé B, Jemenao MI, Medel M, et al. Antiseptics and disinfectants: Aiming at rational use. recommendations of the advisory committee on healthcare associated infections. Sociedad Chilena de infectología. Rev Chil Infectol. 2017; 34: 156–174. https://doi.org/10.4067/S0716-10182017000200010 PMID: 28632831

106. Slaughter RJ, Watts M, Vale JA, Grieve JR, Schep LJ. The clinical toxicology of sodium hypochlorite. Clin Toxicol. 2019; 57: 303–311. https://doi.org/10.1080/15563650.2018.1543889 PMID: 30689457

107. Nikpour S, Masoumi-Moghaddam E, Pazoki S, Hassanian-Moghaddam H, Zamani N. Upper Gastrointestinal Endoscopic Evaluation Following Household Sodium Hypochlorite Ingestion. J Burn Care Res. 2017; 39: 1. https://doi.org/10.1097/BCR.0000000000000608 PMID: 28661987

Supporting information

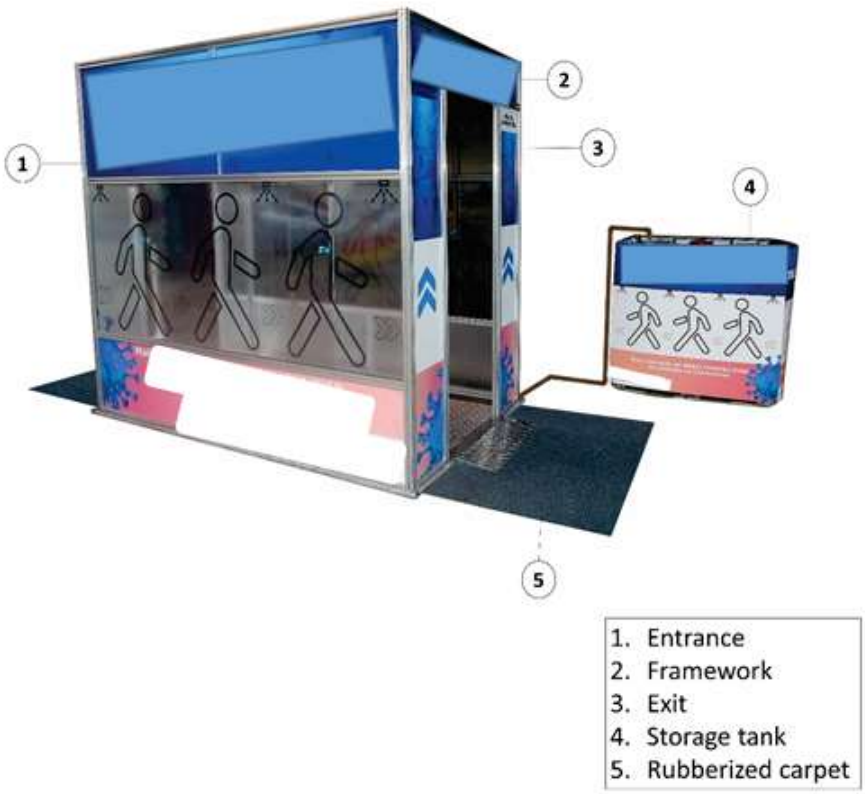

S1 Fig. Image of the disinfection chamber: spray disinfection technology for instant decontamination of personal protective equipment.

S2 Fig. Images of the manikin suitably dressed with PPEs used to simulate the use of the disinfection chamber by healthcare workers in nosocomial environments

S1 Table. Raw data of stability of sodium hypochlorite regarding pH and active chlorine analysis (mean ± standard deviation).

Time (days)	pH	Active chlorine (%)
0	12.3 ± 0.02	0.259 ± 0.01
3	12.2 ± 0.01	0.252 ± 0.001
6	12.3 ± 0.05	0.251 ± 0.001
10	12.3 ± 0.07	0.251 ± 0.001
13	12.3 ± 0.05	0.252 ± 0.005

4. ARTIGO II

Numerical and experimental analyses for the improvement of surface instant decontamination technology through biocidal agent dispersion: Potential of application during pandemic

Artigo publicado em ***PloS ONE*** 16(5): e0251817, 2021.

Paulo Roberto Freitas Neves[1], Turan Dias Oliveira[1], Tarcísio Faustino Magalhães[1], Paulo Roberto Santana dos Reis[1], Luzia Aparecida Tofaneli[1], Alex Álisson Bandeira Santos[1], Bruna Aparecida Souza Machado[1,2*], Fabricia Oliveira Oliveira[2], Leone Peter Correia da Silva Andrade[1,2], Roberto Badaró[2] and Luis Alberto Brêda Mascarenhas[1,2]

[1] SENAI CIMATEC, National Service of Industrial Learning – SENAI, Computational Modeling and Industrial Technology, University Center SENAI/CIMATEC, 41650-010, Salvador, Bahia, Brazil.
[2] SENAI CIMATEC, National Service of Industrial Learning – SENAI, SENAI Institute of Innovation (ISI) in Health Advanced Systems (CIMATEC ISI SAS), University Center SENAI/CIMATEC, 41650-010, Salvador, Bahia, Brazil.

DOI: 10.1371/journal.pone.0251817

Neste artigo foi avaliado, por meio de simulações CFD e ensaios experimentais, o desempenho de uma câmara de desinfecção projetada para aspersão instantânea de solução de agente biocida, e proposto ajustes na configuração melhorando a aspersão do agente biocida sobre as superfícies de contato e, consequentemente, a eficácia do equipamento desenvolvido. O detalhamento das condições de contorno da modelagem computacional desenvolvida, está disposto no Apêndice A.

Por ser um trabalho interdisciplinar, o artigo contou com o apoio de algumas áreas do SENAI CIMATEC, sendo: Área de Eficiência Energética, contribuiu para o projeto e desenvolvimento da nova configuração da câmara de desinfecção, metodologia, realização de ensaios experimentais e simulações CFD. Instituto SENAI de Inovação em Sistemas Avançados em Saúde, contribuiu com a metodologia e ensaios experimentais. No final do artigo são apresentadas as contribuições da cada um dos autores no desenvolvimento do trabalho.

PLOS ONE

RESEARCH ARTICLE

Numerical and experimental analyses for the improvement of surface instant decontamination technology through biocidal agent dispersion: Potential of application during pandemic

Paulo Roberto Freitas Neves[1], Turan Dias Oliveira[1], Tarcísio Faustino Magalhães[1], Paulo Roberto Santana dos Reis[1], Luzia Aparecida Tofaneli[1], Alex Álisson Bandeira Santos[1], Bruna Aparecida Souza Machado[1,2]*, Fabricia Oliveira Oliveira[2], Leone Peter Correia da Silva Andrade[1,2], Roberto Badaró[2], Luis Alberto Brêda Mascarenhas[1,2]

1 SENAI CIMATEC, National Service of Industrial Learning–SENAI, Computational Modeling and Industrial Technology, University Center SENAI/CIMATEC, Salvador, Bahia, Brazil, **2** SENAI CIMATEC, National Service of Industrial Learning–SENAI, SENAI Institute of Innovation (ISI) in Health Advanced Systems (CIMATEC ISI SAS), University Center SENAI/CIMATEC, Salvador, Bahia, Brazil

* brunam@fieb.org.br, brunamachado17@hotmail.com

Citation: Freitas Neves PR, Oliveira TD, Magalhães TF, dos Reis PRS, Tofaneli LA, Bandeira Santos AÁ, et al. (2021) Numerical and experimental analyses for the improvement of surface instant decontamination technology through biocidal agent dispersion: Potential of application during pandemic. PLoS ONE 16(5): e0251817. https://doi.org/10.1371/journal.pone.0251817

Editor: Amitava Mukherjee, VIT University, INDIA

Received: February 9, 2021

Accepted: April 28, 2021

Published: May 19, 2021

Data Availability Statement: All relevant data are within the paper.

Funding: The author(s) received no specific funding for this work.

Competing interests: The authors have declared that no competing interests exist.

Abstract

The transmission of SARS-CoV-2 through contact with contaminated surfaces or objects is an important form of transmissibility. Thus, in this study, we evaluated the performance of a disinfection chamber designed for instantaneous dispersion of the biocidal agent solution, in order to characterize a new device that can be used to protect individuals by reducing the transmissibility of the disease through contaminated surfaces. We proposed the necessary adjustments in the configuration to improve the dispersion on surfaces and the effectiveness of the developed equipment. Computational Fluid Dynamics (CFD) simulations of the present technology with a chamber having six nebulizer nozzles were performed and validated through qualitative and quantitative comparisons, and experimental tests were conducted using the method Water-Sensitive Paper (WSP), with an exposure to the biocidal agent for 10 and 30 s. After evaluation, a new passage procedure for the chamber with six nozzles and a new configuration of the disinfection chamber were proposed. In the chamber with six nozzles, a deficiency was identified in its central region, where the suspended droplet concentration was close to zero. However, with the new passage procedure, there was a significant increase in wettability of the surface. With the proposition of the chamber with 12 nozzles, the suspended droplet concentration in different regions increased, with an average increase of 266%. The experimental results of the new configuration proved that there was an increase in wettability at all times of exposure, and it was more significant for an exposure of 30 s. Additionally, even in different passage procedures, there were no significant differences in the results for an exposure of 10 s, thereby showing the effectiveness of the new configuration or improved spraying and wettability by the biocidal agent, as well as

in minimizing the impact caused by human factor in the performance of the disinfection technology.

Introduction

COVID-19, a disease characterized by a severe acute respiratory syndrome and caused by coronavirus-2 (SARS-CoV-2), first occurred in Wuhan, China and spread worldwide in a few weeks [1–4]. On March 11, 2020, the World Health Organization (WHO) declared COVID-19 to be a pandemic [5–7]. The United States, India, and Brazil are the three countries with the highest number of reported cases, representing 51% of the total SARS-CoV-2 infections worldwide [8].

Although there have been warnings about the threat of viruses that cause respiratory diseases [9], the SARS-CoV-2 virus has spread at an unprecedented rate, and there is an urgent need to formulate various approaches to face this pandemic [10–13]. The transmission of SARS-CoV-2 can occur through direct contact with contaminated surfaces or by air, mainly through direct contact with contaminated people and biological secretions [14–20]. Since the beginning of the pandemic, different countries adopted different challenging measures to reduce infection rates and avoid the collapse of health systems [21, 22]. A variety of non-pharmaceutical interventions were adopted, such as complete regional blockages, closing of non-essential activities/commerce, mass testing of the population, quarantine measures, tracking the infected, construction of hospitals for the treatment of COVID-19, and development of new disinfection technologies [23, 24]. Transmission through contact with contaminated surfaces or objects has been described as an important form of transmissibility [25, 26], which has even been demonstrated for SARS-CoV-2 [27, 28]. The search and evaluation of the efficacy of some biocidal agents and technologies that disinfect contaminated environments and surfaces is based on previous studies, mainly with related viruses, such as SARS-CoV (Severe Acute Respiratory Syndrome Coronavirus) and MERS (Middle Eastern Respiratory Syndrome Coronavirus) [29–31]. To date, there is no specific treatment for SARS-CoV-2, however, since the beginning of the pandemic, a race against time has begun to make a vaccine for disease prevention available quickly. Currently, the vaccination against COVID-19 could be achieved mainly through emergency approvals for use by the regulatory agencies in each country. These approvals are mechanisms to facilitate the use of medicines in emergency situations, that may be used (even if not officially approved), but if certain statutory criteria have been met, including for example, that there are no other available alternatives [32]. The disinfection measures are also part of this race for preventive methodologies, especially at the time when vaccines were not yet available and also during the vaccination process, since this process has not yet been able to cover the entire population.

Disinfection measures can help inhibit the transmissibility of the virus, provided that they are safe for use. When it comes to transmissibility, it is important to emphasize that several studies have been bringing more and more data about the importance of disinfection measures, given the virus' ability to stay alive in the environment for considerable periods of time. The environmental risks associated with COVID-19, such as the waste generated and contaminated by the virus, have been receiving great attention from researchers [33]. Hospitals, home care and quarantine facilities, for example, are generating a large amount of waste. Face masks, personal protective equipment (PPE), nitrile gloves, disposable caps, among others, despite the importance of their use for individual protection, are considerable sources of contamination. And for this reason, the concern with the disinfection measures applied to these residues is also important in the context of the pandemic [34, 35]. Still, it is worth to note that the search

for new disinfection measures can not only be applied to the current pandemic of COVID-19, but also to other situations that may occur in the future, since the growth in the number of infections associated with new diseases may become an increasingly frequent factor in the future.

Since the beginning of the pandemic, new technologies and protocols have been developed with the purpose of exercising microbial control efficiently, thereby targeting a reduction in the infection rate [36, 37]. Here, we discuss technologies that have been adopted to help combat contamination by SARS-CoV-2. For example, previous studies have demonstrated the benefits of using ultraviolet light devices for disinfecting hospital environments [38], portable devices with spray systems for surface decontamination [39], and disinfection chambers with different biocidal agents [40]. These new developments have been shown to assist in the control of microbial load based on evidence from tests on different microorganisms and have mainly been applied in nosocomial environments, which are one of the main public health problems worldwide [41, 42] and therefore have considerable potential for application during and after the COVID-19 pandemic.

An equipment was recently developed to disperse a solution containing biocidal materials for the instant disinfection of personal protective equipment (PPE), worn by healthcare workers when leaving hospital areas intended for treatment of patients with SARS-CoV-2 in some of the reference hospitals for the treatment of COVID-19 in Brazil. The evaluation of its effectiveness, safety, and acceptance among professionals was carried out through experimental tests using previously contaminated surfaces and qualitative analysis of the deposition of particles in the study regions [43], as well as by collecting information using structured questionnaires involving more than 400 professionals who have used it. This equipment, called disinfection chamber, was designed as an alternative strategy to the current possibilities of protection against COVID-19, and its objective is to decontaminate potential surfaces, such as PPE, which may contribute to the high transmission of SARS-CoV-2 among health professionals during the process of doffing step. It is worth mentioning that the use of this equipment may also be applied in other situations, not only in nosocomial environments, increasing the scope of protection to individuals.

In addition to the disinfection properties of the solution, the effectiveness of this technology is also dependent on the configuration and form of use of the equipment. The nozzle arrangement and passage procedure can influence the wettability of the surfaces and thus the disinfection performance [44].

Numerical simulations have been shown to be useful for assessing air flow and particulate trajectory, where it is important to understand the physical phenomenon for medical and research purposes [45–48]. Some studies have shown the development of disinfection chambers using CFD and have illustrated validation techniques using such type of simulations [44, 49]. Hence, CFD can be an interesting alternative for evaluating existing technologies or new propositions [49, 50].

Thus, this study evaluated the performance of a disinfection chamber designed for instantaneous dispersion of biocidal agent solution. We proposed the necessary adjustments in the configuration to improve the dispersion on surfaces and the effectiveness of the developed equipment. Therefore, different exposure times, passage procedures inside the chamber, and nebulizer nozzle configurations were evaluated to improve the application of the technology as an additional barrier against contamination by SARS-CoV-2.

Materials and methods

Experiments and numerical simulations were used to test a previously developed disinfection chamber [43]. The experimental tests were conducted with the objective of providing input

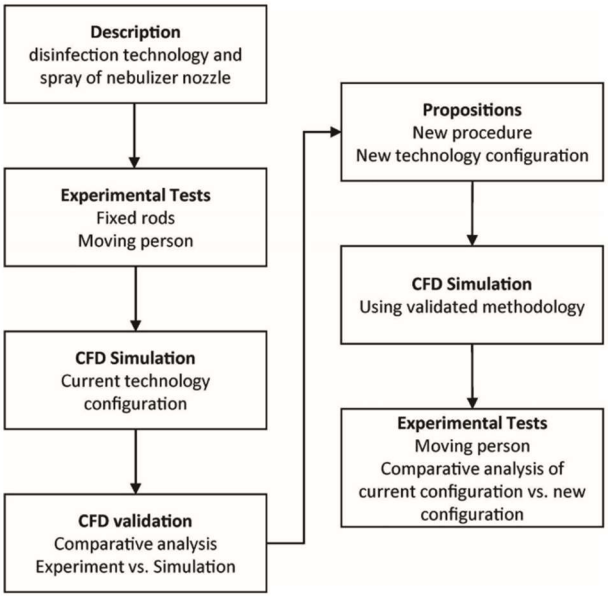

Fig 1. General scheme of the methodology used in this study to evaluate the performance of the disinfection technology (chamber) in relation to the dispersion of the biocidal agent.

https://doi.org/10.1371/journal.pone.0251817.g001

information for the simulations and comparative analyses, applying flow measurement methods, thermography, and water sensitive paper (WSPs) [33, 35, 51–55]. The simulations were carried out in two stages. The first stage involved the nebulizer nozzle to gain a proper understanding of the dispersion behavior in the nozzle, and the second stage was related to the effectiveness of the biocidal agent dispersion in the disinfection system (chamber). Fig 1 presents the scheme of the methodology applied in this study to evaluate the dispersion of the biocidal agent solution (aqueous solution of sodium hypochlorite with a concentration of up to 0.25%).

Disinfection technology (chamber)

The disinfection chamber used in this study was developed as a modular structure, with the dimensions 2,4 x 1,5 x 3,0 m (HxWxL), composed of aluminum profiles and closure in material acrylic and PVC (polyvinyl chloride). Internally, the chamber had a nebulization system composed of six nebulizer nozzles installed on the sides (horizontal position), ceiling (vertical position), a water filter, submerged pump, and storage tank with a capacity of 1000 L (Fig 2). A control unit was responsible for activating the system, with the presence sensor for activation of the nebulizer nozzles if an individual passed through the chamber [56, 57].

Characterization of the spray formed by the nebulizer nozzle

The spray formed by the nebulizer nozzle had different angles, droplet sizes, and flow rates. These variables were used as input data in the numerical simulations [47, 58–60]. Hence, the nozzle volumetric flow was determined by collecting three samples of solution volumes (one minute per sample) and then calculating the average volumetric flow.

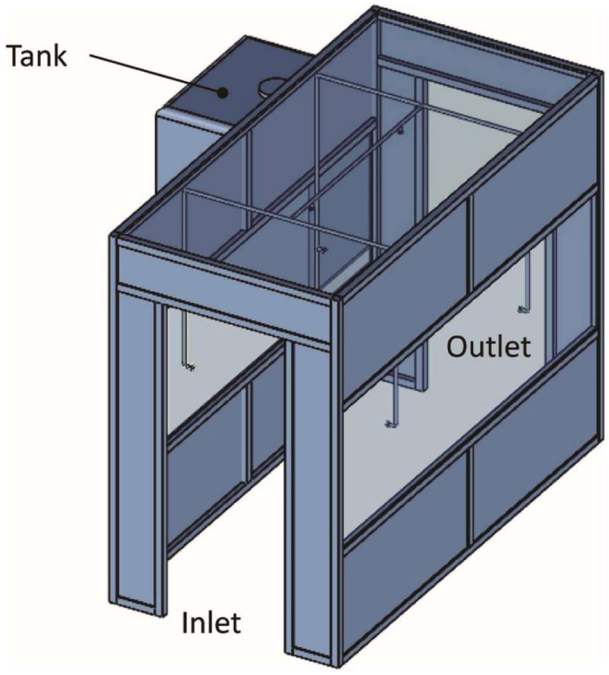

Fig 2. Representation of the disinfection chamber developed for instant decontamination of surfaces using biocidal agents.

https://doi.org/10.1371/journal.pone.0251817.g002

The angle formed by the spray was measured by collecting thermal images of the spray using a thermographic camera, according to the methodology proposed by Jiao et al. [60] obtained images to visualize the spray due to the difference between the temperatures of the fluid and the internal walls of the disinfection chamber. For the measurement of this parameter, six thermal images were captured at vertical and horizontal positions of the nozzle at different instants.

The measurement of the spray particle size was performed thrice, collecting droplets of the spray formed by the nebulizer nozzle using WSPs positioned in front of the nozzle at a distance of 65 mm. After collection, the WSPs were read using WSP reading technology (DropScope, Brazil). Thus, it was possible to detect overlapping droplets [61], with a minimum recorded size of 24.18 μm. The obtained data were compiled and adjusted to a Rosin–Rammler distribution function, suitable for representing the distribution of particles and droplets [62–64]. This distribution is characterized by a scale factor d_e and form factor γ.

Wettability analysis

Wettability analysis was performed using the WSP method in two different ways. Initially, 18 WSPs were applied to rods fixed in the ranges identified as 1, 2, and 3 arranged in the central area of the disinfection chamber, as shown in Fig 3A. Thus, the WSPs were exposed for a period of 10 s and then analyzed using DropScope technology, and the percentage of wet area of each WSP was calculated. In the second step, 44 WSPs were applied to different regions of the body of a person previously dressed with PPE (cap, glasses, mask, gloves, coat, and shoes)

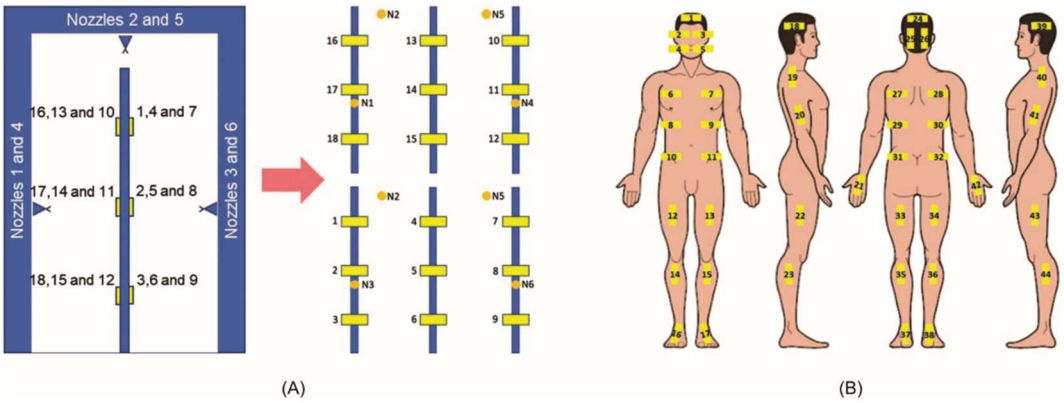

Fig 3. Illustration of the regions where WSPs were applied. (A) Experiment with the rods in the central area of the chamber; (B) experiment with the properly dressed individual in PPE.

https://doi.org/10.1371/journal.pone.0251817.g003

(Fig 3B) in order to qualitatively assess the wettability of the surfaces in different regions of the PPE during exposure in the disinfection chamber. For this analysis, two exposure times to the biocidal agent, 10 and 30 s, were used, where the individual made a 360˚ rotation during the passage through the chamber. Additionally, for 10 s exposure, the direct passage through the chamber was also evaluated (without turning in the center). All experimental tests for wettability analysis were performed twice.

Computational fluid dynamics

Simulation of nebulizer nozzle. To study the flow in the disinfection chamber, it was necessary to conduct simulations of the nebulizer nozzles to determine the speed of injection of the droplets. Here, ANSYS CFX 17.1 software was used to simulate the flow of nozzles. The modeled computational domain presents the geometric characteristics in which there is continuous flow of the solution before it leaves the nebulizer nozzle, as shown in Fig 4. The green region represents the internal part of the nebulizer nozzle, and the red extension is modeled for numerical stability.

The Eulerian approach through the finite volume method [65] was adopted to obtain the solution of the equations that describe the flow through the continuous medium of the nozzle. The method in question solves the equations of conservation of mass (continuity) and momentum (Navier-Stokes), described by Eqs 1–4:

$$\frac{\partial \rho}{\partial t} + div(\rho \vec{u}) = 0 \tag{1}$$

$$\frac{\partial(\rho u)}{\partial t} + div(\rho u \vec{u}) = -\frac{\partial p}{\partial x} + div(\mu\, grad\, u) + S_{Mx} \tag{2}$$

$$\frac{\partial(\rho v)}{\partial t} + div(\rho v \vec{u}) = -\frac{\partial p}{\partial y} + div(\mu\, grad\, v) + S_{My} \tag{3}$$

$$\frac{\partial(\rho w)}{\partial t} + div(\rho w \vec{u}) = -\frac{\partial p}{\partial z} + div(\mu\, grad\, w) + S_{Mz} \tag{4}$$

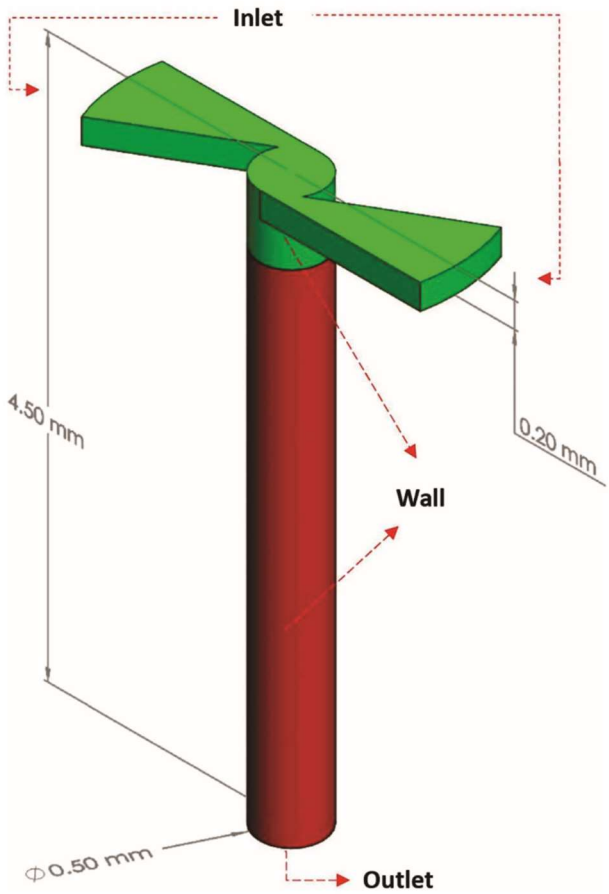

Fig 4. Computational domain illustration of the nebulizer nozzle.

https://doi.org/10.1371/journal.pone.0251817.g004

where p is the pressure; t is time; ρ is density; x, y, and z are the three Cartesian directions; u, v, and w are the speeds in the x, y, and z directions, respectively; $\vec{u}$ is the three-dimensional velocity vector; μ is the viscosity of the fluid; S_{Mx}, S_{My}, and S_{Mz} are the source terms of momentum in the directions x, y, and z, respectively. n the present simulation, the Shear Stress Transport (SST) k–ω turbulence model was used. The application of this model requires the solution of two more transport equations (one for turbulent kinetic energy, k, and another for turbulent frequency, ω), as shown in Eqs 5 and 6:

$$\frac{\partial(\rho k)}{\partial t} + div\left(\rho k \vec{u}\right) = div(\Gamma\, grad\, k) + S_k \tag{5}$$

$$\frac{\partial(\rho \omega)}{\partial t} + div\left(\rho \omega \vec{u}\right) = div(\Gamma\, grad\, \omega) + S_\omega \tag{6}$$

where S_k and S_ω are the source terms of k and ω, respectively. In the simulation of the flow of the nozzle to a stationary regiment, the derivatives in time are treated as zero.

In order to know if the turbulence model is being used appropriate, it is necessary to evaluate Yplus. The Yplus represents a dimensionless distance from the first node to the wall and, depending on the numerical treatment given to the boundary layer, turbulence models have different ranges suitable for Yplus values. The standard k- ε model, for example, requires an Yplus value on the wall between approximately 30 to 300. According to Salim and Cheah [66] for Yplus values below 30, the k—ε turbulence model is not suitable, being the SST k—ω model more appropriate, as it is a hybrid model between ok—ε and K–ω [67].Once the nozzle computational domain was modeled, it was discretized into control volumes for the application of the discretized governing equations. Fig 5 shows the computational mesh of the simulated geometry with 8,856,031 elements composed of tetrahedrals and pyramids.

For the developed dispersion chamber, it is possible to use different types of products with biocidal properties as well as different concentrations (for example, percentage of dilution in water). For this study, all experiments were performed using sodium hypochlorite at concentrations up to 0.25% as a biocidal agent [68]. Sodium hypochlorite is considered to be one of the most relevant and prevalent disinfectants for disinfecting surfaces against SARS-CoV-2 [69]. For the proposed numerical model, the physical properties were considered as identical to that of water [44]. Thus, they were valid for aqueous solutions of sufficiently low concentrations such that the properties were not significantly impacted. Table 1 shows the boundary conditions (according to the regions named in Fig 4) applied for the simulations with the six

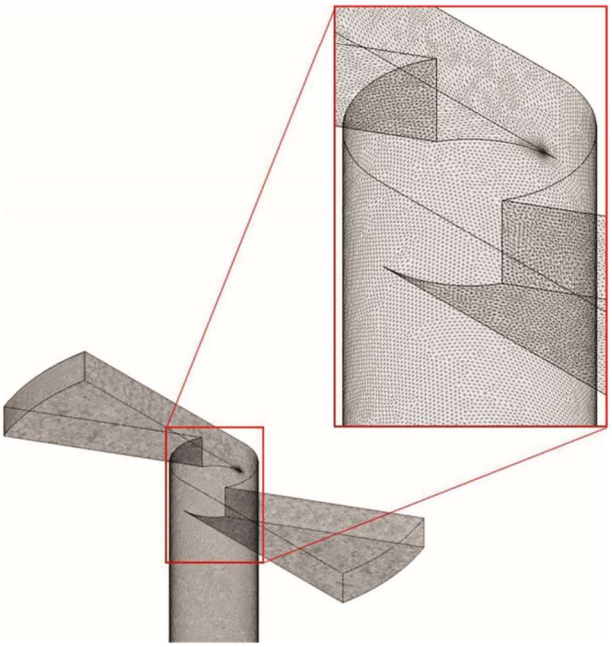

Fig 5. Computational mesh of the nebulizer nozzle.

https://doi.org/10.1371/journal.pone.0251817.g005

Table 1. Contour conditions of the disinfection chamber nebulizer nozzles.

Locations	Boundary Conditions
Inlet	Average flow rates for each nebulizer nozzle
Outlet	Atmosferic Pressure
Wall	No-slip wall

https://doi.org/10.1371/journal.pone.0251817.t001

nebulizer nozzles in the disinfection chamber. For this study, the flow was considered isothermal and incompressible.

Simulation of the disinfection technology (chamber). The disinfection technology (chamber) is represented by a fluid domain that contained the arrangement of the six nebulizer nozzles, as shown in Fig 6. The flow was analyzed through an Eulerian–Lagrangian approach, in which the internal region of the disinfection chamber (continuous medium–ambient air) interacts with the fluid particles (disperse medium) that are generated through the nebulizer nozzles [70, 71].

For the simulation of the disinfection chamber, the continuous medium (air) was treated with an Eulerian approach, using the same mass and moment conservation equations previously presented (Eqs 1–4) but in a transient regime. The biocidal agent solution was treated using a Lagrangian approach as a dispersed fluid (droplets). In this approach, the resulting force on each particle is the sum of the drag (F_D) and thrust (F_B) forces due to gravity [72]. The particle trajectory can be described according to Eqs 7 and 8:

$$F_p = F_D + F_B \tag{7}$$

$$m_p \frac{\partial v_p}{\partial t} = \frac{1}{2} * C_D \rho_f A_p \left(v_f - v_p\right) |v_f - v_p| + \frac{\pi}{6} * d_p^3 \left(\rho_p - \rho_f\right) * g \tag{8}$$

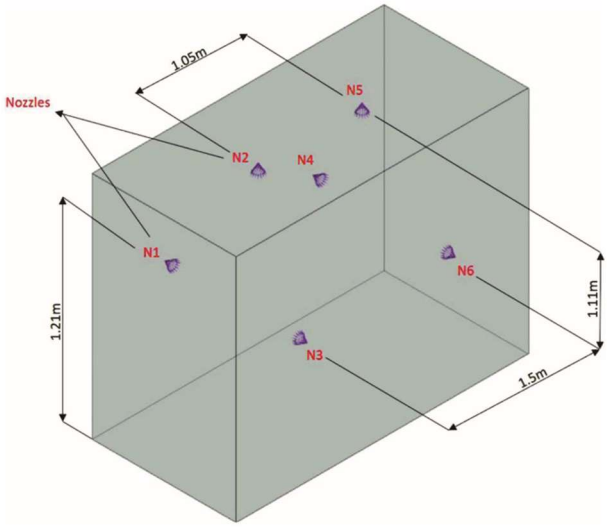

Fig 6. Computational domain of the disinfection chamber.

https://doi.org/10.1371/journal.pone.0251817.g006

where f indicates the value for the fluid, p indicates the value for the particle, m is the mass, C_D is the drag coefficient, ρ is the density, A is the frontal area, v is the speed, d is the diameter, and g is the gravity.

The drag coefficient is calculated using the Schiller–Naumann model [73], according to Eq 9:

$$C_D = \max\left(\frac{24}{Re} * (1 + 0.15Re^{0.687}), 0.44\right) \quad (9)$$

where Re is the Reynolds number.

Three meshes were evaluated for the disinfection chamber with different number of elements (approximately $6.6x10^5$, $1.3x10^6$, and $3.0x10^6$). Each nozzle was considered as a punctual injection of droplets, with mass flow rates defined according to the experimental results. The speeds were set such that they maintained the moment flow resulting from the nozzle simulations. The nozzle dispersion angle value was adopted as determined experimentally. The adopted particle size distribution was described by adjusting the Rosin–Rammler distribution function, which was also evaluated experimentally. All disinfection technology walls were considered "no-slip" with restitution coefficients equal to zero.

Ethics approval and consent to participate

This study was conducted after its approval by the Ethics and Research Committee of University Center SENAI/CIMATEC (No. 4,132,735), and by following the ethical principles and a written informed consent was obtained.

For this study, only one volunteer was recruited to perform the WSP tests. During the tests, the participant was properly dressed, using all PPE. To avoid contact of the biocidal agent with mucous membranes and skin, as well as to avoid inhalation of the spray formed, the participant used all PPE, including N95 mask, goggles, waterproof coat, gloves, protective shoe and cap.

The participant was followed throughout the study on any type of adverse event. The participant did not manifest or reported any adverse effects related to the use of the disinfection chamber and had no previous allergy to the tested biocidal agent.

The consent form was read and signed by the study volunteer. In addition, participant was also made aware of possible risks, such as the occurrence of an adverse event during or after the use of the chamber, and the benefits, such as reducing the SARS-CoV-2 spread rate.

Results and discussion

Spray characterization

Table 2 shows the flow rates for each nozzle and their respective standard deviations. The maximum relative deviation is 3.34%, showing that the individual measured values are slightly different from the average.

The angle formed by the spray in the two positions is 60˚. The captured thermal images (Fig 7) show profiles similar to the characteristic angle.

Bian et al. [74] performed experiments with the orientation angles of the nebulizer nozzle varying from 0˚ to 90˚. The spray cone angles measured through images varied between 60˚ and 62˚, showing that the angle formed by the spray was not affected by the nozzle orientation angle [74].

Fig 8 shows the cumulative particle size distribution (average of the data collected from the WSPs) and the Rosin–Rammler distribution function curve with $d_e = 78.6\ \mu m$ and $\gamma = 1.87$.

Table 2. Flow rates of the nebulizer nozzles.

	Flow rates Nozzles [L/h]					
Measurement	Nozzle 1	Nozzle 2	Nozzle 3	Nozzle 4	Nozzle 5	Nozzle 6
M1	5.58	5.70	7.50	7.80	5.52	6.72
M2	5.70	5.64	7.50	7.68	5.40	6.84
M3	5.70	6.00	7.50	7.74	5.34	6.90
Average	5.66	5.78	7.50	7.74	5.42	6.82
Standard deviation	0.07	0.19	0.00	0.06	0.09	0.09
	1.22%	3.34%	0.00%	0.78%	1.69%	1.34%

https://doi.org/10.1371/journal.pone.0251817.t002

The adjusted curve shows a coefficient of determination $R^2 = 0.998$, characterizing that the adjustment is valid for the representation of the experimental data.

Wettability analysis

The samples of the experiment carried out with WSPs applied to the three ranges inside the disinfection chamber and exposed to the biocidal agent for 10 s are shown in Fig 9. The percentages of the wet area for each WSP are also shown.

In the two samples, the areas affected by the solution of the biocidal agent were similar, showing that the method used for evaluation is acceptable. It should be noted that it was not possible to read the WSP with number 12 from sample 1 (Fig 9A). When comparing the WSPs numbered 12 of the two samples, a large difference is visually observed in the area affected by the biocidal agent during exposure. Thus, for this study, the WSP 12 obtained for sample 1 is not considered in the qualitative and quantitative analyses.

In range 2, corresponding to the central region of the disinfection chamber, no significant deposition of particles is observed. Therefore, this can be considered as a limitation of the functionality of the developed equipment and may compromise its effectiveness, regardless of the biocidal agent used (Fig 9).

In a study carried out by Joshi [44], it was observed (side view of the chamber) that even after 12 s of disinfectant dispersion, at regions close to the ends of the structure, the concentration of droplets in the suspension was lower than that in the regions close to the nebulizer nozzles. Thus, it can be guessed that if Joshi [44] experimentally evaluated the dispersion of droplets using the WSP method, the results would be close to those of the samples presented in Fig 9. However, the central region would have a higher concentration of suspended droplets in relation to the ends of the developed chamber.

Simulation

Fig 11A illustrates the Yplus contours for the walls of the simulation for the nebulizer nozzle and represents the dimensionless distance to the first computational node. The maximum

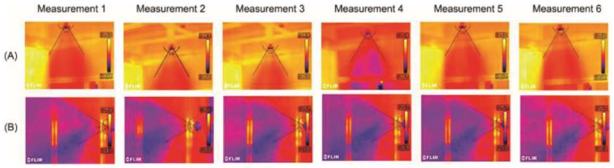

Fig 7. Measurement of the angle formed by the spray generated in the nebulizer nozzles. (A) Vertical position; (B) Horizontal position.

https://doi.org/10.1371/journal.pone.0251817.g007

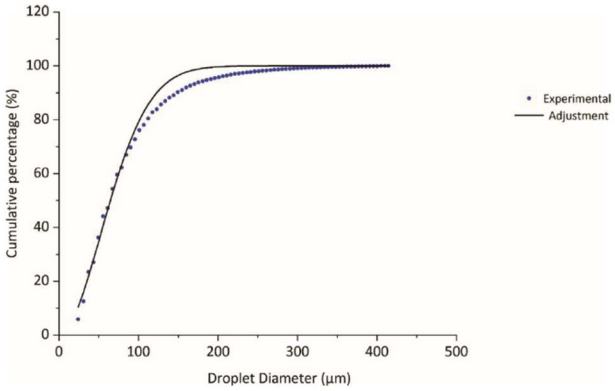

Fig 8. Rosin–Rammler distribution function for the data collected from the WSPs.

https://doi.org/10.1371/journal.pone.0251817.g008

value of Yplus is 14, thus validating the methodology used for the treatment of the turbulence. This is because the use of the SST model presents good solutions in the treatment close to the wall for a wide range of Yplus [67].

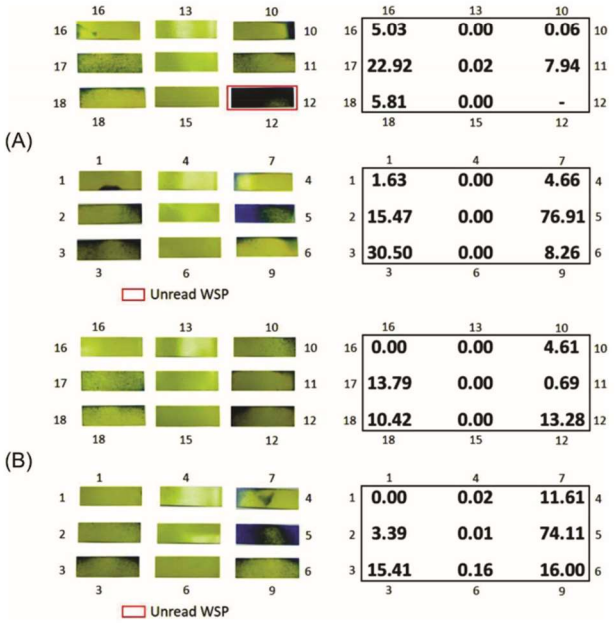

Fig 9. WSPs exposed to the biocidal agent for 10 s and their percentage wet area values. (A) Sample 1; (B) Sample 2.

https://doi.org/10.1371/journal.pone.0251817.g009

Table 3. Flow rates and velocities of the fluid at the exit of the disinfection chamber nebulizer nozzles.

	Nozzles					
	1	2	3	4	5	6
Guidance	Horizontal	Horizontal	Vertical	Horizontal	Vertical	Horizontal
Mass Flow (g/s)	1.57	1.61	2.08	2.15	1.51	1.89
Velocity (m/s)	35.5	33.9	42.6	49.1	35.8	44.5

https://doi.org/10.1371/journal.pone.0251817.t003

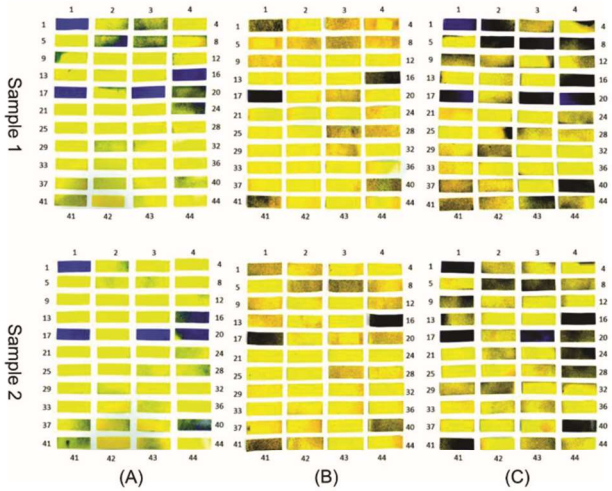

Fig 10. WSPs applied to the body of an individual properly dressed in PPE and exposed to the biocidal agent in the disinfection chamber composed of six nozzles. (A) Exposure for 10 s without turning in the central area of the chamber; (B) exposure for 10 s with 360˚ rotation in the central area of the chamber; (C) exposure for 30 s with 360˚ rotation in the central area of the chamber.

https://doi.org/10.1371/journal.pone.0251817.g010

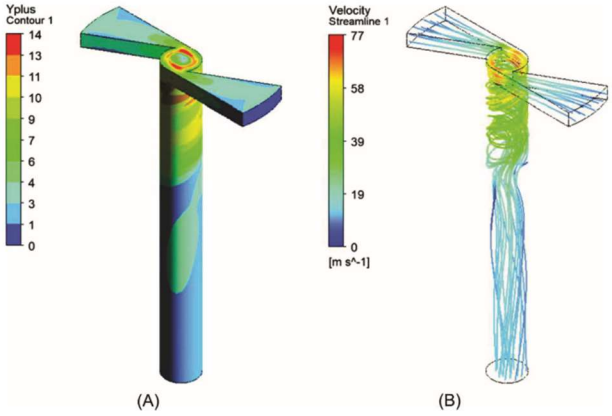

Fig 11. Contours of the nebulizer nozzle. (A) Yplus; (B) Streamline.

https://doi.org/10.1371/journal.pone.0251817.g011

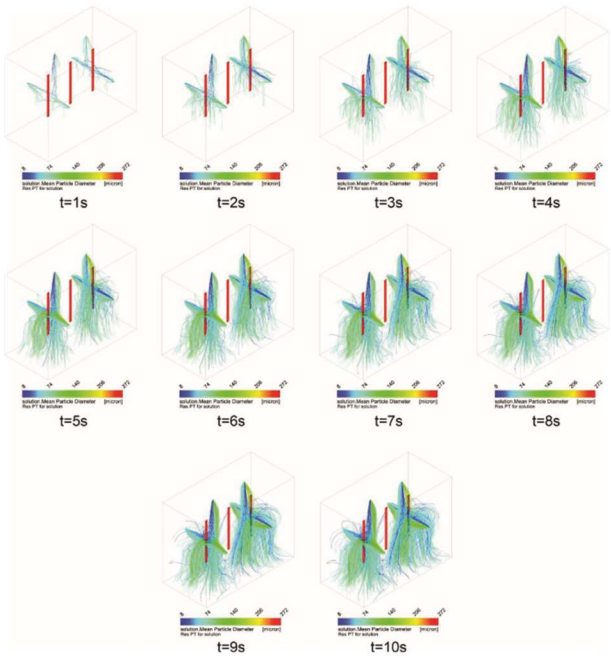

Fig 13. Dispersion of the droplets generated by the six nebulizer nozzles in the disinfection chamber during the exposure time of 10 s.

https://doi.org/10.1371/journal.pone.0251817.g013

where ρ_{ar} is the specific mass, V_{relmax} is the maximum relative speed, d_{pmax} is the maximum droplet diameter, σ is the surface tension, and Oh is the Ohnesorge number.

In the calculation of the critical Weber number (We_{crit}), only positive values greater than 12 can be achieved. However, in the calculation of the maximum Weber number, consideration of the maximum values for velocity V_{rel} and droplet diameter d_p results in a value of 7.12, thereby meeting the criterion of no secondary rupture.

Fig 13 shows the dispersion of the particles over a time of 10 s for the current configuration of six nozzles of the disinfection chamber. As previously described, the intensity of the flow of droplets is evaluated in the ranges 1, 2, and 3 (Fig 3A), and it is observed that the intensity of the flow increases up to 10 s (Fig 13). It is verified that, in the region of range 2, even within the time of 10 s, there is insignificant concentration of suspended droplets. From the results, a new procedure is proposed for the passage/use of the disinfection chamber, where the need for 360˚ rotation is modified compared to the central region of the chamber (more specifically in range 2). Thus, based on the simulation results, a new method is proposed with two 360˚ turns in two different regions of the disinfection chamber (with six projected nozzles). The turning positions should be fixed in the regions with the highest volume of droplets dispersed inside the chamber, i.e., in the regions identified as ranges 1 and 3. It is noted that the droplets that hit the ground at t = 9 s and t = 10 s (Fig 13) stop recirculating within the environment. This occurs because the restitution coefficients are zero, similar to the physical phenomenon in which droplets adhere to solid surfaces [75, 76].

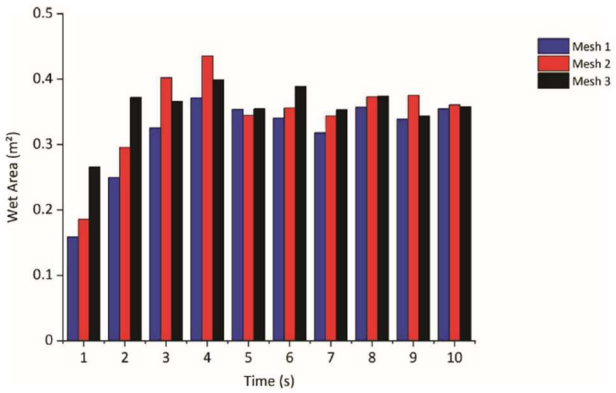

Fig 12. Mesh convergence study.

https://doi.org/10.1371/journal.pone.0251817.g012

Fig 11B shows the representation of the current lines of flow inside the nebulizer nozzles. It is observed that, owing to the geometric characteristics of the nebulizer nozzle, the highest speeds occur when the flow is redirected to the circular section outlet, causing "swirl" zones.

Table 3 shows the results obtained for the speeds with each average flow of the nebulizer nozzles, which are the boundary conditions for the simulation. The Reynolds number (Re) assumes a minimum value of 4,484 and a maximum value of 6,403, varying according to the average flow of the nozzles.

To analyze the mesh convergence (an important parameter for the stability of the simulation), the wet area results were used in the simulation, along with varying the mesh refinement. Fig 12 shows the results of the wet area in the central plane of the studied device for three different meshes at each instant of time up to a total of 10 s. Meshes 1, 2, and 3 have approximately $6.6x10^5$, $1.3x10^6$, and $3.0x10^6$ elements, respectively. The average relative discrepancy between the results of meshes 2 and 1 is 9.38%, and that between meshes 3 and 2 is 9.36%. Hence, we used mesh 2 to obtain a good relationship between processing time and accuracy.

The injection of particles can occur in two atomization regimes. These include primary atomization, which occurs in the initial conditions for the droplets that leave the nozzle, and secondary atomization, which occurs when the external forces act on the droplets and generate smaller droplets. The secondary rupture of the particles occurs when their Weber number is greater than the critical Weber number [73]:

$$We_{crit} < \mathrm{We}$$

For the evaluation of the maximum Weber number, Eqs 10–12 are used.

$$We_{max} = \frac{\rho_{ar} * V_{relmax}^2 * d_{pmax}}{\sigma} \tag{10}$$

$$We_{crit} = 12 * (1 + 1,077 * Oh^{1,6}) \tag{11}$$

$$\mathrm{Oh} = \frac{\mu_{solução}}{\sqrt{\rho_{solução} * \sigma * d_p}} \tag{12}$$

In another study, Joshi [44] presented the results of CFD simulations based on 12-s dispersion times within the developed chamber. However, it was not informed whether the droplets that touched the solid walls of the structure or the floor were discarded. This information is important because, in practice, when a droplet touches a solid surface, it is not dispersed in air (for negligible air velocity on the surface). Without this consideration, the result of the dispersion of droplets in a certain time may be erroneous because some droplets may hit solid surfaces and no longer recirculate in that region.

Comparative analysis of simulation and experimental tests

The angle of the spray formed by the nebulizer nozzle in the simulation shows a behavior close to the angle measured in the experiment, as shown in Fig 14. In Fig 15, the average percentages of the wet area in each of the three ranges are shown, according to the experimental results (Fig 9) and the percentages of the numerical simulation. The results show an agreement between the experiment and simulation. Once again, it is identified that in range 2, there is no dispersion of droplets and that the greatest dispersion occurs in the region of range 3. The experimental results thus confirm that the simulation yields results that identify the need for proposals to achieve improvements in the configuration of the disinfection chamber for better performance, which is the objective of this study. In Fig 16, the dispersion contours of the droplets for nozzles N1 (horizontal) and N2 (vertical) are shown. Distance d1 (Fig 16A) is greater than d3 (Fig 16C) in the front view, and distance d2 (Fig 16B) is greater than d4 (Fig 16D) in the side view of the camera. A greater dispersion of the droplets for the nozzle is

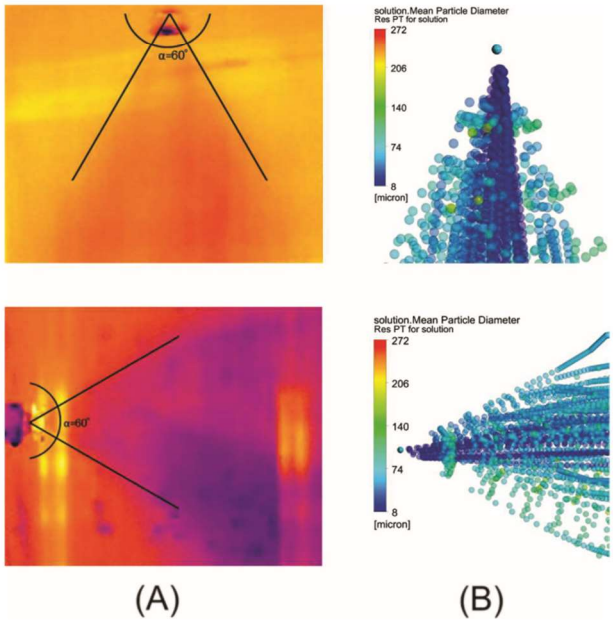

Fig 14. Angle formed by the spray on the nebulizer nozzles in the vertical and horizontal positions. (A) Thermal image; (B) CFD simulation.

https://doi.org/10.1371/journal.pone.0251817.g014

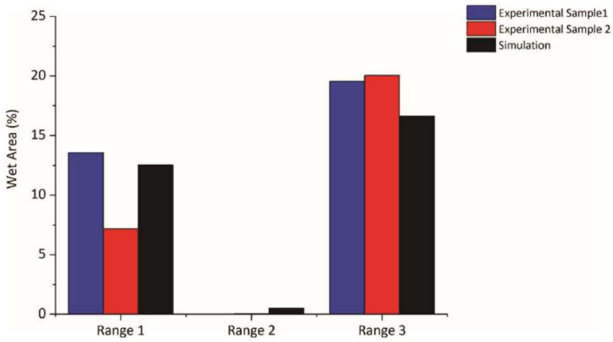

Fig 15. Percentage of wet area in the ranges analyzed inside the disinfection chamber with six nebulizer nozzles (experimental and simulation results).

https://doi.org/10.1371/journal.pone.0251817.g015

observed in the horizontal position compared to the vertical position. Hence, a new configuration of the chamber is proposed in this study. The nozzles must be positioned horizontally to improve the dispersion of droplets in the environment and consequently the effectiveness of the disinfection chamber.

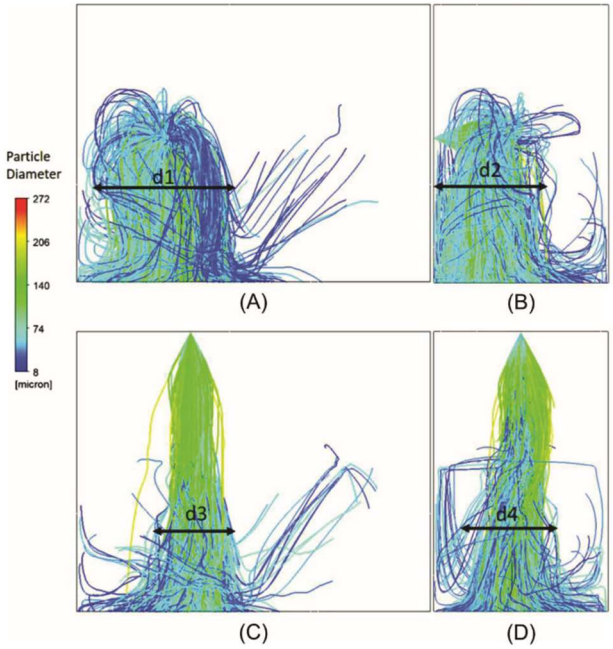

Fig 16. Contours of the nozzles N1 and N2. (A) Front view and (B) Side view of the horizontal nozzle (N1); (C) Front view and (D) Side view of the vertical nozzle (N2).

https://doi.org/10.1371/journal.pone.0251817.g016

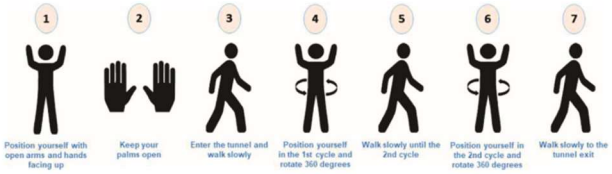

Fig 17. Newly proposed passage procedure for using the disinfection chamber.

https://doi.org/10.1371/journal.pone.0251817.g017

Proposed new procedure of using the disinfection chamber

From the experimental and simulation results obtained for the dispersion of the biocidal agent solution in range 2 of the previously developed disinfection chamber, a new passage procedure can be proposed, as shown in Fig 17. According to the proposal, the individual performs two complete 360˚ turns in the regions of ranges 1 and 3, where there is a higher concentration of suspended droplets. Hence, there is greater possibility of the biocidal agent adhering to the surface of the PPE. This can improve the performance of the disinfection chamber, considering that the proposed use is to promote the instant disinfection of PPE before the doffing step.

The proposed new procedure was tested experimentally, and improvement was confirmed with an increase in WSP wettability. Fig 18 shows the results obtained for the analysis with the WSPs (two samples from the experiment carried out under the same conditions). From the comparative analysis between the tests performed within the passage procedure with a 360˚ turn in the central area of the chamber (range 2) (Fig 10C) and with two turns in ranges 1 and 3 of the chamber (Fig 18), the improvement in the use of the disinfection chamber is demonstrated. However, to increase the operational reliability of the system and to ensure that users utilize the technology in the best possible manner, a new configuration for the equipment itself is also proposed with 12 nozzles. It is worth mentioning that the proposed new construction configuration addresses the understanding of the functioning and influence of human factors in human–machine interaction. This is because, in integrated and complex systems, reducing failures requires an understanding of the complexity of human functioning and its cognitive processes [77, 78].

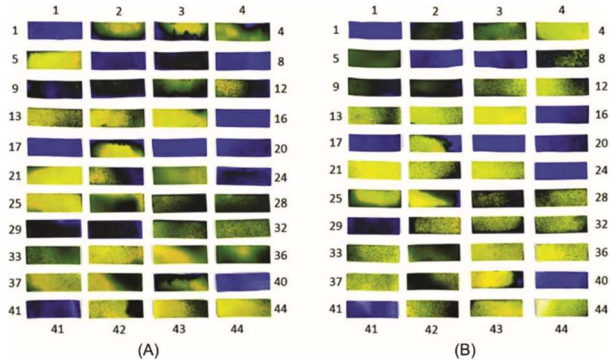

Fig 18. WSPs applied to different regions of the body of an individual properly dressed with PPE and exposed to the biocidal agent during passage through the disinfection chamber with six nozzles in 30 s. (A) Sample 1; (B) Sample 2.

https://doi.org/10.1371/journal.pone.0251817.g018

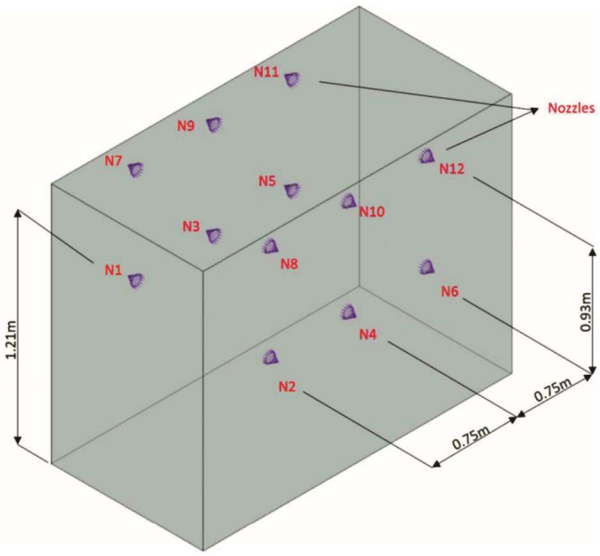

Fig 19. New proposed configuration for the disinfection chamber designed with 12 nebulizer nozzles.

https://doi.org/10.1371/journal.pone.0251817.g019

New proposed configuration for the disinfection chamber

Geometry. After the simulation analysis, a new configuration is proposed for the chamber, using 12 horizontally mounted nozzles, which allows greater wettability capacity of the exposed area. The new proposed configuration is shown in Fig 19. The wettability allows the uniform and homogeneous action of the biocidal agent in the application of the chamber and its use for instant disinfection of contaminated surfaces. In the proposed configuration, all 12 nozzles are positioned horizontally, with two nozzles at different heights for each side of ranges 1, 2, and 3 (Fig 19). The proposed configuration also aims to minimize possible interference related to human factors. Thus, even if the user passes through the interior of the chamber without making a complete 360° turn in the center of the chamber, the arrangement can ensure that droplets of the biocidal agent solution are deposited on the surface of interest.

Simulation. Fig 20 shows the dispersion of the solution over time (10 s) for the new configuration proposed for the disinfection chamber, i.e., with 12 nebulizer nozzles. Thus, the intensity of the flow of droplets is evaluated in the ranges 1, 2, and 3 for 10 s, and an increased flow intensity is observed for this new configuration, as compared to the previous configuration of six nozzles. Significantly improved droplet deposition behavior is observed in the region of range 2 (Figs 13 and 20). It is noteworthy that in this configuration, the region of range 2 behaves similar to the ranges 1 and 3, and the suspended droplets are capable of reaching the surfaces of all areas evaluated in this study.

Fig 21 presents the results for the percentage of wet area in the ranges 1, 2, and 3 obtained from the simulations of chamber configurations with six and twelve nebulizer nozzles. The comparative analysis in relation to the percentage of the wet area shows that the proposed new configuration significantly increases the suspended droplet configuration in all the studied ranges. It is important to highlight that, with the new configuration, range 2 represents the region with the highest concentration of suspended droplets (39.94%) (represented by the

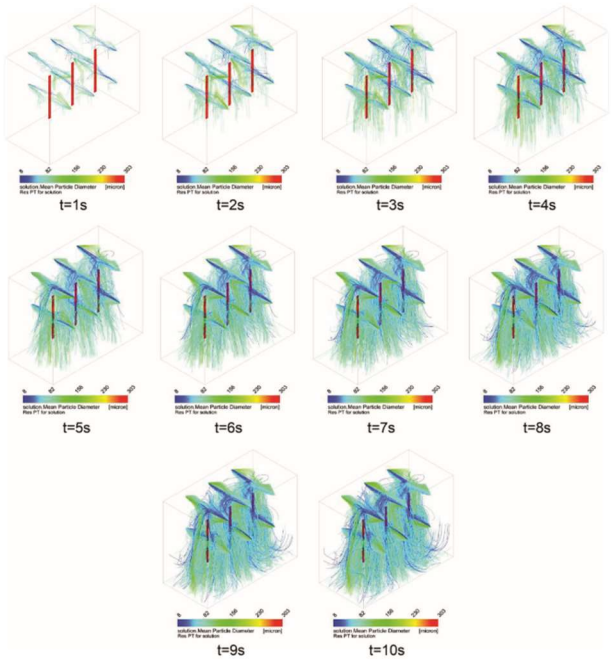

Fig 20. Dispersion of the droplets generated by the 12 nebulizer nozzles according to the new configuration of the disinfection chamber.

https://doi.org/10.1371/journal.pone.0251817.g020

central area of the disinfection chamber), thus demonstrating the potential for application of the proposed new configuration.

Experimental tests. To confirm the simulation results with the new configuration, experiments were also carried out to analyze the wettability using WSPs, and the results are shown in

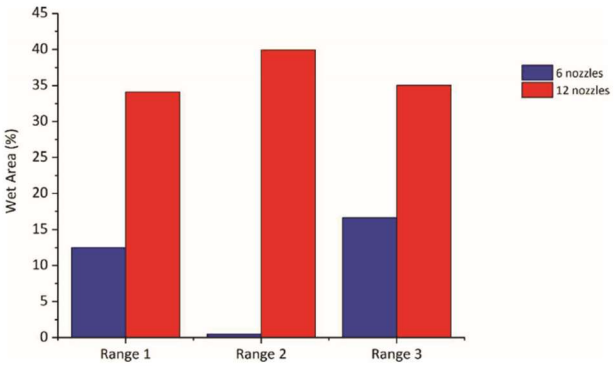

Fig 21. Percentage of wet area in the configurations analyzed for the disinfection chamber with 6 and 12 nebulizer nozzles.

https://doi.org/10.1371/journal.pone.0251817.g021

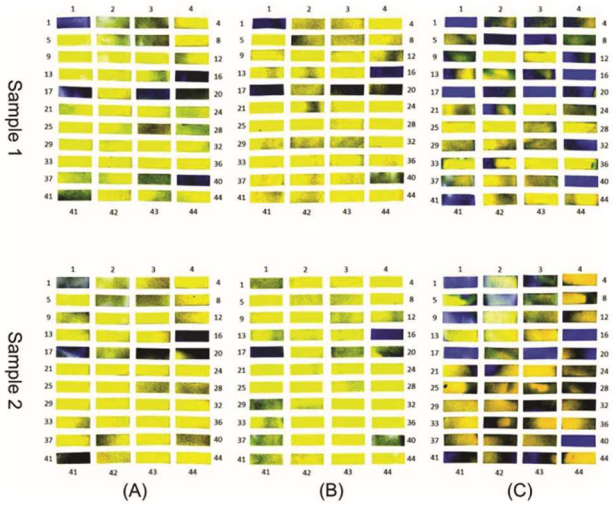

Fig 22. WSPs applied to the body and exposed to the biocidal agent (12 nozzles). (A) Exposed for 10 s without turning; (B) Exposed for 10s with turning in the center; (C) Exposed for 30 s with turning in the center.

https://doi.org/10.1371/journal.pone.0251817.g022

Fig 22. From this analysis, a similar wettability pattern is observed. This pattern is justified by WSPs 1, 16, 17, 19, 20, and 40, which wet more intensively in all samples, even with different exposure times and passage procedures. It is also observed that the WSPs exposed to the biocidal agent for 30 s (Fig 22C) have the highest droplet deposition. Another important detail is that, for the same time of 10 s, the WSPs in Fig 22A and 22B show similar wettability.

Comparison of wettability between the chambers with six and 12 nozzles. From the comparative analysis between the chambers with six nozzles (Fig 13) and twelve nozzles (Fig 20), the configuration with greater number of nozzles shows better performance with respect to the dispersion of droplets, covering all the equipment. In this way, and as previously mentioned, even if users perform turns in different regions between ranges 1 and 3, greater wettability is achieved when compared to the procedure of turning in the center of the equipment in the configuration with six nozzles. In Fig 21, it is evident that there is a significant increase in the concentration of suspended droplets in the regions between the ranges 1 and 3. In addition, comparing the WSPs of the experimental tests shown in Figs 10 and 22, it is observed that there is an increase in the wet area (blue color) in all experiments. This increase is more significant for the exposure time of 30 s (Figs 10C and 22C). Another important detail is that even though the passage procedure was performed differently (Fig 22A and 22B), the WSPs show similar behavior. This is in contrast to the WSPs obtained for the chamber with six nozzles (Fig 10A and 10B). Thus, with the new configuration, the human factor can be significantly minimized.

This study demonstrated the effectiveness of aspersion the disinfection chamber. Thus, these technical parameters and data found can help subsidize an increase in scale for the equipment tested, in future development studies, since the technical characteristics of construction and application of the equipment were amply explained in this research. This may allow a greater expansion of the application of this equipment through its distribution to other sites, covering a larger number of hospitals, for example, or other areas where the principle of the technology can be applied for the decontamination of potential surfaces.

Conclusion

The experimental tests were carried out twice and showed similar results, thus demonstrating that the applied methodology is adequate for the proposed study. It is important to say that the evaluation performed was for the passage of one person at a time inside the chamber. However, the possibility of more than one person at a time may be considered in future studies, applying the same evaluation of the new configuration performed in this study to affirm the non-interference in the results by passing through the chamber in a shared manner.

The mesh of the geometry used in the numerical simulations shows good convergence, and its parameters are within the reported range in literature. Comparing the experimental and simulation results of the current configuration, it is concluded that the use of the CFD tool is sufficient to understand the flow behavior within the chamber. A good agreement between the numerical and experimental results was observed. This model can be used to propose new configurations for the disinfection technology.

The mathematical model was validated, and simulations of the proposed new configuration were performed. The simulation results confirm that the proposed configuration increases the wettability of the human body. In this new configuration, it is possible to considerably increase the suspended droplets in ranges 1, 2, and 3. The droplet concentration increases from 12.53% to 34.11% in range 1, from 0.51% to 39.94% in range 2, and from 16.65% to 35.05% in range 3.

The experimental results of the new configuration prove that there is an increase in wettability at all exposure times, and it is more significant for an exposure time of 30 s. Even with different passage procedures, there are no significant differences in the results, thus demonstrating the effectiveness of the new configuration in minimizing the impact of human factors on the disinfection technology.

The present study is limited to the geometry conditions of the disinfection chamber and the operational parameters studied (either through simulation or experimentally). Conclusions about other conditions need to be evaluated since the flow profiles may undergo significant changes.

Acknowledgments

The authors thank the Bahia Department of Health (Secretaria de Saúde do Estado da Bahia–SESAB), Directorate of Sanitary and Environmental Surveillance of Bahia (Diretoria de Vigilância Sanitária e Ambiental do Estado da Bahia–DIVISA BA), and Hospital Espanhol of Salvador (COVID-19 Campaign Hospital).

Author Contributions

Conceptualization: Paulo Roberto Freitas Neves, Turan Dias Oliveira, Luzia Aparecida Tofaneli, Alex Álisson Bandeira Santos, Bruna Aparecida Souza Machado, Leone Peter Correia da Silva Andrade, Roberto Badaró, Luis Alberto Brêda Mascarenhas.

Data curation: Tarcísio Faustino Magalhães, Paulo Roberto Santana dos Reis, Luzia Aparecida Tofaneli, Alex Álisson Bandeira Santos, Bruna Aparecida Souza Machado, Roberto Badaró, Luis Alberto Brêda Mascarenhas.

Formal analysis: Paulo Roberto Freitas Neves, Turan Dias Oliveira, Tarcísio Faustino Magalhães, Paulo Roberto Santana dos Reis, Luzia Aparecida Tofaneli, Alex Álisson Bandeira Santos, Bruna Aparecida Souza Machado, Fabricia Oliveira Oliveira, Leone Peter Correia da Silva Andrade, Luis Alberto Brêda Mascarenhas.

Investigation: Paulo Roberto Freitas Neves, Turan Dias Oliveira, Luzia Aparecida Tofaneli, Alex Álisson Bandeira Santos, Bruna Aparecida Souza Machado, Roberto Badaró, Luis Alberto Brêda Mascarenhas.

Methodology: Paulo Roberto Freitas Neves, Turan Dias Oliveira, Tarcísio Faustino Magalhães, Paulo Roberto Santana dos Reis, Luzia Aparecida Tofaneli, Alex Álisson Bandeira Santos, Bruna Aparecida Souza Machado, Fabricia Oliveira Oliveira, Luis Alberto Brêda Mascarenhas.

Project administration: Alex Álisson Bandeira Santos, Bruna Aparecida Souza Machado, Leone Peter Correia da Silva Andrade, Roberto Badaró, Luis Alberto Brêda Mascarenhas.

Software: Paulo Roberto Freitas Neves, Paulo Roberto Santana dos Reis, Alex Álisson Bandeira Santos, Fabricia Oliveira Oliveira.

Supervision: Alex Álisson Bandeira Santos, Bruna Aparecida Souza Machado, Leone Peter Correia da Silva Andrade, Luis Alberto Brêda Mascarenhas.

Validation: Alex Álisson Bandeira Santos, Bruna Aparecida Souza Machado, Leone Peter Correia da Silva Andrade, Roberto Badaró, Luis Alberto Brêda Mascarenhas.

Visualization: Paulo Roberto Freitas Neves, Roberto Badaró, Luis Alberto Brêda Mascarenhas.

Writing – original draft: Paulo Roberto Freitas Neves, Turan Dias Oliveira, Tarcísio Faustino Magalhães, Paulo Roberto Santana dos Reis, Luzia Aparecida Tofaneli, Alex Álisson Bandeira Santos, Bruna Aparecida Souza Machado, Leone Peter Correia da Silva Andrade, Roberto Badaró, Luis Alberto Brêda Mascarenhas.

References

1. Weber DJ, Kanamori H, Rutala WA. 'No touch' technologies for environmental decontamination. Curr Opin Infect Dis. 2016; 29: 424–431. https://doi.org/10.1097/QCO.0000000000000284 PMID: 27257798
2. Donskey CJ. Decontamination devices in health care facilities: Practical issues and emerging applications. Am J Infect Control. 2019; 47: A23–A28. https://doi.org/10.1016/j.ajic.2019.03.005 PMID: 31146846
3. Shereen MA, Khan S, Kazmi A, Bashir N, Siddique R. COVID-19 infection: Emergence, transmission, and characteristics of human coronaviruses. J Adv Res. 2020; 24: 91–98. https://doi.org/10.1016/j.jare.2020.03.005 PMID: 32257431
4. Wang L, Didelot X, Yang J, Wong G, Shi Y, Liu W, et al. Inference of person-to-person transmission of COVID-19 reveals hidden super-spreading events during the early outbreak phase. Nat Commun. 2020; 11: 5006. https://doi.org/10.1038/s41467-020-18836-4 PMID: 33024095
5. Rudberg A-S, Havervall S, Månberg A, Jernbom Falk A, Aguilera K, Ng H, et al. SARS-CoV-2 exposure, symptoms and seroprevalence in healthcare workers in Sweden. Nat Commun. 2020; 11: 5064. https://doi.org/10.1038/s41467-020-18848-0 PMID: 33033249
6. World Health Organization. WHO Director-General's opening remarks at the media briefing on COVID-19–11 March 2020. In: WHO [Internet]. 2020 [cited 10 Sep 2020]. Available: www.who.int/dg/speeches/detail/who-director-general-s-opening-remarks-at-the-media-briefing-on-covid-19—11-march-2020
7. Bertacchini F, Bilotta E, Pantano PS. On the temporal spreading of the SARS-CoV-2. Di Gennaro F, editor. PLoS One. 2020; 15: e0240777. https://doi.org/10.1371/journal.pone.0240777 PMID: 33119625
8. Johns Hopkins University & Medicine. Global Map—OVID-19 Dashboard by the Center for Systems Science and Engineering (CSSE). In: Baltimore. 2020.
9. Shi Z, Gewirtz AT. Together forever: Bacterial–viral interactions in infection and immunity. Viruses. MDPI AG; 2018. https://doi.org/10.3390/v10030122 PMID: 29534424
10. Wojewodzic MW. Bacteriophages Could Be a Potential Game Changer in the Trajectory of Coronavirus Disease (COVID-19). PHAGE. 2020; 1: 60–65. https://doi.org/10.1089/phage.2020.0014

11. Moozhipurath RK, Kraft L, Skiera B. Evidence of protective role of Ultraviolet-B (UVB) radiation in reducing COVID-19 deaths. Sci Rep. 2020; 10: 17705. https://doi.org/10.1038/s41598-020-74825-z PMID: 33077792
12. Anderson RM, Heesterbeek H, Klinkenberg D, Hollingsworth TD. How will country-based mitigation measures influence the course of the COVID-19 epidemic? Lancet. 2020; 395: 931–934. https://doi.org/10.1016/S0140-6736(20)30567-5 PMID: 32164834
13. Zhang B, Zhou H, Zhou F. Study on SARS-CoV-2 transmission and the effects of control measures in China. PLoS One. 2020; 15: e0242649. https://doi.org/10.1371/journal.pone.0242649 PMID: 33253212
14. De Vitis R, Passiatore M, Perna A, Proietti L, Taccardo G. COVID-19 contagion and contamination through hands of trauma patients: what risks and what precautions? J Hosp Infect. 2020; 105: 354–355. https://doi.org/10.1016/j.jhin.2020.03.037 PMID: 32259547
15. Gambardella C, Pagliuca R, Pomilla G, Gambardella A. COVID-19 risk contagion: Organization and procedures in a South Italy geriatric oncology ward. J Geriatr Oncol. 2020; 11: 1187–1188. https://doi.org/10.1016/j.jgo.2020.05.008 PMID: 32467027
16. Koçak Tufan Z, Kayaaslan B. Crushing the curve, the role of national and international institutions and policy makers in COVID-19 pandemic. Turkish J Med Sci. 2020; 50: 495–508. https://doi.org/10.3906/sag-2004-167 PMID: 32299201
17. Rothe C, Schunk M, Sothmann P, Bretzel G, Froeschl G, Wallrauch C, et al. Transmission of 2019-nCoV Infection from an Asymptomatic Contact in Germany. N Engl J Med. 2020; 382: 970–971. https://doi.org/10.1056/NEJMc2001468 PMID: 32003551
18. Younes N, Al-Sadeq DW, AL-Jighefee H, Younes S, Al-Jamal O, Daas HI, et al. Challenges in Laboratory Diagnosis of the Novel Coronavirus SARS-CoV-2. Viruses. 2020; 12: 582. https://doi.org/10.3390/v12060582 PMID: 32466458
19. Kampf G, Todt D, Pfaender S, Steinmann E. Persistence of coronaviruses on inanimate surfaces and their inactivation with biocidal agents. J Hosp Infect. 2020; 104: 246–251. https://doi.org/10.1016/j.jhin.2020.01.022 PMID: 32035997
20. Di Carlo P, Chiacchiaretta P, Sinjari B, Aruffo E, Stuppia L, De Laurenzi V, et al. Air and surface measurements of SARS-CoV-2 inside a bus during normal operation. Moore G, editor. PLoS One. 2020; 15: e0235943. https://doi.org/10.1371/journal.pone.0235943 PMID: 33151953
21. Yabe T, Tsubouchi K, Fujiwara N, Wada T, Sekimoto Y, Ukkusuri S V. Non-compulsory measures sufficiently reduced human mobility in Tokyo during the COVID-19 epidemic. Sci Rep. 2020; 10: 18053. https://doi.org/10.1038/s41598-020-75033-5 PMID: 33093497
22. Dobrovolny HM. Modeling the role of asymptomatics in infection spread with application to SARS-CoV-2. Lo Iacono G, editor. PLoS One. 2020; 15: e0236976. https://doi.org/10.1371/journal.pone.0236976 PMID: 32776963
23. Flaxman S, Mishra S, Gandy A, Unwin HJT, Mellan TA, Coupland H, et al. Estimating the effects of non-pharmaceutical interventions on COVID-19 in Europe. Nature. 2020; 584: 257–261. https://doi.org/10.1038/s41586-020-2405-7 PMID: 32512579
24. Bhatia R. Need for integrated surveillance at human-animal interface for rapid detection & response to emerging coronavirus infections using One Health approach. Indian J Med Res. 2020; https://doi.org/10.4103/ijmr.IJMR_623_20 PMID: 32202259
25. Henwood AF. Coronavirus disinfection in histopathology. J Histotechnol. 2020; 43: 102–104. https://doi.org/10.1080/01478885.2020.1734718 PMID: 32116147
26. World Health Organization. Modes of transmission of virus causing COVID-19: implications for IPC precaution recommendations. In: Genebra [Internet]. 2020 [cited 20 Oct 2020]. Available: https://www.who.int/news-room/commentaries/detail/modes-of-transmission-of-virus-causing-covid-19-implications-for-ipc-precaution-recommendations
27. Otter JA, Donskey C, Yezli S, Douthwaite S, Goldenberg SD, Weber DJ. Transmission of SARS and MERS coronaviruses and influenza virus in healthcare settings: the possible role of dry surface contamination. J Hosp Infect. 2016; 92: 235–250. https://doi.org/10.1016/j.jhin.2015.08.027 PMID: 26597631
28. Chan JF-W, Yuan S, Kok K-H, To KK-W, Chu H, Yang J, et al. A familial cluster of pneumonia associated with the 2019 novel coronavirus indicating person-to-person transmission: a study of a family cluster. Lancet. 2020; 395: 514–523. https://doi.org/10.1016/S0140-6736(20)30154-9 PMID: 31986261
29. Drosten C, Günther S, Preiser W, van der Werf S, Brodt H-R, Becker S, et al. Identification of a Novel Coronavirus in Patients with Severe Acute Respiratory Syndrome. N Engl J Med. 2003; 348: 1967–1976. https://doi.org/10.1056/NEJMoa030747 PMID: 12690091
30. Zaki AM, van Boheemen S, Bestebroer TM, Osterhaus ADME, Fouchier RAM. Isolation of a Novel Coronavirus from a Man with Pneumonia in Saudi Arabia. N Engl J Med. 2012; 367: 1814–1820. https://doi.org/10.1056/NEJMoa1211721 PMID: 23075143

31. Whitworth J. COVID-19: a fast evolving pandemic. Trans R Soc Trop Med Hyg. 2020; 114: 241–248. https://doi.org/10.1093/trstmh/traa025 PMID: 32198918

32. U.S Food & Drug Administration. Emergency Use Authorization for Vaccines Explained [Internet]. 2020 [cited 12 Apr 2021]. Available: v/vaccines-blood-biologics/vaccines/emergency-use authorization-vaccines-explained%22 https://www.fda.gov/vaccines-blood-biologics/vaccines/emergency-use authorization-vaccines-explained

33. Barcelo D. An environmental and health perspective for COVID-19 outbreak: Meteorology and air quality influence, sewage epidemiology indicator, hospitals disinfection, drug therapies and recommendations. J Environ Chem Eng. 2020; 8: 104006. https://doi.org/10.1016/j.jece.2020.104006 PMID: 32373461

34. Singh N, Tang Y, Ogunseitan OA. Environmentally Sustainable Management of Used Personal Protective Equipment. Environ Sci Technol. 2020; 54: 8500–8502. https://doi.org/10.1021/acs.est.0c03022 PMID: 32597663

35. Ilyas S, Srivastava RR, Kim H. Disinfection technology and strategies for COVID-19 hospital and biomedical waste management. Sci Total Environ. 2020; 749: 141652. https://doi.org/10.1016/j.scitotenv.2020.141652 PMID: 32822917

36. Ning P, Shan D, Hong E, Liu L, Zhu Y, Cui R, et al. Disinfection performance of chlorine dioxide gas at ultra-low concentrations and the decay rules under different environmental factors. J Air Waste Manage Assoc. 2020; 70: 721–728. https://doi.org/10.1080/10962247.2020.1769768 PMID: 32412353

37. Silva DF, Toledo Neto JL, Machado MF, Bochnia JR, Garcez AS, Foggiato AA. Effect of photodynamic therapy potentiated by ultrasonic chamber on decontamination of acrylic and titanium surfaces. Photodiagnosis Photodyn Ther. 2019; 27: 345–353. https://doi.org/10.1016/j.pdpdt.2019.06.011 PMID: 31279916

38. Dellinger EP. Prevention of Hospital-Acquired Infections. Surg Infect (Larchmt). 2016; 17: 422–426. https://doi.org/10.1089/sur.2016.048 PMID: 27248978

39. Cadnum JL, Jencson AL, Livingston SH, Li DF, Redmond SN, Pearlmutter B, et al. Evaluation of an electrostatic spray disinfectant technology for rapid decontamination of portable equipment and large open areas in the era of SARS-CoV-2. Am J Infect Control. 2020; 48: 951–954. https://doi.org/10.1016/j.ajic.2020.06.002 PMID: 32522608

40. Ishikawa S, Ueno S, Mitsui M, Matsumura Y, Hatsuoka T. Construction of Its Evaluation System in Originally Designed Test-Chamber System and Sporicidal Activity of Aerosolized Hypochlorite Solution to Bacillus subtilis Spores. Biocontrol Sci. 2019; 24: 57–65. https://doi.org/10.4265/bio.24.57 PMID: 30880314

41. World Health Organization. Prevention of Hospital-Acquired Infections: A Practical Guide. In: Genebra. 2002.

42. Carter H, Weston D, Betts N, Wilkinson S, Amlôt R. Public perceptions of emergency decontamination: Effects of intervention type and responder management strategy during a focus group study. West JC, editor. PLoS One. 2018; 13: e0195922. https://doi.org/10.1371/journal.pone.0195922 PMID: 29652927

43. Mascarenhas LAB, Alex Alisson BS, Roberto B, Leone PC da SA, Bruna ASM. Potential application of novel technology developed for instant decontamination of personal protective equipment before the doffing step. PLoS One. 2021;

44. Joshi JR. COVSACK: an innovative portable isolated and safe COVID-19 sample collection kiosk with automatic disinfection. Trans Indian Natl Acad Eng. 2020; 5: 269–275. https://doi.org/10.1007/s41403-020-00139-1

45. Mutuku JK, Hou W-C, Chen W-H. An Overview of Experiments and Numerical Simulations on Airflow and Aerosols Deposition in Human Airways and the Role of Bioaerosol Motion in COVID-19 Transmission. Aerosol Air Qual Res. 2020; 20: 1172–1196. https://doi.org/10.4209/aaqr.2020.04.0185

46. Peng S, Chen Q, Liu E. The role of computational fluid dynamics tools on investigation of pathogen transmission: Prevention and control. Sci Total Environ. 2020; 746: 142090. https://doi.org/10.1016/j.scitotenv.2020.142090 PMID: 33027870

47. Gao N, Niu J. Transient CFD simulation of the respiration process and inter-person exposure assessment. Build Environ. 2006; 41: 1214–1222. https://doi.org/10.1016/j.buildenv.2005.05.014 PMID: 32287998

48. Shin E, Kim JJ, Lee S, Ko KS, Rhee BD, Han J, et al. Hemodynamics in diabetic human aorta using computational fluid dynamics. Chalmers J, editor. PLoS One. 2018; 13: e0202671. https://doi.org/10.1371/journal.pone.0202671 PMID: 30138473

49. Hariharan P, D'Souza GA, Horner M, Morrison TM, Malinauskas RA, Myers MR. Use of the FDA nozzle model to illustrate validation techniques in computational fluid dynamics (CFD) simulations. Borazjani I, editor. PLoS One. 2017; 12: e0178749. https://doi.org/10.1371/journal.pone.0178749 PMID: 28594889

50. Liu Y-Y, Yang G, Xu Y, Peng F, Wang L-Q. Effect of space diffuser on flow characteristics of a centrifugal pump by computational fluid dynamic analysis. Gurka R, editor. PLoS One. 2020; 15: e0228051. https://doi.org/10.1371/journal.pone.0228051 PMID: 32012173

51. Syngenta Crop Protection. Water-Sensitive Paper. In: Syngenta [Internet]. 2002 [cited 2 Sep 2020]. Available: https://www.syngenta.com.au/awri#:~:text=Water-sensitive paper is a,need the addition of dye.

52. Cunha M, Carvalho C, Marcal ARS. Assessing the ability of image processing software to analyse spray quality on water-sensitive papers used as artificial targets. Biosyst Eng. 2012; 111: 11–23. https://doi.org/10.1016/j.biosystemseng.2011.10.002

53. Nishida K, Ishii M, Tsushima S, Hirai S. Detection of water vapor in cathode gas diffusion layer of polymer electrolyte fuel cell using water sensitive paper. J Power Sources. 2012; 199: 155–160. https://doi.org/10.1016/j.jpowsour.2011.10.026

54. Özlüoymak ÖB, Bolat A. Development and assessment of a novel imaging software for optimizing the spray parameters on water-sensitive papers. Comput Electron Agric. 2020; 168: 105104. https://doi.org/10.1016/j.compag.2019.105104

55. Lipiński AJ, Lipiński S. Binarizing water sensitive papers–how to assess the coverage area properly? Crop Prot. 2020; 127: 104949. https://doi.org/10.1016/j.cropro.2019.104949

56. ANVISA. Technical Note no 38/2020 / SEI / COSAN / GHCOS / DIRE3 / ANVISA of May 7, 2020—It presents recommendations on the disinfection of people in public environments and hospitals during the Covid-19 pandemic. In: Brazil [Internet]. 2020 [cited 5 Aug 2020]. Available: https://coronavirus.rs.gov.br/upload/arquivos/202006/12142016-nota-tecnica-28-anvisa-2020-desinfeccao-de-pessoas.pdf

57. Surveillance. D of S and E. Ordinance No. 002, of May 25, 2020. Authorizes the use of equipment, with tested effectiveness, for decontamination of dressing in hospital environments. Official Gazette of Bahia. Salvador, Ba, 29 May. 2020. In: Brazil [Internet]. 2020 [cited 30 Aug 2020]. Available: http://www.saude.ba.gov.br/wp-content/uploads/2020/05/PORTARIA-DIVISA-N°-002-2020-DE-25-DE-MAIO-DE-2020.pdf

58. Beji T, Zadeh SE, Maragkos G, Merci B. Influence of the particle injection rate, droplet size distribution and volume flux angular distribution on the results and computational time of water spray CFD simulations. Fire Saf J. 2017; 91: 586–595. https://doi.org/10.1016/j.firesaf.2017.03.040

59. Fathinia F, Khiadani M, Al-Abdeli YM. Experimental and mathematical investigations of spray angle and droplet sizes of a flash evaporation desalination system. Powder Technol. 2019; 355: 542–551. https://doi.org/10.1016/j.powtec.2019.07.081

60. Jiao L, Dong D, Feng H, Zhao X, Chen L. Monitoring spray drift in aerial spray application based on infrared thermal imaging technology. Comput Electron Agric. 2016; 121: 135–140. https://doi.org/10.1016/j.compag.2015.12.006

61. Sprayx. Dropscope—Operation manual. In: Dropscope [Internet]. 2020 [cited 20 Sep 2020]. Available: https://www.sprayx.com.br/ds/

62. Jain M, John B, Iyer KN, Prabhu SV. Characterization of the full cone pressure swirl spray nozzles for the nuclear reactor containment spray system. Nucl Eng Des. 2014; 273: 131–142. https://doi.org/10.1016/j.nucengdes.2014.02.025

63. Zhang H, Luo M, Pan X, Zheng Q. Numerical analysis of gas turbine inlet fogging nozzle manifold resistance. Proc Inst Mech Eng Part A J Power Energy. 2016; 230: 63–75. https://doi.org/10.1177/0957650915616279

64. Bayat H, Rastgo M, Mansouri Zadeh M, Vereecken H. Particle size distribution models, their characteristics and fitting capability. J Hydrol. 2015; 529: 872–889. https://doi.org/10.1016/j.jhydrol.2015.08.067

65. Versteeg H., Malalasekera W. An introduction to Computational Fluid Dynamics: The Finite Volume Method. [Internet]. Second. Technical LS, editor. England: Edinburgh Gate; 1995. Available: http://ftp.demec.ufpr.br/disciplinas/TM702/Versteeg_Malalasekera_2ed.pdf

66. Salim S, Cheah S. Wall y+ strategy for dealing with wall-bounded turbulent flows. Proceedings of the International MultiConference of Engineers and Computer Scientists. 2009. pp. 1–6. Available: http://citeseerx.ist.psu.edu/viewdoc/download?doi=10.1.1.149.722&rep=rep1&type=pdf

67. Menter FR. Review of the shear-stress transport turbulence model experience from an industrial perspective. Int J Comut Fluid Dyn. 2009; 23: 305–316. https://doi.org/10.1080/10618560902773387

68. World Health Organization. Water, sanitation, hygiene, and waste management for SARS-CoV-2, the virus that causes COVID-19: Interim guidance. 29 July 2020. In: Genebra [Internet]. 2020 [cited 22 Sep 2020]. Available: https://www.who.int/publications/i/item/water-sanitation-hygiene-and-waste-management-for-the-covid-19-virus-interim-guidance

69. Kampf G. Potential role of inanimate surfaces for the spread of coronaviruses and their inactivation with disinfectant agents. Infect Prev Pract. 2020; 2: 100044. https://doi.org/10.1016/j.infpip.2020.100044

70. Delele MA, Vorstermans B, Creemers P, Tsige AA, Tijskens E, Schenk A, et al. Investigating the performance of thermonebulisation fungicide fogging system for loaded fruit storage room using CFD model. J Food Eng. 2012; 109: 87–97. https://doi.org/10.1016/j.jfoodeng.2011.09.030

71. Pinilla JA, Asuaje M, Ratkovich N. Study of a fogging system using a computational fluid dynamics simulation. Appl Therm Eng. 2016; 96: 228–239. https://doi.org/10.1016/j.applthermaleng.2015.10.117

72. Ali M, Yan C, Sun Z, Wang J, Gu H. CFD simulation of dust particle removal efficiency of a venturi scrubber in CFX. Nucl Eng Des. 2013; 256: 169–177. https://doi.org/10.1016/j.nucengdes.2012.12.013

73. Incorporation A. ANSYS CFX—Solver Modeling Guide. 2011.

74. Bian J, Zhang D, Sun R, Wu Y, Tian W, Su GH, et al. Experimental study on spray characteristics of pressure-swirl nozzle in China advanced PWR containment. Nucl Eng Des. 2019; 350: 158–175. https://doi.org/10.1016/j.nucengdes.2019.05.013

75. Breuninger P, Krull F, Huttenlochner K, Müller-Reno C, Ziegler C, Merz R, et al. Microstructuring of steel surfaces via cold spraying with 316L particles for studying the particle-wall collision behavior. Surf Coatings Technol. 2019; 379: 125054. https://doi.org/10.1016/j.surfcoat.2019.125054

76. Asgari B, Amani E. An improved spray-wall interaction model for Eulerian-Lagrangian simulation of liquid sprays. Int J Multiph Flow. 2021; 134: 103487. https://doi.org/10.1016/j.ijmultiphaseflow.2020.103487

77. Reason J. Human Error [Internet]. Cambridge University Press; 1990. https://doi.org/10.1017/CBO9781139062367

78. Henriqson E, Saurin TA. Análise do campo conceitual da engenharia de sistemas cognitivos e proposta de uma nova agenda de pesquisa. Production. 2013; 24: 405–419. https://doi.org/10.1590/S0103-65132013005000056

5. CONCLUSÃO

Uma câmara de desinfecção foi projetada e construída em estrutura modular com dimensões 2,4 x 1,5 x 3,0 m (AxLxC) com de alumínio e fechamento em material acrílico e PVC. Para armazenamento e transporte do agente biocida, foi utilizado um reservatório de 1000 L, uma bomba submersa e um filtro de disco. Além disso, na parte interna da câmara foram instalados, na proposta inicial, um sistema de aspersão composto por 6 bicos nebulizadores instalados nas laterais (posição horizontal), teto (posição vertical). Após avaliação e proposição de nova configuração, o sistema de aspersão foi alterado para 12 bicos nebulizadores todos instalados nas laterais da câmara (posição horizontal).

Ensaios experimentais foram realizados em duplicata para avaliação da eficácia da câmara de desinfecção e análise de molhabilidade com uso de papeis sensíveis a água (WSPs). As amostras apresentaram resultados semelhantes, demonstrando que a metodologia aplicada foi adequada para o estudo proposto. É importante dizer que a avaliação realizada foi para a passagem de uma pessoa por vez dentro da câmara.

A câmara de desinfecção mostrou-se uma tecnologia potencial para a desinfecção rápida e eficaz da superfície dos EPIs, independente do item avaliado, utilizada rotineiramente pelos profissionais de saúde para proteção contra agentes infecciosos. O sistema de pulverização com o agente biocida foi eficaz na redução da carga microbiana, sendo a redução percentual igual a> 99% e, consequentemente, trazendo o número de células viáveis para <10 UFC / mL e <0,33 UFC / cm² após tempos de exposição de 10 e 30 s em 96,93% das condições experimentais analisadas.

Os resultados deste estudo mostram que a câmara de desinfecção com hipoclorito de sódio a 0,25% pode ser uma alternativa para o controle da biocarga em ambientes nosocomiais, principalmente para evitar a autocontaminação dos profissionais de saúde na etapa de desparamentação. A importância do uso da câmara por profissionais de saúde devidamente vestidos também é enfatizada para evitar o contato direto com o agente biocida testado. Além disso, por se tratar de um estudo inédito, esses resultados podem contribuir para o desenvolvimento e uso seguro de

equipamentos de desinfecção em ambientes onde a biocarga ambiental deve ser controlada. É importante destacar também que o delineamento experimental do estudo foi realizado com o objetivo de simular como a câmara de desinfecção seria utilizada pelos profissionais de saúde em ambiente hospitalar, antes da etapa de desparamentação. Desse modo, a manipulação de cepas virais não seria adequada nas condições testadas, visto que o manuseio desses microrganismos requer um ambiente laboratorial com maior nível de biossegurança. Porém, embora a eficácia virucida não tenha sido determinada diretamente, a câmara pode ser uma alternativa para reduzir as taxas de contaminação entre os profissionais de saúde diante de diferentes tipos de microrganismos emergentes, reduzindo os impactos na área de saúde pública.

Comparando os resultados experimentais e de simulação da configuração atual, conclui-se que o uso da ferramenta CFD é suficiente para entender o comportamento do fluxo dentro da câmara, havendo concordância entre os resultados numéricos e experimentais. Este modelo pode ser usado para propor novas configurações para a tecnologia de desinfecção.

O modelo matemático foi validado e simulações da nova configuração proposta foram realizadas. Os resultados da simulação confirmam que a configuração proposta aumenta a molhabilidade do corpo humano. Nesta nova configuração, câmara com 12 bicos nebulizadores instalados nas laterais (posição horizontal), foi possível aumentar as gotas suspensas nas faixas 1, 2 e 3. A concentração de gotículas aumenta de 12,53% para 34,11% na faixa 1, de 0,51% para 39,94% na faixa 2 e de 16,65% para 35,05% na faixa 3.

Os resultados experimentais da nova configuração evidenciaram um aumento na molhabilidade em todos os tempos de exposição, e é mais significativo para um tempo de exposição de 30 s. Mesmo com diferentes procedimentos de passagem, não havendo diferenças significativas nos resultados, demonstrando a eficácia da nova configuração em minimizar o impacto de fatores humanos na tecnologia de desinfecção.

5.1. Sugestão para Trabalhos Futuros

O presente estudo limita-se à passagem de apenas uma pessoa por vez e às condições de geometria da câmara de desinfecção com 6 e 12 bicos e aos parâmetros operacionais estudados, como por exemplo, a vazão do agente biocida na saída dos bicos (por simulação ou experimentalmente). Desta forma, sugere-se os seguintes tópicos a serem abordados em trabalhos futuros:

- Realizar ensaios experimentais prevendo a passagem de pessoas de forma contínua, onde se possa avaliar a eficácia da tecnologia com mais de uma pessoa passando por dentro da câmara;
- Caracterizar bicos de aspersão utilizando tecnologias óticas de medição de tamanho de gotas;
- Variar a vazão do agente biocida na saída dos bicos e avaliar o comportamento do perfil de molhabilidade;
- Avaliar novas geometrias de câmaras de desinfecção com a pessoa parada em seu interior;
- Correlacionar a inativação de vírus e bactérias com a molhabilidade da superfície atingida pelo agente biocida.

APÊNDICE A – Condições de Contorno da Modelagem

As condições de contorno determinam as características inicias do domínio computacional a ser simulado. Dentre essas características são necessárias inserir informações como, condições de parede, velocidade do fluido, pressão e outras variáveis relevantes para o caso.

Na Figura A.1 é apresentado o domínio computacional do bico nebulizador.

Figura A.1: Ilustração do domínio computacional do bico nebulizador [1].

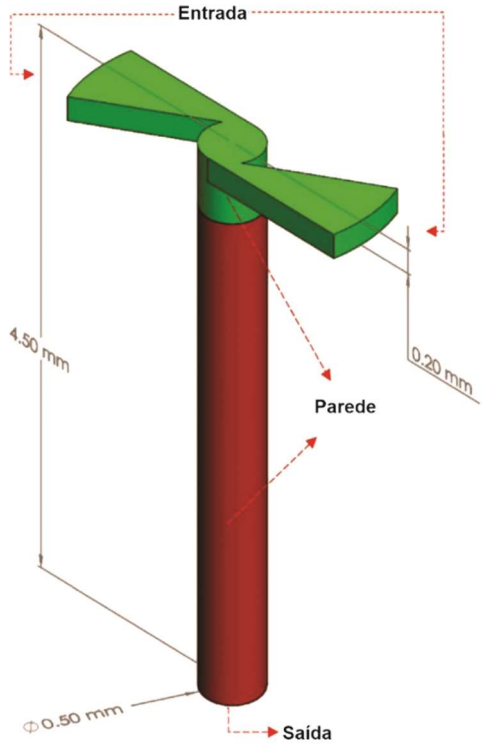

Nas simulações o domínio está parado e o fluido (água) se movimenta dentro dele, formando o escoamento característico de swirl em sua saída. A região verde representa a parte interna do bico nebulizador, e a extensão vermelha é modelada para estabilidade numérica (evitar recirculação na região de contorno).

A abordagem euleriana por meio do método dos volumes finitos [2] foi adotada para se obter a solução das equações que descrevem o escoamento pelo meio contínuo do bico.

Para o modelo numérico proposto, as propriedades físicas foram consideradas similares às da água [3]. Assim, eles eram válidos para soluções aquosas de concentrações suficientemente baixas de modo que as propriedades não fossem significativamente impactadas.

A Tabela A.1 mostra as condições de contorno de acordo com as regiões nomeadas na Figura A.1 aplicado para as simulações das câmaras de desinfecção com 6 e 12 bicos nebulizadores. Para este estudo, o fluxo foi considerado isotérmico e incompressível.

Tabela A.1: Condições de contorno do bico nebulizador [1].

Localizações	**Condições de contorno**
Entrada	Fluxo de massa médio para cada bico nebulizador
Saída	Pressão Atmosférica
Parede	Condição de não deslizamento

Na Figura A.2 são apresentados os domínios computacionais das câmaras de desinfecção com 6 e 12 bicos nebulizadores.

Figura A.2: Ilustração do domínio computacional das câmaras de desinfecção (A) 6 bicos nebulizadores; (B) 12 bicos nebulizadores [1].

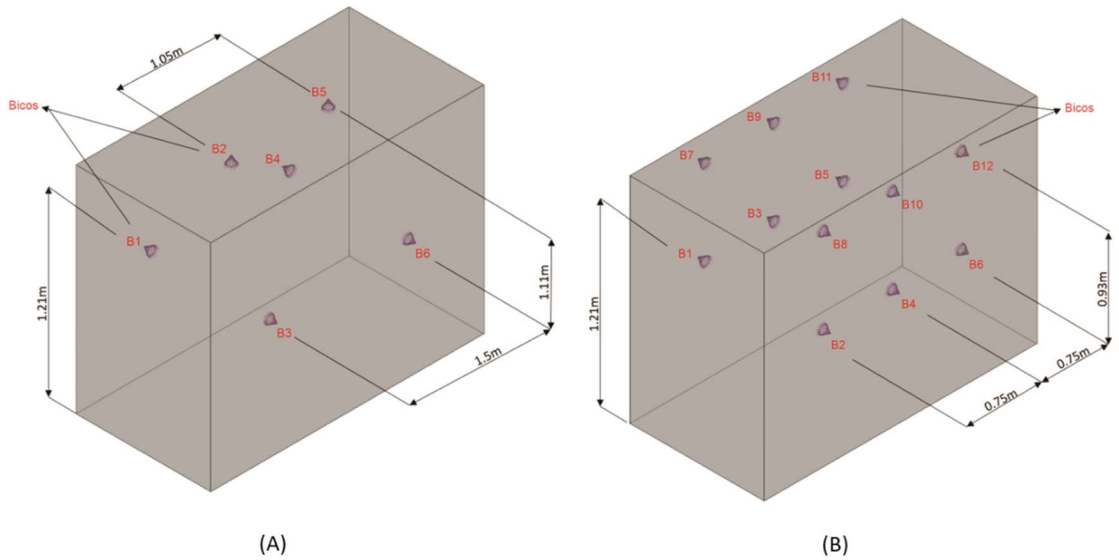

A câmara de desinfecção é representada por um domínio de fluido contínuo em duas configurações com 6 e 12 bicos nebulizadores, conforme mostrado na Figura A.2. O fluxo foi analisado por meio de uma abordagem Euleriana-Lagrangeana, na qual a região interna da câmara de desinfecção (meio contínuo - ar ambiente) interage com as partículas de fluido (meio disperso) que são geradas através dos bicos nebulizadores [4,5].

Para a simulação da câmara de desinfecção, o meio contínuo (ar) foi tratado com uma abordagem Euleriana, usando as mesmas equações de conservação de massa e momento apresentadas no capitulo 2 (Equações 1–4), mas em regime transiente, devido a necessidade de se analisar de forma quantitativa o percentual de área molhada na região central da câmara. A solução do agente biocida foi tratada usando uma abordagem Lagrangeana como um fluido disperso (gotículas).

Cada bico foi considerado como uma injeção pontual de partículas (gotas), com taxas de fluxo de massa definidas de acordo com os resultados experimentais. As velocidades foram ajustadas de forma que mantivessem o fluxo de momento resultante das simulações dos bicos nebulizadores. O valor do ângulo de dispersão do bico foi adotado conforme determinado experimentalmente. A distribuição de tamanho de partícula adotada foi descrita ajustando a função de distribuição de Rosin-Rammler [1], que também foi avaliada experimentalmente. Todas as paredes da tecnologia foram consideradas como sem deslizamento e com coeficientes de restituição iguais a zero.

REFERÊNCIAS

1. Freitas Neves PR, et al. Numerical and experimental analyses for the improvement of surface instant decontamination technology through biocidal agent dispersion: potential of application during pandemic. 2021 May;16(5). http://dx.doi.org/10.1371/journal.pone.0251817.

2. Versteeg H., Malalasekera W. An introduction to Computational Fluid Dynamics: The Finite Volume Method. [Internet]. Second. Technical LS, editor. England: Edinburgh Gate; 1995. Available: http://ftp.demec.ufpr.br/disciplinas/TM702/Versteeg_Malalasekera_2ed.pdf

3. Joshi JR. COVSACK: an innovative portable isolated and safe COVID-19 sample collection kiosk with automatic disinfection. Trans Indian Natl. Acad. Eng. 2020 Jul;5:269–275. https://doi.org/10.1007/s41403-020-00139-1.

4. Delele MA, Vorstermans B, Creemers P, Tsige AA, Tijskens E, Schenk A, Opara UL, Nicolai BM, Verboven P. Investigating the performance of thermonebulisation fungicide fogging system for loaded fruit storage room using CFD model. Journal of Food Rngineering. 2012 Mar;109(1):87-97. https://doi.org/10.1016/j.jfoodeng.2011.09.030.

5. Pinilla JA, Asuaje M, Ratkovich N. Study of a fogging system using a computational fluid dynamics simulation. Applied Thermal Engineering. 2015 Mar;96:228-239.http://dx.doi.org/10.1016/j.applthermaleng.2015.10.117.